



CHIP-TO-CHIP OPTICAL INTERCONNECTION  
USING MEMS MIRRORS

THESIS

Tod Laurvick, Captain, USAF

AFIT/GE/ENG/09-27

DEPARTMENT OF THE AIR FORCE  
AIR UNIVERSITY

**AIR FORCE INSTITUTE OF TECHNOLOGY**

Wright-Patterson Air Force Base, Ohio

APPROVED FOR PUBLIC RELEASE; DISTRIBUTION UNLIMITED.

The views expressed in this thesis are those of the author and do not reflect the official policy or position of the United States Air Force, Department of Defense, or the United States Government.

CHIP-TO-CHIP OPTICAL INTERCONNECTION  
USING MEMS MIRRORS

THESIS

Presented to the Faculty  
Department of Electrical and Computer Engineering  
Graduate School of Engineering and Management  
Air Force Institute of Technology  
Air University  
Air Education and Training Command  
In Partial Fulfillment of the Requirements for the  
Degree of Master of Science in Electrical Engineering

Tod Laurvick, B.S.E.E.  
Captain, USAF

March 2009

CHIP TO CHIP OPTICAL INTERCONNECTION  
USING MEMS MIRRORS

Tod Laurvick, B.S.E.E.

Captain, USAF

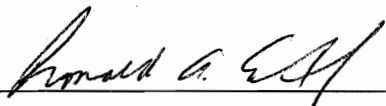
Approved:



LaVern A. Starman, PhD, Maj, USAF  
(Chairman)

26 Feb 09

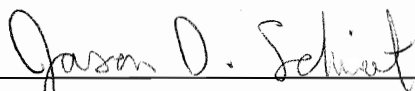
date



Ronald A. Coutu Jr., PhD, PE, LtCol,  
USAF (Member)

19 Feb 09

date



Jason D. Schmidt, PhD, Maj, USAF  
(Member)

19 Feb 09

date

*Abstract*

This research explores the use of microelectromechanical systems (MEMS) mirrors to direct subsurface optical signals to another device and reception of those signals for use in chip to chip communications. Devices were built in polysilicon multi-user MEMS processes (PolyMUMPs) to test the feasibility of building prototype optical paths to and from the device controlling horizontal and vertical beam direction and tilting in the outgoing signal and MEMS beam splitters for the incoming signal.

Several elements of the steerable mirrors were successful, and those which needed improvement indicate a high probability of success with limited trials needed. Currently successful design elements could still be improved within the scope of PolyMUMPs. The stationary mirror elements were unsuccessful as designed. The issues encountered using flat-foldability would probably not be successful with PolyMUMPs, but show promise with a more sophisticated process. With flip chip bonding however, the incoming beam path could have been realized with a high probability of success and minimal design work. With both the stationary and movable mirrors, an incoming and outgoing beam path could be realized. This comprises all the elements needed for a prototype proof of concept device.

With a more sophisticated fabrication process (such as SUMMiT), drastic improvements could be made to both beam paths and potentially allow for a variety of more sophisticated designs to be incorporated to improve design compactness, improve controllability, tighten tolerances on moving parts, increase mirror quality, and allow for the design and testing of foldable MEMS structures.

It was determined that PolyMUMPs would likely be usable for constructing steerable mirrors and actuating them but not for the incoming beam paths as designed. PolyMUMPs would not however provide adequate mirror surfaces for bottom reflection and while progress was made in making bottom reflecting mirrors, a success-

ful method has not yet been finalized. With the added capability of flip-chip bonding, PolyMUMPs could be used to prototype both beam path structures (but with the same backside mirror challenge). If SUMMiT (or a similarly sophisticated process) were made available, there is a much greater chance that a single device could be built without the need for flip-chip bonding and would likely not require additional reflective surfaces for prototype structures. If in the event mirror material was needed with SUMMiT however, the added capability of the process itself allows for alternate solutions for this problem to be explored.

## *Acknowledgements*

I would first like to thank my family for the never ending support, dedication and belief.

To the staff at AFIT (Maj Starman, LtCol Coutu and Maj Schmidt) for allowing me to pursue my interests while keeping me honest and on track.

Most importantly I would like to thank my fellow MEMS students (Luke Rederus, Mauricio Kossler, Adam Gubbels, James Shields, Dan Gallagher, Nicholas Coleman, Mimi Ledet, and Tom Lagoski) - without your support, dedication, great ideas and much needed comic relief this would not have been possible.

Tod Laurvick

# Table of Contents

	Page
Abstract . . . . .	iv
Acknowledgements . . . . .	vi
Table of Contents . . . . .	vii
List of Figures . . . . .	ix
List of Abbreviations . . . . .	xii
I. Introduction . . . . .	1
1.1 Chip-to-Chip Optical Interface (C2OI) . . . . .	1
1.2 The Micro-Electromechanical Approach . . . . .	2
II. Comparable Work in Micro-Optics Emitting and Sensing . . . . .	6
2.1 Signal Generation . . . . .	6
2.2 Structures of Beam Directing Devices . . . . .	8
2.2.1 Outgoing Beam Path - Actuated Mirrors . . . . .	9
2.2.2 Incoming Beam Path - Stationary Mirrors . . . . .	12
2.3 Methods of Actuation . . . . .	16
2.3.1 Piezoelectric Actuation . . . . .	16
2.3.2 Electrostatic Actuation . . . . .	17
2.3.3 Electrothermal Actuation . . . . .	18
2.4 Photo-detection . . . . .	21
2.5 Applicable Works . . . . .	25
III. Theory of Operation . . . . .	27
3.1 Fabrication Considerations . . . . .	28
3.2 Overall Design Approach . . . . .	32
3.2.1 Incoming Beam Path . . . . .	33
3.2.2 Outgoing Beam Path . . . . .	39
IV. Simulated Modeling and Test Results . . . . .	47
4.1 Incoming Beam Path . . . . .	48
4.1.1 Backside Mirrors . . . . .	48
4.1.2 45° Overhead Mirrors . . . . .	50
4.1.3 Floating Joint Structures . . . . .	59
4.2 Outgoing Beam Path . . . . .	60



	Page
4.2.1 Beam-Positioning Mirrors . . . . .	60
4.2.2 Beam-Tilting Mirrors . . . . .	60
4.2.3 Mirror Attachments . . . . .	63
4.2.4 Thermal Actuation and Pawl Motion . . . . .	66
4.2.5 Mirror Actuation and Gearing . . . . .	67
V. Conclusions and Recommendations . . . . .	71
5.1 Processing . . . . .	71
5.1.1 Wet and Dry Release . . . . .	72
5.1.2 Drying Technique . . . . .	72
5.2 Incoming Beam Path . . . . .	73
5.2.1 Bottom-side Mirrors . . . . .	73
5.2.2 45° Overhead Mirrors . . . . .	74
5.2.3 Beam Splitters . . . . .	76
5.3 Outgoing Beam Path . . . . .	77
5.3.1 Bottom-side Mirrors . . . . .	77
5.3.2 Mirror Hinging and Support Structure . . . . .	78
5.3.3 Mirror Movement and Gearing . . . . .	80
5.3.4 Thermal Actuators and Pawl Motion . . . . .	80
5.3.5 Additional Mirror Designs . . . . .	81
5.4 Recommendations . . . . .	81
Appendix A. Forward Kinematic Analysis . . . . .	84
Appendix B. PolyMUMPs Design Overview . . . . .	94
B.1 Run 83 . . . . .	94
B.2 Run 84 . . . . .	96
Appendix C. Post Processing . . . . .	98
C.1 Mirrors and Hinges . . . . .	98
C.2 Process Followers . . . . .	101
Appendix D. Intermediate Results . . . . .	103
D.1 Foundry Issues From PolyMUMPs . . . . .	103
D.2 Post Processing . . . . .	104
Bibliography . . . . .	108
Index . . . . .	112

## *List of Figures*

Figure		Page
1.1.	Conceptual Design Overview . . . . .	3
2.1.	VCSEL to MEMS interface . . . . .	7
2.2.	MEMS Beam Splitter . . . . .	9
2.3.	Embedded Lead Multi-axis MEMS Mirror . . . . .	10
2.4.	Horizontally Controllable MEMS Mirror . . . . .	11
2.5.	MEMS mirrors assembled with solder balls . . . . .	13
2.6.	Dissimilar Material Bending . . . . .	14
2.7.	MEMS Assembly Using Polymer Hinges . . . . .	14
2.8.	Vertical MEMS Mirror From Deep Reactive Ion Etching . . . . .	15
2.9.	Examples of applied origami . . . . .	16
2.10.	MEMS Mirror Using Piezoelectric Bimorph Actuation . . . . .	17
2.11.	MEMS Mirror Using Electrostatic Actuation . . . . .	18
2.12.	Electrostatic Phased Array Multiaxis Actuation . . . . .	19
2.13.	Dissimilar Material Hinges Using Thermal Actuation . . . . .	20
2.14.	Embedded Ring Thermal Actuators . . . . .	20
2.15.	Photodiodes . . . . .	22
2.16.	Nanowire Photodetectors . . . . .	23
2.17.	Angular Restriction of Quantum Well Infrared Photodetectors . . . . .	24
2.18.	Multiple Band Quantum Well Infrared Photodetectors . . . . .	25
3.1.	Single Device Concept Overview . . . . .	27
3.2.	PolyMUMPs Overview . . . . .	29
3.3.	SUMMiT V Overview . . . . .	30
3.4.	Sample SUMMiT Devices . . . . .	31
3.5.	Three Layer Hinge Design . . . . .	33
3.6.	Incoming stationary mirror designs . . . . .	36

Figure		Page
3.7.	Top Mirror Ring Conceptual Assembly . . . . .	38
3.8.	45° Overhead Mirror . . . . .	40
3.9.	Vertical Beam Positioning Mirror . . . . .	41
3.10.	Horizontal Beam Positioning Mirror . . . . .	42
3.11.	Horizontal Beam Turning Mirror . . . . .	42
3.12.	Vertical Beam Turning Mirror . . . . .	43
3.13.	Outgoing Movable Mirror Designs . . . . .	44
3.14.	Pawl Operation Description . . . . .	46
4.1.	Backside Mirror . . . . .	49
4.2.	Fused 45° Overhead Mirror . . . . .	50
4.3.	Overhead 45° Angle Definitions . . . . .	51
4.4.	Overhead 45° Point Definitions . . . . .	53
4.5.	45° Overhead Mirror Step 1 . . . . .	56
4.6.	45° Overhead Mirror Step 3 . . . . .	56
4.7.	45° Overhead Mirror Step 4 . . . . .	57
4.8.	45° Overhead Mirror Step 5 . . . . .	58
4.9.	Four States of 45° Overhead Mirror . . . . .	58
4.10.	Pyramid SEM . . . . .	59
4.11.	Designs of Beam Positioning Mirrors . . . . .	61
4.12.	Designs of Beam Turning Mirrors . . . . .	62
4.13.	Assembled Tilting Mirror . . . . .	64
4.14.	Assembled Steering Mirror . . . . .	65
4.15.	Five Bank vs. Two Bank Actuators . . . . .	67
4.16.	Engaged Pawl . . . . .	68
4.17.	Linear Actuator SEM . . . . .	69
5.1.	Flip Chip Bonding . . . . .	75
5.2.	Etched Beam Splitter . . . . .	77
5.3.	Fabricated Thermal Actuators . . . . .	79

Figure		Page
A.1.	Overhead 45° Angle Definitions . . . . .	85
B.1.	LEdit Design for PolyMUMPs Run 83 . . . . .	95
B.2.	LEdit Design for PolyMUMPs Run 84 . . . . .	97
C.1.	Process Follower For Bottom Side Mirror Deposition . . . . .	101
D.1.	PolyMUMPs Foundry Results, Run 83 . . . . .	104
D.2.	PolyMUMPs Foundry Results, Run 84 . . . . .	105
D.3.	LOR Undercut . . . . .	106
D.4.	SU-8 Depositions . . . . .	107
D.5.	Metal Deposition . . . . .	107

## *List of Abbreviations*

Abbreviation		Page
MEMS	microelectromechanical systems . . . . .	iv
PolyMUMPs	polysilicon multi-user MEMS processes . . . . .	iv
DARPA	defense advanced research projects agency . . . . .	1
MTO	microsystems technology office . . . . .	1
C2OI	chip to chip optical interconnects . . . . .	1
VCSEL	vertical cavity surface emitting laser . . . . .	6
SEM	scanning electron microscope . . . . .	9
SUMMiT	Sandia ultra-planar multi-level technology . . . . .	10
QWIP	quantum wells infrared photodetector . . . . .	24
HF	hydrofluoric acid . . . . .	29
SacOx	sacrificial oxide . . . . .	30
Poly	polysilicon . . . . .	30
LPCVD	low pressure chemical vapor deposition . . . . .	30
CMP	chemical mechanical polishing . . . . .	30
PECVD	plasma enhanced chemical vapor deposition . . . . .	31

# CHIP-TO-CHIP OPTICAL INTERCONNECTION USING MEMS MIRRORS

## I. Introduction

As advancements in microelectronics continue, the common challenges which continually present themselves require newer and more ingenious methods to overcome. To this end, the advantages of photonics-based alternatives become more and more appealing. When one considers the general advantages of these systems versus their electronic counterparts (in areas such as noise reduction, increased data transmission speeds, security, reliability, reduction in heat, computational speed increases, etc.), the importance of developing all areas of this technology become apparent. One such obstacle lies in the ability to direct optical signals from one device to another through open air, such that individual photonic components may one day be assembled as easily as their electronic counterparts are today, but without any limitations on their capabilities.

### *1.1 Chip-to-Chip Optical Interface (C2OI)*

The Defense Advanced Research Projects Agency (DARPA) sponsors several programs which address a variety of technological challenges [1]. Among these programs is one overseen by the Microsystems Technology Office (MTO) called Chip to Chip Optical Interconnects (C2OI) [1]. The overall objective of this program is to ‘remove the chip boundary as a significant obstacle to data transport and demonstrate between-chip interconnects that have comparable performance to on-chip non-local electrical interconnects’ [1]. The limitations specifically cited with current electrical base technology include [1]:

- achieving high packing density,
- reduce cross-talk between channels,

- minimize frequency-dependent losses,
- and lower power dissipation.

While current technologies are beginning to utilize optical communications, most of the state of the art components are designed for computer networking applications and do not specifically address the above issues [1].

## ***1.2 The Micro-Electromechanical Approach***

Presumably, the long-term application for this experiment would be the communications between two all-optical devices. One possible example may be a theoretical ‘all-optical’ microprocessor and memory storage device. While the exact specifications of such devices can only be theorized at this time, in order to be applicable this design will need to be both general and flexible. Considering the above example of microprocessor and memory communication, whatever the source of the signal emission from the microprocessor, that device needs to be engineered in such a way that it can be integrated with this design and still function as intended. While the parameters which would define the ideal system are not currently known, it is presumed that this design can be modified to meet these unforeseen needs (such as changing mirror material to reflect a different range of frequencies for a different operational bandwidth and center frequency). In order to actually proceed with design and testing using current technology, design limitations on current emission and detection devices will be important limiting factors.

The focus of this work will be to explore the feasibility of addressing this challenge using MEMS. The approach will be to design a single ‘standard’ system which can be integrated on the top surface of any pair of chips containing optical signals that need to communicate. Each device would include the system of mirrors and any supporting electronics required to drive beam control for both the incoming and outgoing signal (analogous to a single port on a computer and a similar port on a

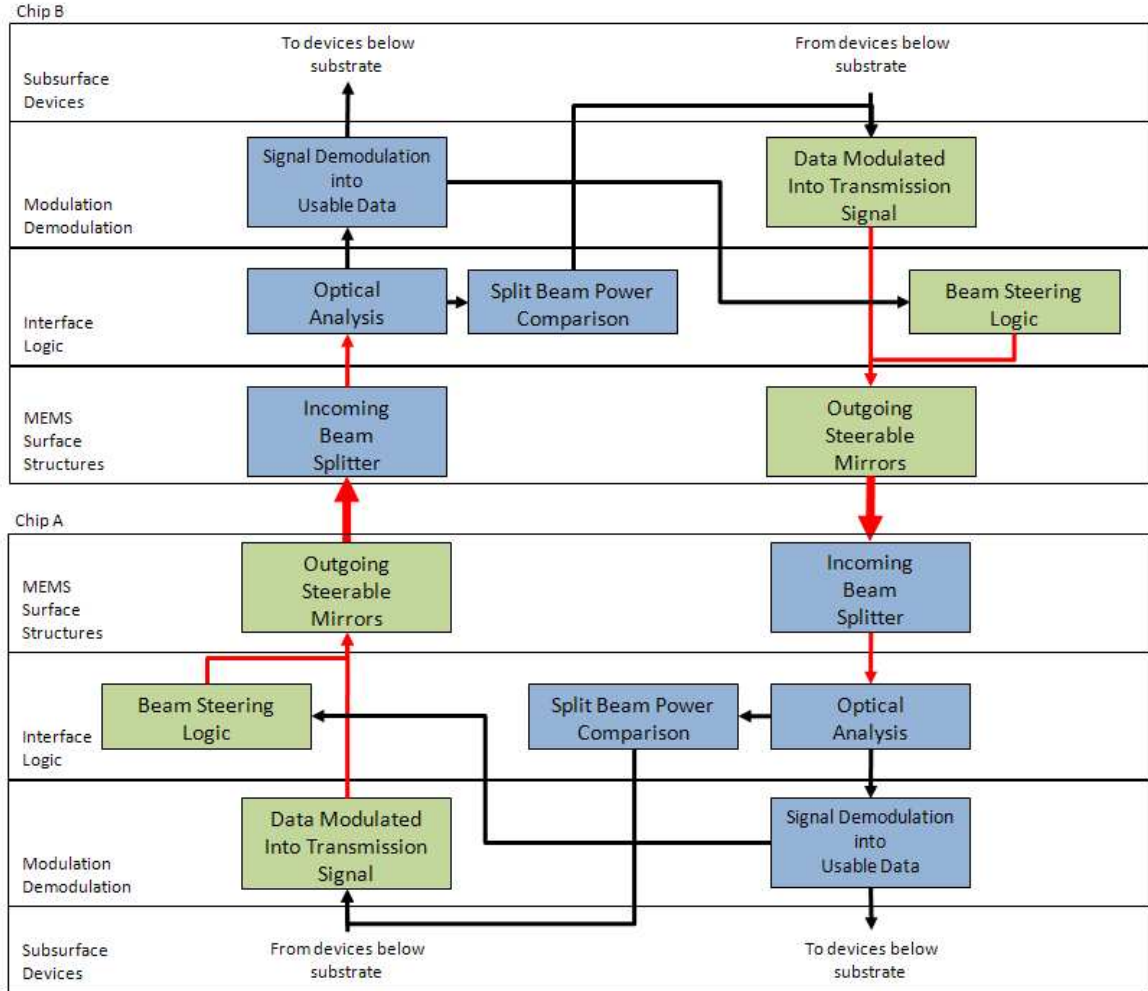


Figure 1.1: Concept of operation between two devices

connecting serial device). A flowchart outlining this control scheme is provided in Figure 1.1 with optical paths shown in red and electrical paths in black.

In order to evaluate the feasibility of this scheme, the following steps will be required:

1. demonstrate the manufacturability and controllability of the MEMS components
2. characterize the capabilities of these structures
3. compare the results to the overall constraints required by the design as a whole (i.e. what are the limitations in distance, temperature, air purity, vibration, etc.) to identify and address deficiencies in the design



4. join these refined MEMS components with VCSELs and photodetectors below the substrate, and prove alignment is possible while maintaining required performance metrics
5. develop and test the control algorithms needed to drive these devices along with the full control modulation scheme (i.e. how much bandwidth needs to be used for mirror control)
6. construct a minimum of two prototype devices which can then be tested as a functioning pair

During the bulk of this work, the outgoing and incoming beam paths will be considered separately. For simplicity, the outgoing beam path is composed of movable mirrors capable of directing the beam to the correct spot on the second device. The incoming beam path is comprised of the stationary mirrors needed to take this directed beam, split it and direct the individual signals to photodetectors. This simplification assumes that the incoming beam path is close enough to centerline to be usable but does not prevent the possibility of adding steerable mirrors to the incoming beam path as well to compensate for large misalignments. Such structures would however be very similar to those present in the outgoing beam path and thus will not be included at this time. The separation of these two systems is simply to provide a logical division in discussing the two kinds of structures. Once these structures can be characterized, the location, size, type and functionality of each mirror in both beam paths can be adjusted accordingly.

Should the above steps prove successful, the resulting design should address the four limitations outlined in the C2OI program, specifically:

- be of sufficiently small size as to allow for at least one outgoing and incoming beam path on any one side of a typically sized integrated circuit
- utilize only optical signals to transmit and receive data eliminating any crosstalk
- utilize fix bandwidths (determined by the devices generating and receiving the optical signal) which would offer the speed of optically communicated signals

without the frequency-dependent factors introduced with conventional electronics

- operate with minimal-power light generation devices sufficient for the small distances required but strong enough to provide an acceptable signal-to-noise ratio, along with minimal absorption in any reflecting component in the beam path (to minimize losses from device to device)

To evaluate the potential of such a project, Chapter II will discuss relevant work and evaluate the most pertinent related areas not only to help guide the design process through utilization of other successful projects, but also to help bound design limitations and provide a solid foundation for decisions made throughout this experiment. Next in Chapter III, the theory of operation will be discussed, which takes the foundation built by prior works and attempts to frame the next logical steps as well as bound the scope of what devices are to be built and tested in the time allotted with available resources. A discussion of the devices built is covered next in Chapter IV where the successes and failures of these devices will be discussed. Finally, this experiment will be summarized and next steps defined for each of the areas explored in Chapter V.

## II. Comparable Work in Micro-Optics Emitting and Sensing

With the exception of a few specific areas such as micro-mirror arrays, applications utilizing MEMS which are directly applicable to this kind of an experiment are still relatively rare. In research however, a great deal of work has been performed in not only MEMS structures but also many of the required components needed to demonstrate the effectiveness of this design.

Because this application as a whole incorporates a relatively large number of concepts, the overall design will be broken down in four general areas:

1. signal generation
2. structure of beam directing devices
3. methods of actuation
4. photo-detection

### *2.1 Signal Generation*

As a whole, this area addresses how the transmitted beam is to be generated. Keeping in mind the overall design presented in Chapter I, this includes not only the outgoing data stream (from device A) but may also include data regarding the positioning of the incoming beam (from device B to device A) derived from whatever detection method is employed.

Since the development of the micro-scale light emitting diode in the 1960s [2], continued research has produced several variations of this technology to suit a wide range of applications. This basic design lead to the development of edge emitting lasers by utilizing a Fabry-Perot cavity to provide reflection through the lasing medium [3]. Eventually the ability to create quantum wells and precisely deposit layers of material with varying indexes of refraction lead to the development of the vertical cavity surface emitting laser (VCSEL) [4].

The typical means of integrating a MEMS device with a subsurface device is by flip-chip bonding. This process involves placing metal pads to the bottom of the

MEMS device with corresponding pads on the top of the subsurface device. Gold beads of a specific and uniform diameter are then placed on these pads, and the two devices are positioned together with sufficient heat and pressure to fuse the two structures permanently at a predetermined distance as shown in Figure 2.1. Because of this, of all the types of light emitting devices currently manufacturable, vertically emitting devices will likely be the best suited for this application.

Devices such as this are already in use for several other applications resulting in a large body of work being produced covering a variety of operational aspects, but their use in telecommunications which utilize fiber to transmit data is of particular relevance. Research has been conducted demonstrating it is possible to fabricate these devices in arrays of cells using a quantum dot approach with a resolution greater than even the scale of the devices proposed here. Thus, the possibility exists of

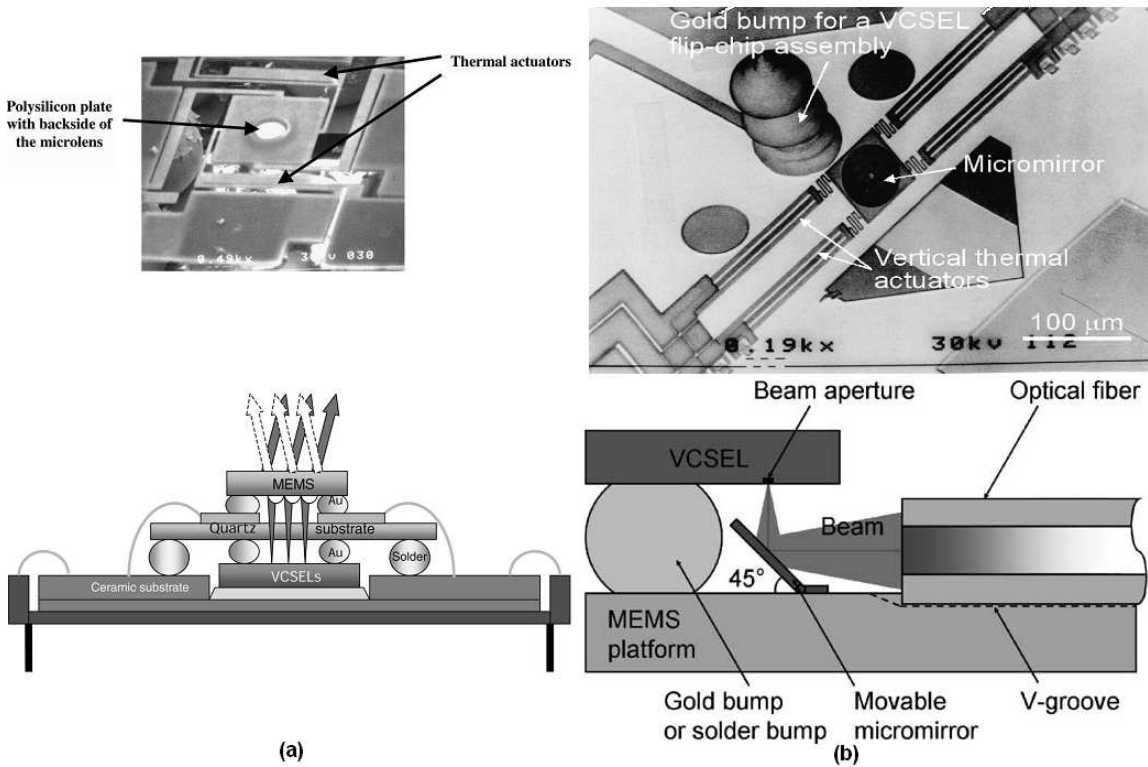


Figure 2.1: Two examples of interfacing VCSELs with MEMS structures (a) using a slide mounted micro lens [5], and (b) using a 45° MEMS mirror to direct beam into a fiber [6]

carrying several independent signals which are steered simultaneously. The behavior of these arrays is still being characterized however, such as modulation effects between adjacent cells [7], etc. For proving the effectiveness of this experiment, single VCSELs can be fabricated to meet the requirements for whatever design parameters are decided upon. While most applications require single-mode operation (i.e. a concentration of power along a single Gaussian shaped beam profile) the ability to engineer multi-mode lasers has also been explored [8–10] and as will be discussed in Chapter III. This leads to the possibility of a single VCSEL producing a multi-mode, yet symmetric, beam (which may lend itself well to a detection mirror geometry).

## ***2.2 Structures of Beam Directing Devices***

Once the desired beam is generated with the required information, structures must be devised which allow for the outgoing beam to be directed at the target based on beam steering information extracted from the received signal. These structures will need to be actuated accordingly, and a detailed outline of how this will be addressed is provided in Chapter III. As will become apparent, the two areas of difficulty with this design will be with the mirrors themselves as well as the hinges between these mirrors and the substrate or the base which actuates the mirror, which will be discussed in Section 2.2.2.

Typically MEMS devices require some electrical conductivity to function, so it is not uncommon for a layer of gold to be deposited as the final step. Even a poor quality gold deposition will function as a mirror, so any mirror built on the topside of the structure is relatively trivial. As is shown in Figure 2.2, sophisticated devices utilizing this technology are already being explored including polysilicon beam splitters, downward reflecting mirrors, and membrane phase modulators [11]. Given the limitations of the foundry process that will be used for this experiment however, there are not sufficient axes available to accomplish the task at hand using most of these kinds of designs. This experiment will still require reflecting a signal downward

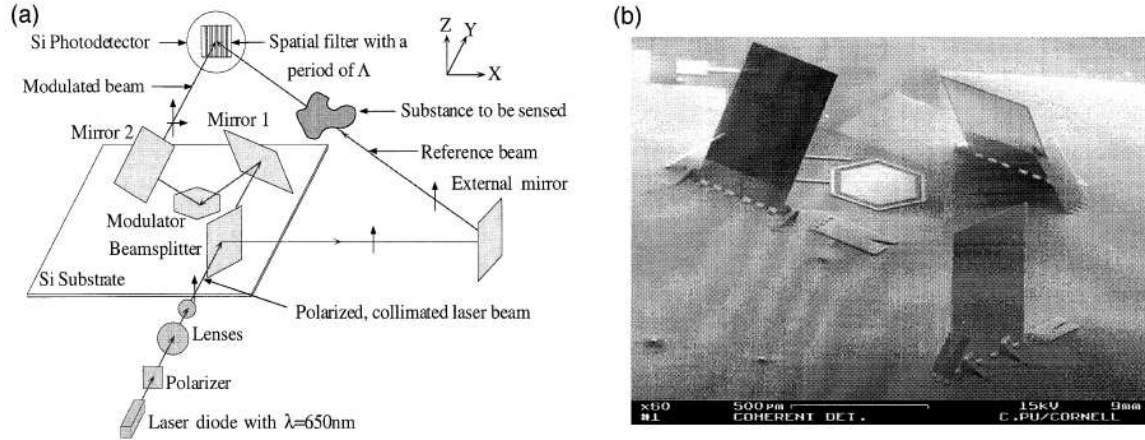


Figure 2.2: Coherent light detection showing schematic (a) and Scanning Electron Microscope (SEM) picture (b) of MEMS structure [11]

(toward the substrate) so this issue will be addressed in a more unconventional method which will be covered in Chapter III.

*2.2.1 Outgoing Beam Path - Actuated Mirrors.* The task of coupling a VCSEL to a horizontal fiber has been accomplished [6,12] by essentially fixing a fiber to a substrate at the end of which is a  $45^\circ$  mirror which interfaces a flip-chip bonded VCSEL to the fiber as was already shown in Figure 2.1. While this may be useful during the manufacturing of a single device with a macroscopic connector, once the device is completed, no further alignment would be possible. Considering the scale of VCSELs which are currently manufacturable, the process of aligning these micro fibers to a completed and enclosed device to create a stable and reliable connection without damaging the fiber would be exceedingly difficult in a laboratory, not to mention a production environment. Additionally, after assembly devices may be shifted due to vibration during operation or some other unintentional physical change. This in turn may cause misalignment or if the fiber were damaged, communications may be cut off entirely with no possibility of repair. An open-air, automated beam control approach eliminates these concerns.

As MEMS mirrors have been designed for directing beams, typically the applications involve micro scale beams directed at macro scale targets (optical displays,

biomedical imaging, optical switching, etc.) such as the one shown in Figure 2.3. This experiment presents a method of constructing two rotational axes from a Poly-MUMPs / Sandia Ultra-Planar Multi-level Technology (SUMMiT) type process (but with several additional buried layers). The mirror surface is constructed in such a way that two pairs of thermally actuated arms hold the structure. The arms themselves serve as thermal actuators, and by utilizing embedded conduction paths, arm actuation provides two axis of rotation [13].

Another proposed method for horizontally steering a VCSEL beam [14] involves using a series of comb drive arrays to provide two dimensions of control. While this configuration of comb drives cannot passively maintain a fixed offset with a large degree of certainty, it may be suitable for an application which requires a cyclic movement, resistance to thermal influences, and minimal stress on moving components (which will be covered in more detail in the next section on actuation methods).

A diffractive lens structure was formed on a moveable platform with a focal length of  $500\text{ }\mu\text{m}$ , a diameter of  $200\text{ }\mu\text{m}$  and was used with a VCSEL which was emitting at a wavelength of  $850\text{ nm}$  [14]. This structure is designed such that it is able to adhere to the polysilicon framework supporting it, is transparent to the

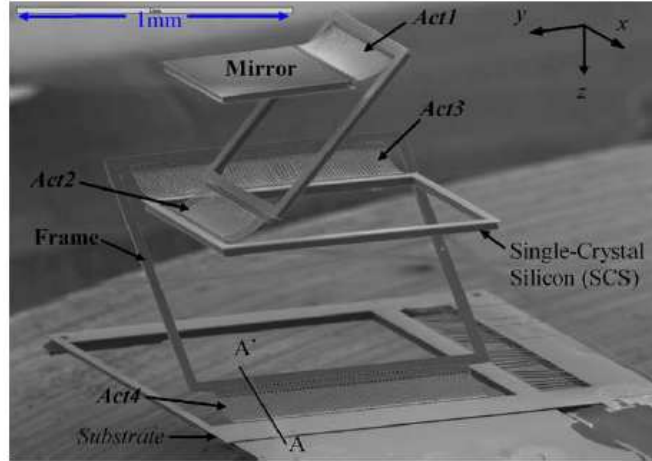


Figure 2.3: SEM of a 2D micromirror with embedded polysilicon circuit paths within the frame structures which drives individual thermal actuation of each mirror segment [13]

frequencies of the light being directed, is rigid enough to hold its shape over a range of temperatures, and is made of a material which can survive the MEMS processing which follows its formation. For this particular experiment, an extremely stable and chemically resistant amorphous fluorocarbon polymer, Cytop<sup>TM</sup>, was selected because it meets the criteria listed above. While a number of methods for actually forming the lens were proposed (such as direct laser beam writing, optical holography, electron-beam lithography, laser ablation, photo lithography and reactive ion etching [14]), this group chose to form the structure in question using hot embossing replication. This material has also been used in the past to fabricate deformable mirrors, wafer bonding, and refractive reflow lenses. Figure 2.4 shows the top view of the movable plate structure and a side view of the structure above the VCSEL in question [5,14].

Depending on what kind of structure these lenses form, this kind of device could be used not only for beam steering but also theoretically for adjusting the focal length of the outgoing beam by moving a lens or series of lenses axially in

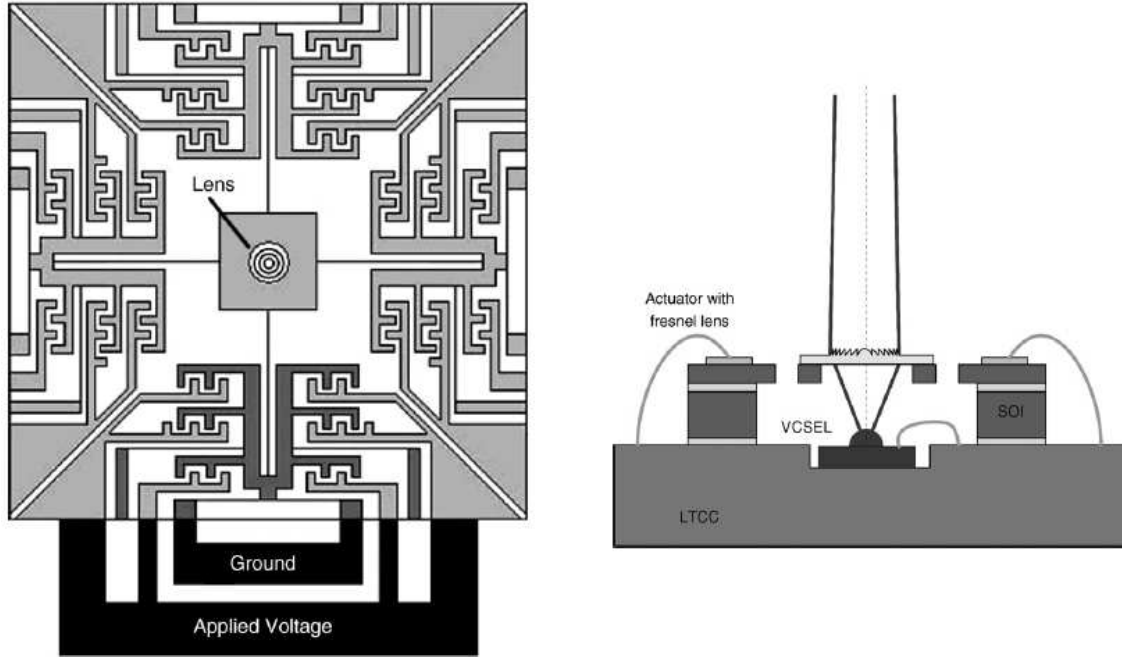


Figure 2.4: Diffraction lens assembly, top view (left) and side view (right) with 2 degrees of freedom using electrostatic actuation [14]



the direction of beam travel. It is also conceivable that if any of these potential lens materials are flexible enough, they could possibly be attached to independent portions of polysilicon and either stretched or compressed (similar to the lens of an eye) to also adjust the target focal length. For the purposes of this project, mirrors will be used instead, keeping in mind that these too can be given curvature through modifications to polysilicon doping creating radially uneven stress prior to metal deposition [15] which can also serve to make small adjustments to the focal length.

*2.2.2 Incoming Beam Path - Stationary Mirrors.* For this experiment, it is presumed that the incoming beam path will be close enough to the expected path that at sufficient distances, with sufficiently small beam diameter and oversized receiving mirrors, a stationary mirror arrangement will suffice. Should this not be the case, then a modified version of the output assembly could instead be employed with intermediate sensors used behind each mirror. This does add a level of complexity to the design which would likely prohibit a process like PolyMUMPs from being used, but as was already mentioned, the concept of micro mirrors serving as beam splitters has been demonstrated [11] and is the only additional item needed in addition to the outgoing assembly to accomplish this task.

Recognizing that with a process which allows additional layers, there is a possibility that stationary designs could in fact be staged and moved. If this is the case and some sort of stationary assembly is sufficient, then what is needed is the ability to construct a mirror arrangement which takes a horizontal beam, directs it down toward the substrate, and splits the signal into individual portions. These individual beams are then metered separately to determine how central the incoming beam is and thus the beam is tracked, similar to a technique used in some telescopes [16]. Thus, a crucial structural element for this experiment is the joint which allows mirror positioning to be accomplished. A variety of methods have been attempted to hinge MEMS devices with varying degrees of success. The first to be discussed is the use of balls of solder placed on a hinge joint in a MEMS device. Using the surface tension

of the solder after it is heated and starts to melt, the mirror is pulled into position as shown in Figure 2.5. For this experiment, this method would be difficult due to the variability which results from mirror to mirror and the large degree of uncertainty regarding the final angle the mirror reaches as a result [17].

Another possible method of controlling mirror position is to use the bending property inherent in two dissimilar materials which are deposited at different temperatures. As these structures reach operating temperature, the internal stresses in the layers will cause bending due to the difference in the coefficients of thermal expansion. One similar paper addresses a variation of this concept as shown in Figure 2.6. In that particular paper, this effect was used in conjunction with actuation which took place using the embedded polysilicon [18].

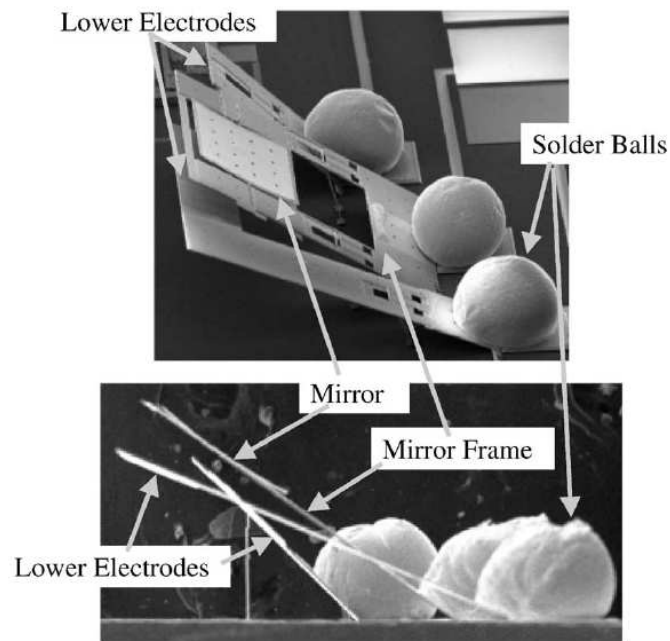


Figure 2.5: SEM images of mirrors assembled using surface tension of molten solder balls to position the mirror and once solidified, hold the mirror in position [17]

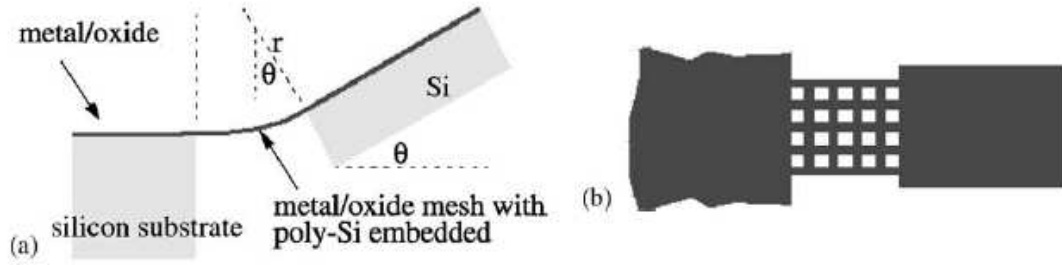


Figure 2.6: Conceptual views of dissimilar materials used to angle a movable mirror, side view (a) and top view (b) [18]

A method similar to solder balls was used to accomplish this task using photoresist as the hinge material as shown in Figure 2.7. This process included strategically placing patterned photoresist such that it joined together neighboring sections of polysilicon. Later in the process this material could then be heated (at a much lower temperature than the solder balls mentioned above) and accomplish the same task but in a much more controllable manner.

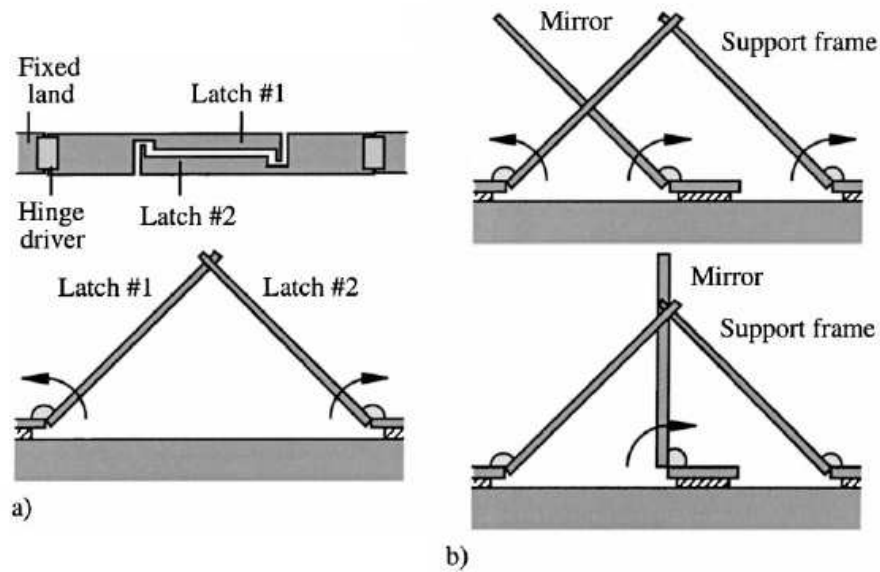


Figure 2.7: Two methods of self assembled mirrors using photoresist to construct simultaneously assembled 45° mirrors (a) and sequentially-assembled 90° mirrors (b) [19]

Vertical mirrors on the side of etched structures have also been achieved as shown in Figure 2.8, but these devices are built by either deposition or etching, and the maximum height limitation due to this is excessively small. Theoretically it is conceivable that the required mirrors could be built in this fashion using a complex variety of patterns with metal depositions at the appropriate stages to build up the required mirror structures. Considering how long the overall depositions would take, the complexity of so many masking steps, and most importantly the lack of on-site capability to accomplish these processes, this option will not be pursued.

While the way in which these structures are assembled is of concern, they must also be both strong and meet fairly complex geometric design constraints. This concern is not unique to MEMS structures, and indeed such challenges exist in many areas of engineering and in several cases have been solved using the concept of flat-foldability mathematics (more commonly referred to as origami). While research

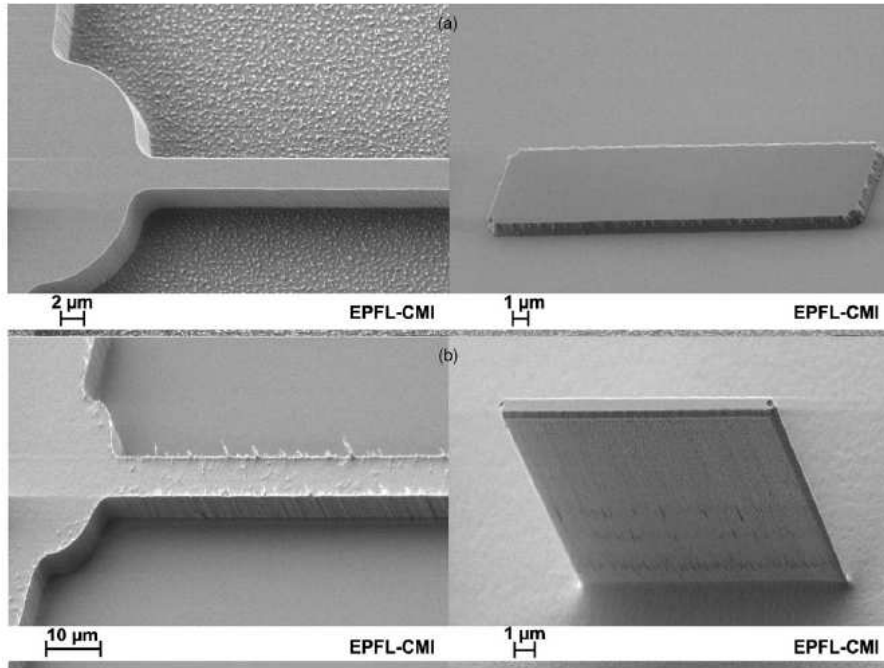


Figure 2.8: SEM images of a vertical mirror structure showing before (a) and after (b) deep reactive ion etching of two parts of the structure - the left shows part of the support arm structure and the right shows the mirror itself [20]

papers exploring this are not common, examples of this concept are shown in Figure 2.9 and include hard-top convertible automobiles as shown in (a) [21], orbital telescopes as shown in (b) [22], and architecture as shown in (c) [23] which have all used this approach to solve some challenging problems.

### 2.3 *Methods of Actuation*

As was mentioned in the previous section, the way in which mirrors are constructed does not necessarily limit the method of actuation. While there have been several research projects conducted for a variety of applications not only for mirror actuation but MEMS actuation in general, these can be explored individually. In general however, the following three broad methods of actuation commonly appear through the literature regarding movable MEMS structures: piezoelectric, electrostatic, and electrothermal.

*2.3.1 Piezoelectric Actuation.* Some materials when deformed (such as in a pressure sensor) produce an electric potential. The reverse of this process is the first driving force to be discussed and is called piezoelectric actuation. This method is not as common in literature partly because of the relatively short list of materials capable of producing large amounts of actuation when compared to electrothermal (which will be discussed in Section 2.3.3). There has been some application of this method

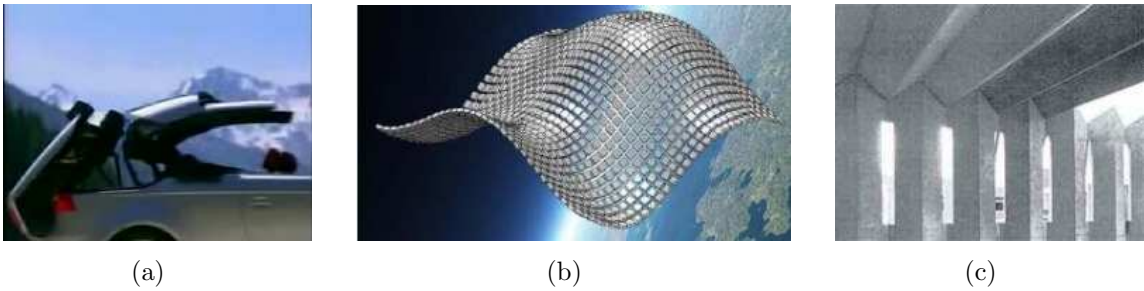


Figure 2.9: (a) Hard top convertible from Volvo [21], (b) Conceptual illustration of origami-inspired orbital space telescope [22], and (c) origami used in building design [23].

in electrophotographic processes however in which a piezoelectric layer is sandwiched between two metal layers, and when a voltage is applied deflection occurs [24]. A similar application shown in Figure 2.10 uses the same method for fast optical beam scanning [25].

*2.3.2 Electrostatic Actuation.* One actuation method which was mentioned in the previous section (see Figure 2.4) is electrostatic actuation to control multiple axes of movement at relatively high speeds. One such design using electrostatic actuation to directly control mirror positioning is shown in Figure 2.11. Unfortunately, this sort of control typically requires relatively large voltages to actuate (which must be maintained to hold those positions), but also provides severe limitations in the maximum achievable deflection.

Still, this sort of design can capitalize on existing micro-mirror formation techniques (as opposed to developing a method of integrating a lens with a MEMS structure) while providing a fast response time. This geometry also hints to the possibility of providing a single device to make small adjustments not only to tilt, but also pis-

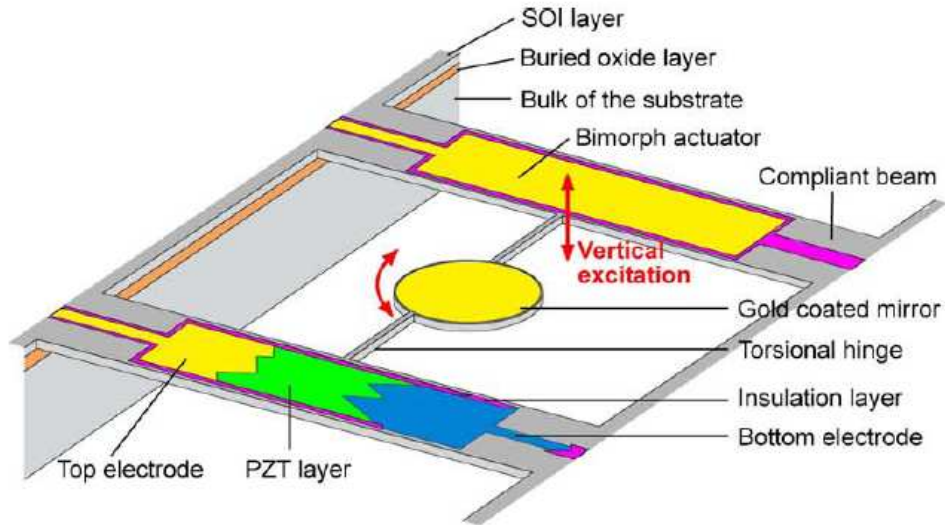


Figure 2.10: Schematic showing a micro-mirror controlled by a piezoelectric bimorph actuator [25]

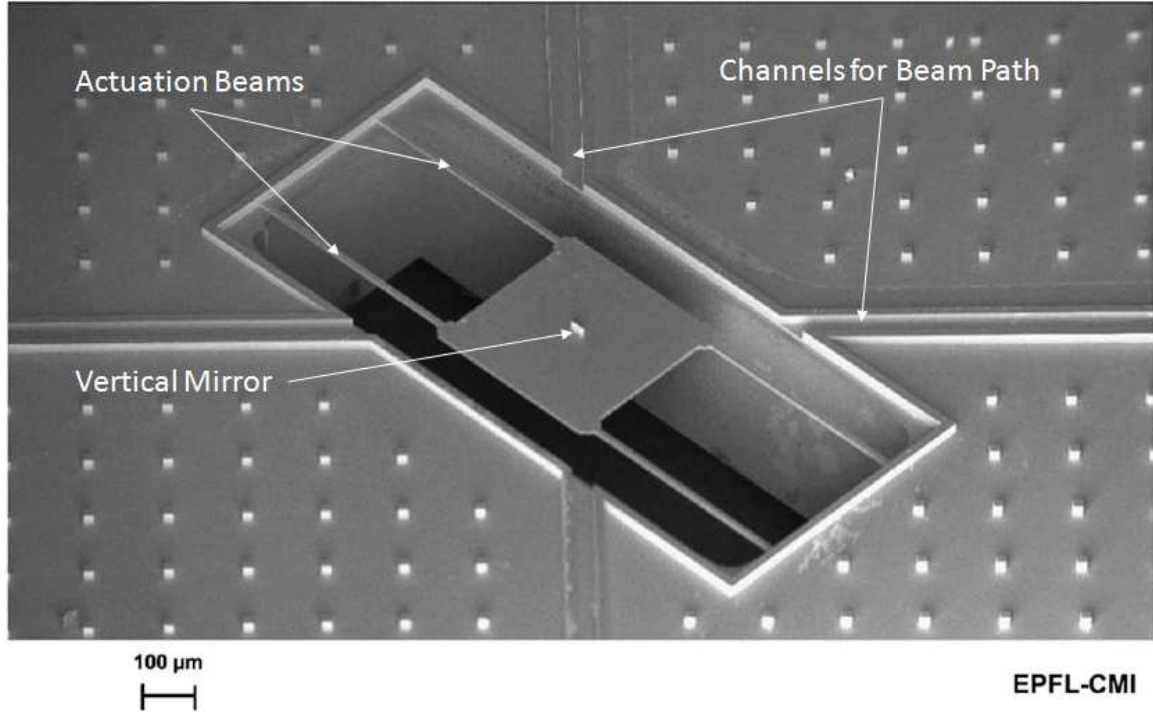


Figure 2.11: SEM image of a four beam electrostatically actuated platform holding a 25 micron tall vertical mirror [20]

toning [26] with the addition of the third axis of control simply with offset actuation surfaces as shown in Figure 2.12.

Depending upon the relative spacing of the top and bottom electrode arrays, as well as the area which captures the rotating mirror, all four electrodes could be controlled in unison to provide not only the tilt mentioned above, but potentially also lift or lower the entire mirror. If the mirror attached is flat, this would provide for subtle changes to path length or if it had some small curvature, this could provide for small focus adjustments based on overall beam path geometry. The ability to design such a structure however requires precise control of layer thicknesses and offsets not currently available for this project. Although, provided more sophisticated fabrication techniques were available, this design does potentially provide some promise.

*2.3.3 Electrothermal Actuation.* An alternate method of actuating a MEMS scale mirror which appears often in research is called thermal actuation. By sending

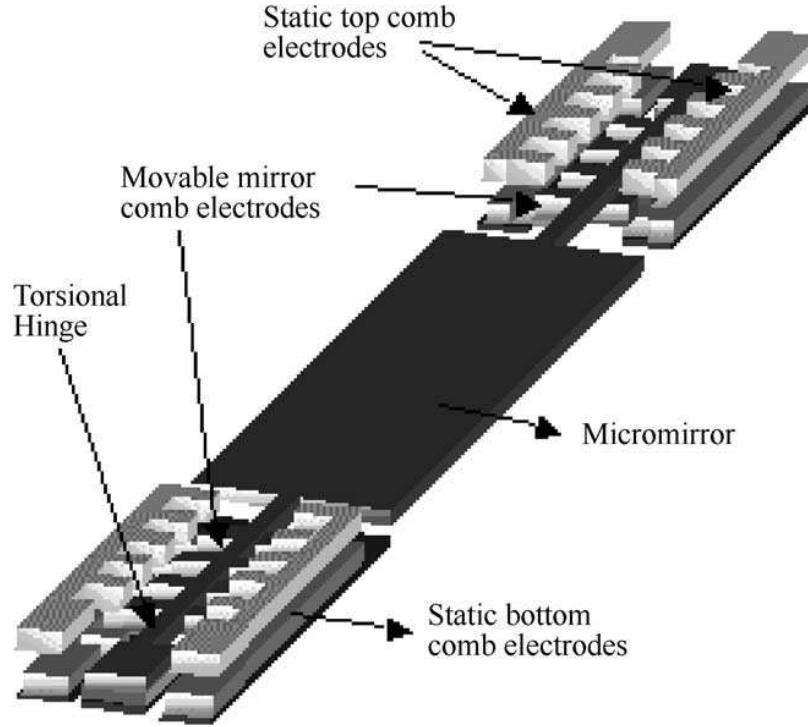


Figure 2.12: Tilting mirror used in phased array assembly [26]

a current through a MEMS structure composed of cross sections of different areas (or through materials with different coefficients of expansion, also known as Bimorph actuation as shown in Figure 2.13), different regions will be forced to carry different amounts of current based on their relative volumes and conductivities.

As the power generated through a resistor is a function of this common current but different resistances, different amounts of heat are generated in the two arms. Depending on their relative heat capacities they will experience different changes in temperature. Based on the coefficients of thermal expansion for each region, their volumes will change by different amounts. This phenomenon can be used to cause motion in a specific direction or manner. The way in which current is directed to the actuator can also be buried as in the structure as illustrated in Figure 2.14.

Here, embedded circuit carrying paths and actuators independently control a portion of the design and its angle relative to the rest of the structure [13]. Both the mirror and outermost ring in Figure 2.14 are moved by actuator 2 (labeled Act2) while



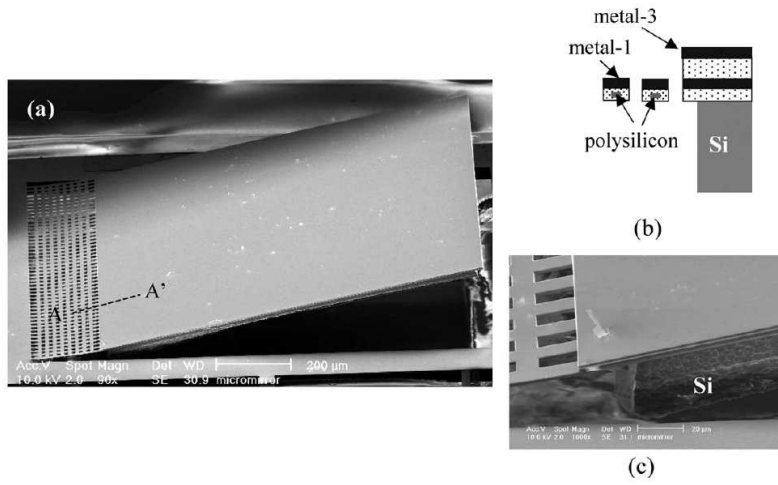


Figure 2.13: SEM images of a released mirror using a combination of dissimilar material stresses with thermal expansion as actuation, (a) wide view of overall structure, (b) cross sectional diagram showing the internal joint structure and (c) close-up of a corner of the structure [18]

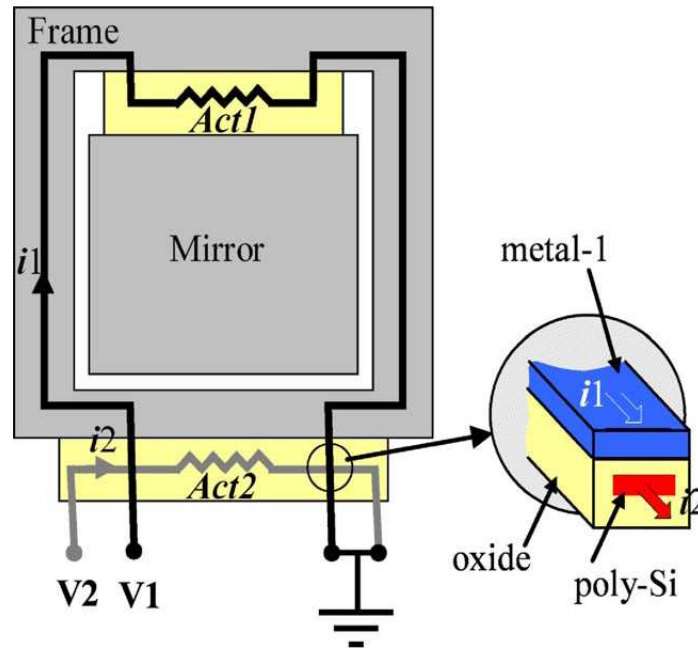


Figure 2.14: Another view of structure from Figure 2.3, multiple imbedded ring structure of 2 axis mirror allow for independent actuation of each loop and the thermal actuator it controls [13]

the mirror is then redirected by actuator 1 (labeled Act1). Signals for these actuators are carried by polysilicon layers embedded within an oxide, insulating each region. This provides for a relatively simple design which accomplishes a wide range of motion in a very compact area with a relatively fast response time. Like the previous case, this would also require continuous current to maintain the temperatures needed to hold any given position and for long-term operation may result in issues with uniform cooling (as relaxing any of these actuators requires the heat to be dissipated and that dissipation rate is dependent on the ambient temperature surrounding the device). Thermal actuators also typically require less voltage to actuate than electrostatic actuators.

As with the staggered resonator design, the limitations of processes available would prohibit the use of these embedded lines of conducting polysilicon for current directing, as several layers would be required to trap polysilicon within oxide. While the details of why this design is not currently available will be held until Chapter III, suffice to say that several depositions would be required beyond what is currently available to have an oxide remain in a structure such as this. Portions of this method (a single-axis mirror actuation for example) would be possible and will be considered.

## ***2.4 Photo-detection***

The final area of consideration is the detection of the beam(s) which not only dictates the structure of the devices below the surface but also the mirrors used to direct light to these detectors. Considering the variety of photon detecting devices available and the pros and cons associated with each, the selection of which to use is not a trivial process and in the end relies heavily upon the signal characteristics and system itself (i.e. data transmission rate, signal to noise ratio, bandwidth(s), optical interference and other physical considerations such as vibrations, temperature variations, etc.) [3]. To fully explore what research has been accomplished which addresses these concerns would be a tremendous undertaking, but to instead bound the problem by reviewing what is considered state of the art and then use that to

limit what the system can then do is a much more feasible approach. To accomplish this task, some of the more critical parameters will be touched on along with some more recent research in those areas.

The first parameter is the type of device to be used. In general, photodetectors and photodiodes are inherently slower devices than phototransistors due to the significant increase in electron mobility which can be engineered into the materials used to make heterojunction devices [3]. As shown in Figure 2.15, a variety of even basic devices exist. Even these basic devices are limited in resolution primarily by lithographic capabilities and electrical isolation between cells. There are intriguing possibilities which in the very near future become realizable based on nano-scale rods of various materials (such as zinc oxide [27] or silicon [28]) capable of photon detection (as shown in Figure 2.16). Current state-of-the-art technology however primarily uses quantum-well-based devices (similar in structure to the quantum wells used to emit light in a VCSEL).

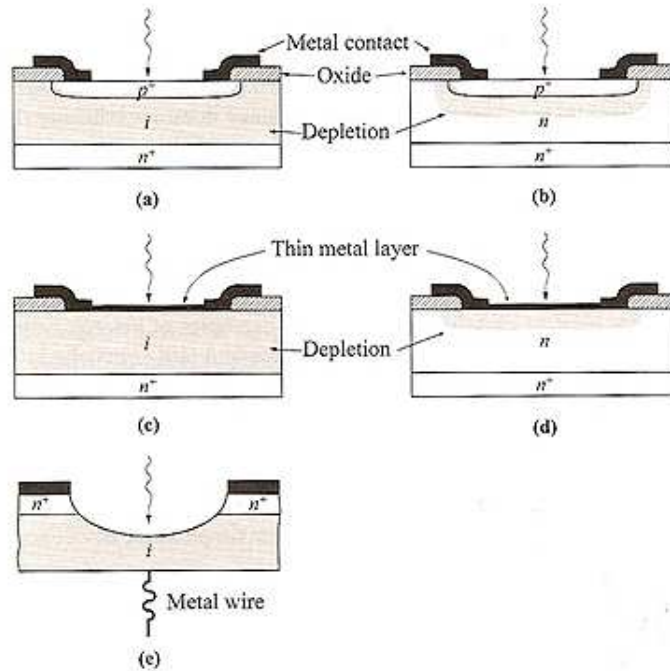


Figure 2.15: High speed photodiodes (a) p-i-n photodiode, (b) p-n photodiode, (c) metal-i-n photodiode, (d) metal-semiconductor photodiode and (e) point-contact photodiode [3]

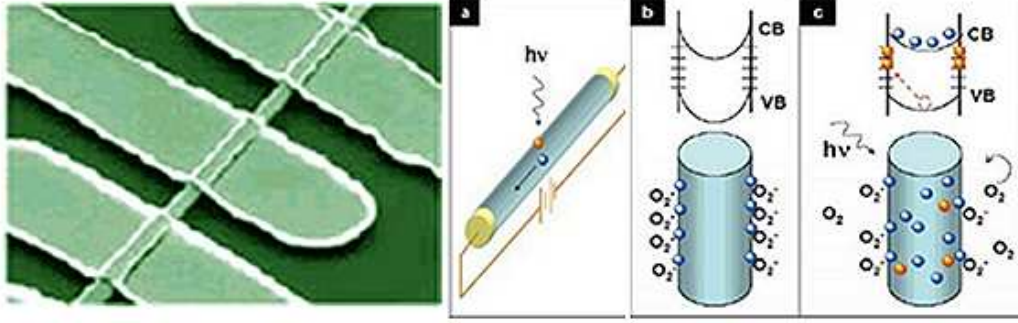


Figure 2.16: Zinc Oxide Nanowire Photodetector [29], drawing of a single nanowire photodetector (a) [30], and schematic of photon trapping with corresponding energy band diagrams (b,c) [31]

An important point to note, however, is that the ability of quantum wells to detect light is usually directly related to the angle of incidence [3]. Unlike photodetectors (and typically any other kind of detector such as nano-rods), light which strikes a series of quantum wells at exactly  $90^\circ$  tends to pass through without any absorption. This phenomenon is due to the fact that electrons displaced within the plane of a quantum well travel easily within that plane, and thus the photon which caused the electron to move in the first place is simply re-emitted. The typical approach to counteract this undesirable effect is shown in Figure 2.17. If the quantum wells are encountered at an angle however, the transverse magnetic (TM) waves will cause out-of-plane displacement and due to the different potentials will hold the electrons and thus cause a photoelectric effect to occur. As this is strictly a question of geometry,  $45^\circ$  is typically considered an ideal. Another approach to overcome this effect is to introduce an array of quantum dots within the quantum well, thus creating localized regions within any one plane of a quantum well which have lower electric potential and thus can still trap electrons effectively [32].

As more materials are used in such devices, the list of possible bands available for communication is continually expanding. If speed is not the primary area of concern however, research focusing on optimization of other areas involved in the photodetection process is currently being explored. For example, a great deal of research is being conducted which still use the quantum-well approach. At terahertz

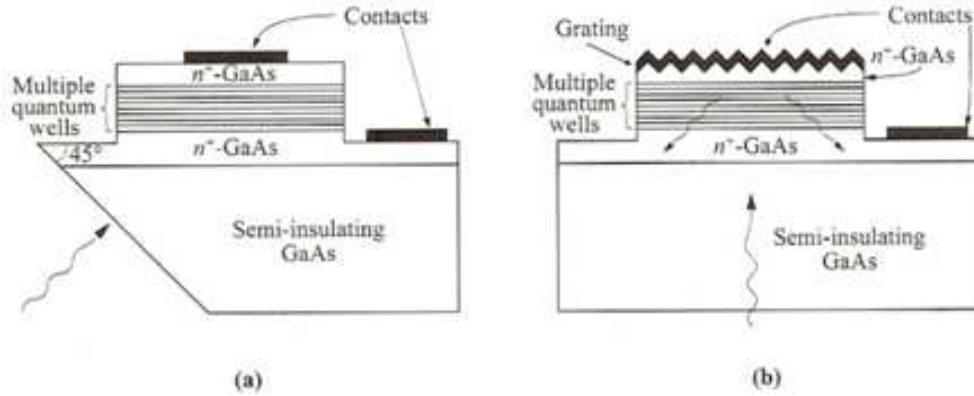


Figure 2.17: Cross section views of GaAs/AlGaAs Quantum Well Infrared Photodetectors showing the two basic approaches to direct light at a usable angle by directing the light at the correct angle (a) and by using a grating to reflect light at the correct angle [3]

frequencies [33] (which are inherently low range signals), this application might be suitable. The infrared spectrum is also a current hot topic in many arenas including ultra-high frequency Quantum Wells Infrared Photodetector (QWIP) [34], ‘multi-color’ infrared detectors (or in other words, breaking down the infrared spectrum into discrete bands) [35] as shown in Figure 2.18, [36,37], integration of infrared-detecting material (GaInAs/InP) onto silicon substrates [38], and near-infrared using metal-semiconductor-metal on a silicon substrate [39]. Within the category of IR detection, more focused research is also being conducted on more specific but equally applicable concerns including low-background-level detection [40], low-temperature dark current consideration [41], and high-speed demodulation considerations [42], just to name a few.

Another important consideration is resolution requirement (i.e. Will a single detecting element sense the entire beam? Will a few detectors detect sectioned parts of the beam or will an array of detectors profile the beam?). The MEMS structures which are to be built and tested will comprise mirrors which are on the order of a few hundred  $\mu\text{m}$  but which are controlled by elements approximately an order of magnitude smaller (based on the resolution of the PolyMUMPs process). Other

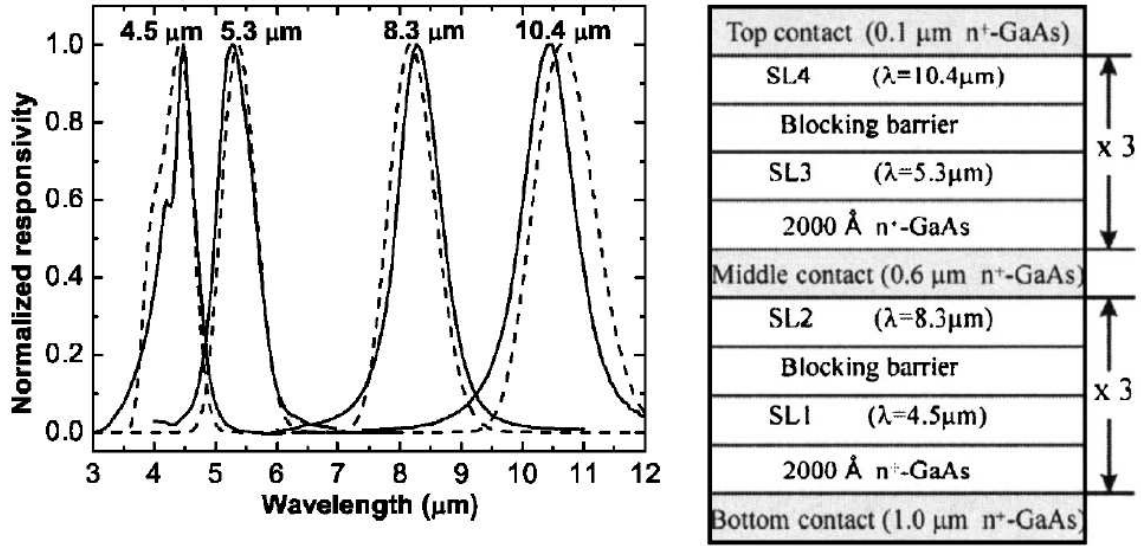


Figure 2.18: Normalized responsivity for four detection bands in a QWIP and corresponding layer structure, including superlattice structures composed of various layered materials, where the top layers are transparent to frequencies detected by lower layers of the structure allowing a single area of a detector the ability to detect multiple bands [37].

processes exist (such as SUMMiT) that can significantly increase this resolution and would then allow for scaled down versions of these structures. For this experiment, mirrors smaller than 100  $\mu\text{m}$  are not practical to attempt to control with any reliability and repeatability. This is orders of magnitude larger than the resolution limits of microelectronic fabrication, so certainly arrays could be constructed if necessary for virtually any of the detection methods mentioned or currently known as the resolution for MEMS devices will always be larger than the electronics they are integrated with. If a more sophisticated approach is taken, it is likely that an array of detectors would be required to accomplish tasks such as characterizing the phase contrast in order to reconstruct an ‘ideal’ signal [43] or reconstruct the wavefront from other algorithmic methods [44].

## 2.5 Applicable Works

In summary, the large variety of works done in the four key areas mentioned above all may play a part in the final design. The driving factor in what approaches

should be taken essentially depend entirely upon how the design is to be used, or more precisely with what devices are the MEMS structure to be integrated with. Once that question is answered for a given application, then the various design concepts, fabrication techniques, integration factors, and control methodologies can be focused in recognizing that for another application other approaches may be more appropriate. For that reason, this project will require a realistic focusing of what will be achievable at this time and using those approaches most likely to succeed even if the superior final design may change dramatically with better tools available.

### III. Theory of Operation

In designing the components which make up this experiment there are several considerations. While the ultimate goal has already been discussed, the immediate goal must fall within additional constraints of available capabilities, materials, and time while still providing the most valuable aspects possible in attaining the end design. As both time and resources are limited, a proof of concept will be the primary goal of this experiment within the capabilities currently available. In Chapter I the overall design outline defined the scope of the MEMS portion of these devices and is presented again in Figure 3.1. The initial designs will attempt to prove that PolyMUMPs can be used to build the basic structures capable of performing these two tasks (directing signals from outside the device to the substrate and directing signals from the substrate in a specific, controllable direction). It is expected however that due to the limitations of PolyMUMPs, additional postprocessing will be needed and will be discussed in more detail in later sections.

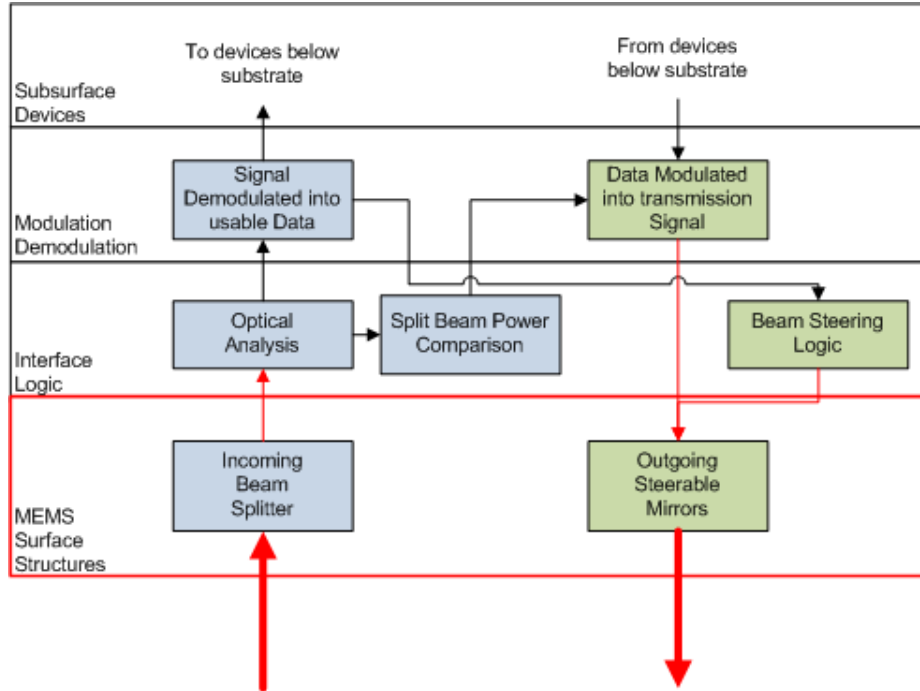


Figure 3.1: Review of the layout of a single working device with MEMS devices outlined in the red box.



This design will be developed with the possibility that eventually no electrical components or signals may be needed. Specifically thermal drives will be used as much as possible for operational actuation as these devices can, in theory be replaced with a photonics-actuated version of the same basic technology. If the assumption is that such chips would operate entirely on photonics, then some elements would for now require an electronic equivalent as these technologies either do not yet exist or are too new to be considered at this time, but at some point in the future these would transition as well. These areas specifically include:

- symmetric ratioing of beam power geometrically
- transferring beam alignment data to outgoing signal
- beam control algorithms from incoming data

As current technology does not yet support these capabilities, approaches which utilize conventional electronics will need to be used and because of this interim measure, some design limitations (such as the minimum beam size producible, data transfer rates, physical control parameters of mirrors, etc.) may also need to be limited. As supporting technology is developed and matures in the future, the design can adapt to better suit the overall objective of using all optical devices.

In order to propose an initial design, fabrication considerations will first need to be discussed in Section 3.1 which merges the immediate capabilities available with a proof of concept design. Once this foundation is layed down, Section 3.2 will then discuss the outgoing and incoming beam paths in two subsections independently leading to a test design which will be fabricated and tested.

### ***3.1 Fabrication Considerations***

The single most important constraint at this point is that all initial testing will occur using the PolyMUMPs process. This foundry process involved repeated masks, depositions and etchings which occur in such a way that predefined patterned layers of doped polysilicon and silicon dioxide are sandwiched together. The final deposition

is patterned gold which allows for a good connection for electrical contacts, and the unreleased structure is then coated in a layer of protected photoresist and delivered to the user. Typically the user will remove the protective layer with acetone then expose the structure to hydrofluoric acid (HF) which removes all exposed silicon dioxide but leaves any exposed polysilicon, nitride, and gold intact thus ‘releasing’ the polysilicon structures designed through careful patterning. Figure 3.2 shows a cross section of the PolyMUMPs process and shows the relative layer positions and thicknesses.

While the final layer of gold is more than adequate for electrical connectivity, the quality is not ideal for good reflectivity and thus any mirror should use an alternate metallic layer deposition through some other means. Additionally, this experiment requires several downward directed mirrors. Considering the way in which these downward mirrors will be designed, this experiment will attempt to suspend a layer of reflective gold directly onto the oxide but within a polysilicon frame. Once this is released and assembled, these devices will use the bottom side of the mirror instead of the top to reflect the optical signal being directed. While there are designs which

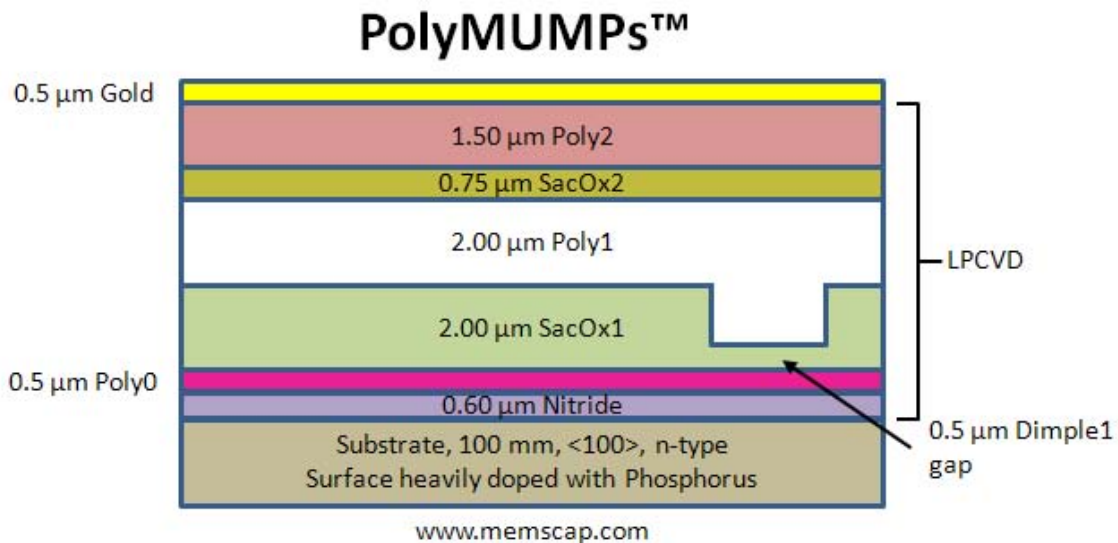


Figure 3.2: Cross section overview of the PolyMUMPs process showing sacrificial oxide (SacOx) locations and thicknesses, polysilicon (Poly) locations and thicknesses and dimple dimension [45].

allow for a topside mirror to be flipped over past  $90^\circ$  to accomplish this, the limited number of releasable layers, the limited resolution, and the available space will prompt that instead, these designs will be attempted using this suspended metal approach. These mirror requirements will then call for post-processing which will be performed and will deposit additional metal(s) prior to release. This will not only provide better reflective layers where needed, but may also help facilitate hinging between otherwise unconnected polysilicon layers by creating a thicker, more rigid hinge.

While PolyMUMPs will be adequate to test initial design concepts, it is likely that at some point in the future, the feasibility of transitioning to some other manufacturing scheme such as the SUMMiT should be addressed. Like PolyMUMPs, this process involves very similar patternings of polysilicon and silicon dioxide, but there are several differences which warrant a brief discussion. A comparable cross-section of the SUMMiT process is provided in Figure 3.3 which even at a glance is considerably more complex.

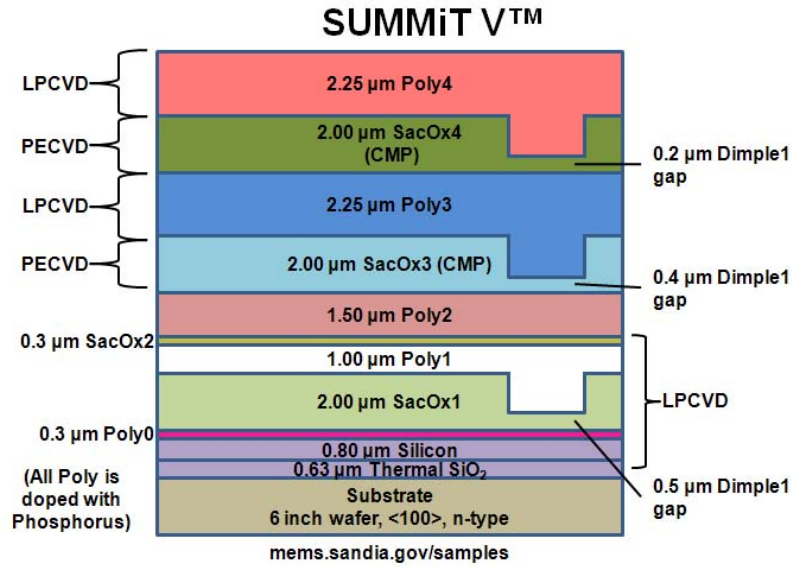


Figure 3.3: Cross-section overview of the SUMMiT process showing sacrificial oxide (SacOx) locations and thicknesses, polysilicon (Poly) locations and thicknesses, low pressure chemical vapor deposition (LPCVD) steps, plasma enhanced chemical vapor deposition steps (PECVD), dimple dimensions and which oxide layers undergo chemical mechanical polishing (CMP) [46].

The first and most notable difference is the addition of two oxide and corresponding polysilicon layers. Having these additional layers available provides for the possibility of significantly more complex designs (such as a hinge structure on a completely movable layer, etc.). While the layout is specifically beneficial for MEMS gearing (such as the ratchet shown in Figure 3.4), the additional layers provided benefits for other applications as well. For example, the top two oxide layers undergo a chemical mechanical polishing which removes any features present due to features of previously deposited layers. Without this polishing, the features of each layer (both silicon and oxide) contribute to the layers above in a conformal manner. With this polishing however, the top layer of polysilicon is extremely flat and any metal deposited on it through a postprocessing step will be a much smoother deposition and better suited for mirror applications. Additionally, the oxides which are deposited through plasma enhanced chemical vapor deposition (PECVD) are of a much higher quality. While this means these oxides then take longer to release, the quality of any metal deposited on them will be increased, and the deposition of polysilicon through patterned openings in this oxide will be more accurate. The etching steps used with SUMMiT ultimately yield  $1\mu\text{m}$  tolerance on most features with alignment tolerance better than  $0.5\mu\text{m}$  [47], compared to PolyMUMPs which requires a minimum of  $2\mu\text{m}$  or more of separation between features for repeatable results.

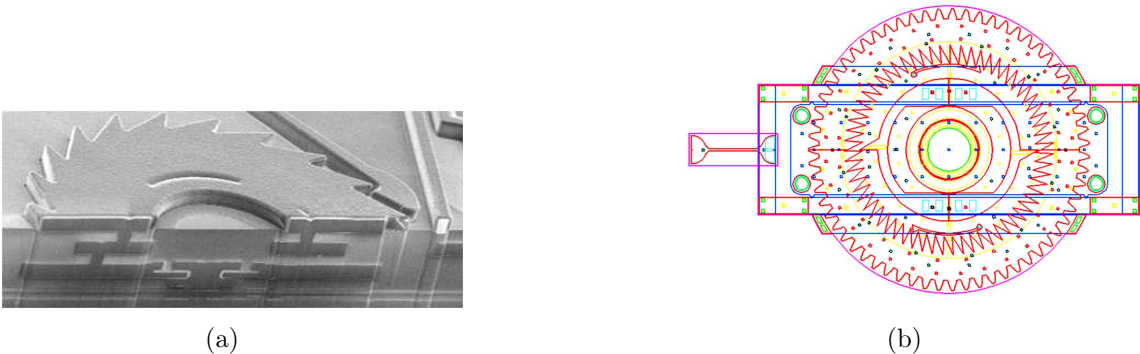


Figure 3.4: a) Focused Ion Beam (FIB) cross-section of double ratchet device fabricated using SUMMiT process [48] and b) example drawing of a premade part from Sandia's device library of a multiple gear arrangement to increase torque or speed [47].

In spite of all the benefits of the SUMMiT process, for initial design testing the expense of such a process is not justified as a single SUMMiT run is significantly more expensive but returns several more devices. When devices manufactured using the SUMMiT process are purchased in quantity however, the price per unit is comparable to PolyMUMPs and the benefits gained more than outweigh the added expense. As SUMMiT comprises additional usable layers of oxide and polysilicon, such a transition would allow for multiple designs to be merged in ways not possible using PolyMUMPs alone and also solve other problems present in PolyMUMPs designs. For example, while an adjustable focal length mirror or a linearly moving stage are both feasible individually using PolyMUMPs, SUMMiT would allow a mirror to be mounted on such a stage simply by designing all the mirror elements one poly level higher and joining the two designs together. This would then add the possibility of an adjustable focus factor to whatever steering mechanism is used and thus accomplish in a single device what would take at least two devices with PolyMUMPs. Another benefit of SUMMiT is illustrated in Figure 3.5 which demonstrates why a minimum of three releasable polysilicon layers are necessary for a floating hinge (which will be of particular interest for this experiment). Also, some designs which may prove problematic with PolyMUMPs may also become feasible with the tighter tolerances, better quality polysilicon depositions, and the non-conformal surface the SUMMiT process provides.

### ***3.2 Overall Design Approach***

In addition to PolyMUMPs, other basic processes are available and will be explored in this experiment. Most significant is the ability to pattern and deposit metal (either by evaporation or sputtering) only in specified areas. While it is also possible to instead uniformly deposit such metals over the entire device and etch the areas where metal is not needed, the metal deposited during the PolyMUMPs process is at risk of being damaged during this process. This could effect electrical conductivity and thus will be avoided if possible. Metals other than gold are available but may pose problems during the release process as most are effected (if not removed entirely)

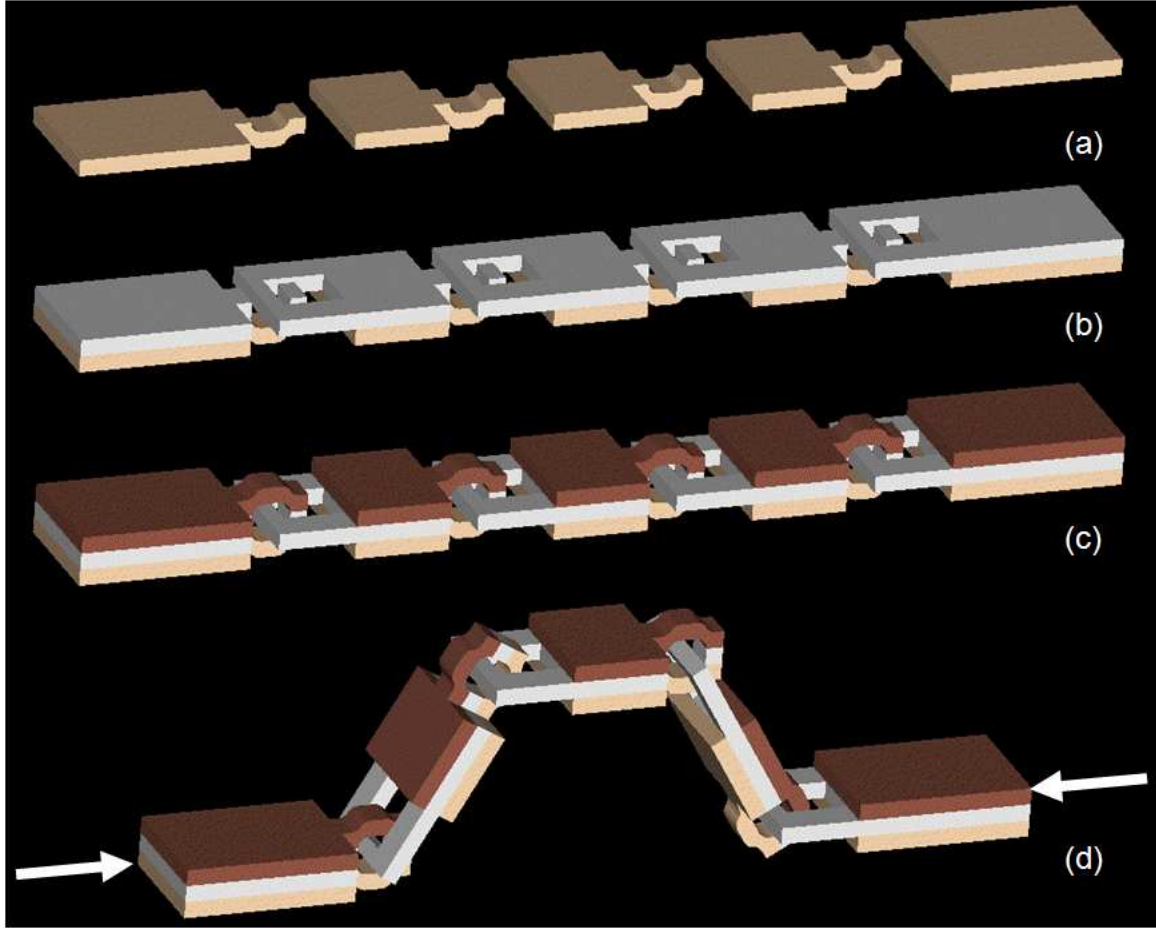


Figure 3.5: Conceptual drawing showing the capability of a hinge built with 3 releasable layers deposited sequentially (a b, and c respectively) and d) bending of the hinge in three dimensions (sacrificial oxide has been omitted from illustration).

by HF. Other materials can be deposited in a similar fashion (in particular a variety of polymers) but in addition to the hydrofluoric acid, the release process requires the use of an organic solvent (typically either isopropyl alcohol or methanol) to prevent polysilicon features from sticking to the substrate, so any material deposited must also survive whatever solvent is to be used as well.

*3.2.1 Incoming Beam Path.* The first and most influential assumption will be that the incoming beam is already at a set height above the substrate, following a path parallel to the substrate and does not experience significant beam spreading over the distances traveled. While it is entirely possible that the transmitting device

cannot achieve this independently, beam steering mirrors would then be need to be added to accomplish this. The mirrors which will be discussed in the next section will accomplish this task. If these are needed for both beam paths, they can be added at a later time. For this stage of the experiment however, this alignment assumption has been made to simplify the design and eliminate duplication of designs that have not yet been proven.

The reception path of such a device could be designed with any level of complexity such that with this added complexity comes greater stability, versatility, and applicability for a variety of application scenarios. On one end of the spectrum, a very simplistic approach could be taken in which a single detector is utilized. The signal received at this detector would be demodulated as normal, but in addition to the data extracted from the signal, the magnitude of the signal is continually monitored. The magnitude of this signal could then feed into an algorithm which directs the transmitting device to vary the beam path slightly and observe if the result is a stronger signal (in which case the new position is assumed to be closer to center) or weaker signal (in which case the change in positioning is undone). This could be repeated until a better signal is received and this process continues constantly in an effort to provide the strongest signal possible. For this kind of a control scheme to work, the corrections would need to be slow enough (relative to the ability to monitor the effect of the change) so that the effect of a single mirror motion can be evaluated before a second correction is made. This sort of a slow feedback would only be feasible to correct constant error or possibly slow variations provided they are occurring much slower than the corrections can be made.

In order to correct for more sudden errors, a slightly more complicated but more effective approach would be to split the incoming beam into a number of individual beams and each of these beams are sent to a single detector. As these would be azimuthally symmetric to the direction of the beam, the individual intensities should be the same at any given time if the beam is centered accurately. Any variation in relative intensities could then be generated in the receiver, embedded in the outgoing

signal and used to determine in which direction the beam needs to be adjusted by the transmitter once it receives this information.

The extreme case would be to direct this beam to a full array of individual detectors which could then reconstruct the full beam profile, provided the array of detectors is larger than the size of the beam (which is reasonable considering the scale of MEMS mirrors are typically on the order of  $100\text{ }\mu\text{m}$  and a single VCSEL can be built which is at least an order of magnitude smaller). This full beam profile should then ideally be centered in the array of photodetectors and could be actively repositioned as it drifts without losing any information in the process. There are also more advanced techniques which could be applied with such arrays that can for example, take the measured profile and compare this to the ‘ideal’ simple Gaussian profile which might be expected by design. Various algorithms could then be applied which infer what kind of aberrations were encountered which could have caused the distortion sensed and correct for it before demodulating the signal and potentially provide a modified signal which produces a better quality beam [43, 44].

As shown in Figure 3.6, the incoming beam path will comprise three basic parts. The first is a  $45^\circ$  mirror which takes a horizontal beam and redirects it directly toward the substrate. Next the beam needs to be split into symmetrical beam paths and third, redirected below the substrate (through holes etched through the backside of the substrate). Figure 3.6 shows two different potential conceptual designs depending upon what kind of photodetector is used. If a detector which can handle perpendicular beam paths (such as a photodiode) is used, then (a) would suffice as the beams which penetrate the substrate do so perpendicular to the substrate. This design would only require an overhead  $45^\circ$  mirror for the first redirection as well as the 4 individual beams. While these could be accomplished using flip-chip bonding (which will be discussed further in Chapter V), this availability would have needed to be identified sooner to have been achievable in this experiment. Other designs have already been presented in Chapter II which demonstrate mirrors such as this could be fabricated and assembled, but these designs would require a tremendous amount of space which



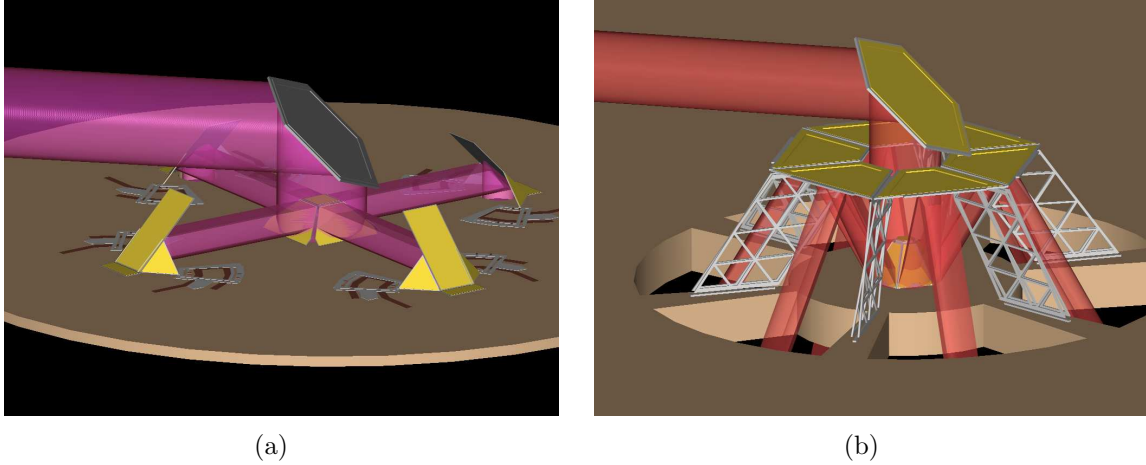


Figure 3.6: Beam splitters for (a)  $90^\circ$  photodiode detection and (b)  $45^\circ$  quantum well detection devices.

also is not practical for this attempt. Instead the bottom side reflection will be attempted along with a fairly complex folding pattern (which will be discussed shortly, but is shown in Figure 3.8).

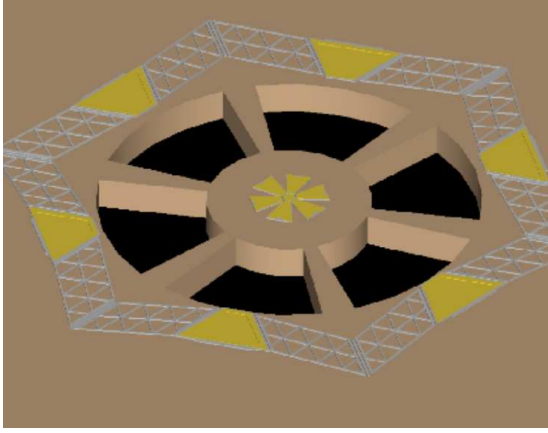
Figure 3.6 (b) shows a similar concept but designed to provide a beam which passes through the substrate at a  $45^\circ$  angle to provide the necessary offset angle needed if a quantum-well type material is used for detection, as the electron displacement caused by a photon passing through most quantum-well materials perpendicularly does not cause a detectable potential change. For these kinds of designs, a rigorous approach could be taken to identify individual structural members in each design, impose what degrees of freedom are allowed from each member to the next, and develop a system of equations which confines the motion of the overall system mathematically. While this rigorous kinematic method is required for systems which involve repetitive movement over a range of values (i.e. designing robotic components) [49] and will be required and discussed in Chapter IV for simulation purposes, designing these systems will be accomplished through a much more straightforward approach. Since the end result is a structure which conforms to specific geometry and more importantly one final resting position, the final structure instead can be modeled using AutoCAD to design the structures in three dimensions. By literally placing the mirror(s) and

supports in three dimensions in the fully assembled position, the structure can then be unfolded to see if it can exist in a flattened state without any overlap. Reassembly can then occur in which intermediate states are evaluated to see if any issues will arise when the model is pushed together.

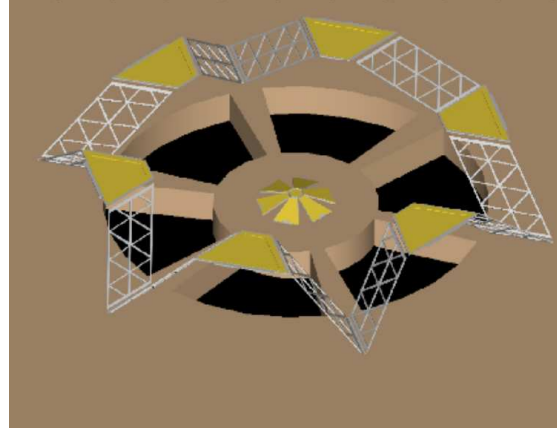
The individual components can thus be shaped to fit and positioned on a single layer the way they would need to appear prior to assembly. The overall change in position and orientation can then be identified for each member and the entire system can be put through a trial assembly in AutoCAD to determine if the range of motion is sufficient for the given design. As the design will contain several geometries which are arbitrary, these can be adjusted to address any conflicts while meeting the geometry targets for final position. The system is then re-examined until a final design is established. Figure 3.7 shows the final conceptual design for the ring mirror structure needed (which corresponds to the overhead mirror ring in Figure 3.6 (b)), but a similar approach will be taken for the 45° overhead mirror which could be used for either of the designs for the two lower pyramid structures.

In order to apply this approach to designs made in PolyMUMPs, the polysilicon used as the skeleton for the structure must be designed in such a way that each piece is the proper size and in the proper orientation relative to each other, but initially supported only by the sacrificial oxides used during the manufacturing process. After the foundry run is complete, the samples will then be masked and patterned and appropriate metals and photoresist will be deposited over the joints and mirror surfaces to attach the rigid polysilicon structures together in such a way that when force is applied, they will have a natural place to fold instead of bending the polysilicon. Scratch drives will be installed at key locations in specific orientations to provide force in the proper direction to induce such folding.

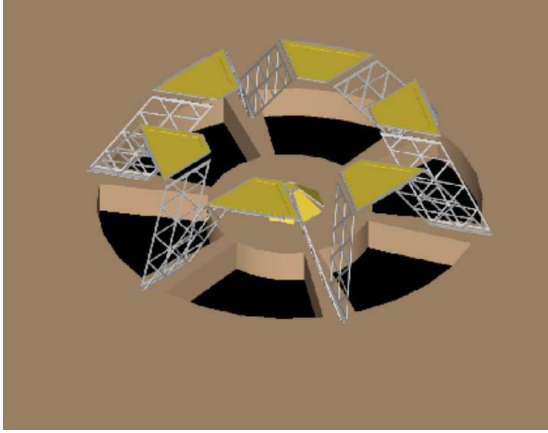
Once fully assembled, the final design will naturally result in two kinds of joints: those which fold upward which will be called valley joints and those which fold downward which will be called mountain joints. Both kinds of hinges will be fabricated



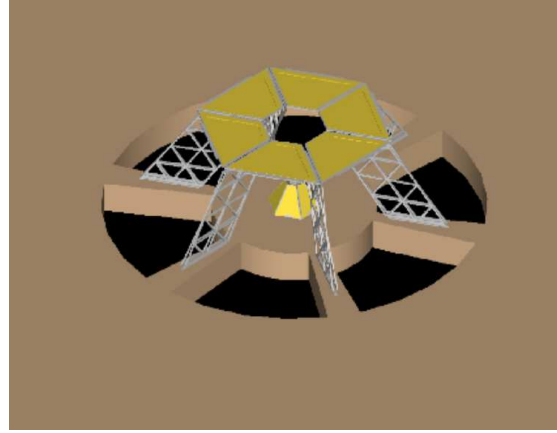
(a)



(b)



(c)



(d)

Figure 3.7: Flat mirror ring structure assembly concept - the bottom surface of each mirror segment will be parallel to substrate at all times, while final position will be determined by geometry of supporting struts.

with empty space between them, but the size of the gap will vary depending upon the geometry of that particular structure, which kind of joint is needed at that location, and the final fully assembled resting angle. Once received, various hinging methods will be attempted by depositing metal and/or photoresist within this gap to attempt to join these polysilicon structures together. Some will be configured such that if the joint has some spring in it (such as the top most joints shown in Figure 3.8 (a)) and thus attempts to return to its original flat position, the tension within the hinge will help to hold the structure together. For these joints, a material should be chosen

such that it provides elastic bending. For other joints however (such as the base joints shown in Figure 3.8 (a)), if the joint attempts to return to its original position, it would actually be detrimental to the rigidity of the overall structure. These joints will require a material which is bent in a more plastic manner and therefore will not feel internal stresses attempting to flatten the structure and return it to its original shape. If a material is used for these joints which can be heated and cooled instead, the geometry will still work, but the rigidity of the cooled joint material will simply help hold the final structure in a stable position.

Where feasible, other structures could be used to help hold the final structure in place (such as support struts, stop posts, etc.). These assemblies also need to be built in such a way that enough translation occurs to place them in the correct positions during assembly or they need actuation capability to move them into position after assembly as shown in Figure 3.8 (b) where the overhead mirror which provides the initial  $90^\circ$  deflection can not be formed directly over the ring so instead it must be formed outside the ring and slid into place. As mentioned previously this will be a challenging, but not necessarily impossible task using PolyMUMPs, but with a more sophisticated and accurate process (such as SUMMiT), it has a much higher chance of success.

*3.2.2 Outgoing Beam Path.* For this application, it is conceivable that once two devices are placed together and beam alignment is achieved through whatever mirror adjustments need to occur, little or no further adjustments may be needed. Because of this, any kind of actuation which requires an input to hold position would not be desirable. By designing intermediate gearing in between the mirrors and their actuation, mirrors can remain stationary in their last working position for indefinite periods of time, but still be actuated as necessary for corrections to position. While many mirror designs could be integrated with geared bases (and therefore include a step-wise adjustment), this would allow for additional levels of potential control and

thus will be mentioned as applicable even though not directly pursuable at this time due to the limitations of the PolyMUMPs process.

The outgoing beam paths serve an entirely different purpose than the incoming structure discussed in the last section and therefore will be considerably different in design. The function of these mirrors is to direct a vertically emitted laser signal from beneath the substrate in a direction dictated by the information received from the other device. If gross misalignment were encountered however, these designs could just as easily be integrated in the incoming path on the other device as well to take a beam which is significantly off-axis but still incident on the receiving device and re-direct it to a more on-axis path. While other beam adjustments may be possible (such as an adjustable focal length mirror integrated with any of the mirrors presented here), the most basic and most influential types of aberrations were addressed in an order which is convenient for the final design, namely: vertical beam misalignment, horizontal beam misalignment, horizontal beam tilt and vertical beam tilt.

*3.2.2.1 Vertical Beam Misalignment.* The first task is to take a beam which has been emitted from a VCSEL (or VCSEL array) through a hole in the substrate and reflect it to a horizontal direction. The height of this reflected beam

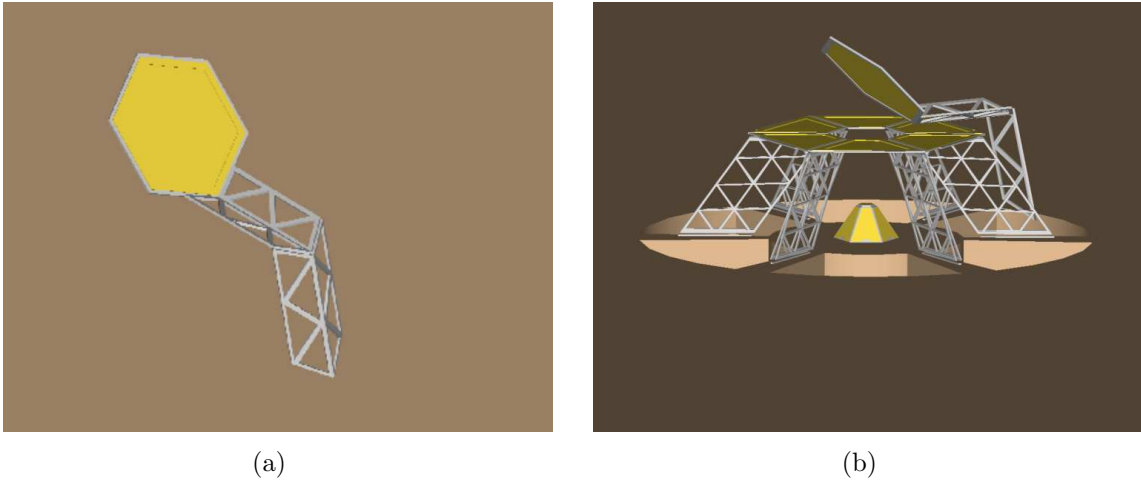


Figure 3.8: (a) Top mirror at correct height and reach with  $45^\circ$  angle to substrate and (b) fully assembled top mirror and beam splitter assembly.

will be directly proportional to the amount of displacement of the mirror as shown in Figure 3.9. While the amount of deflection with a  $45^\circ$  mirror will be equal to the amount of linear displacement of the mirror (which for a MEMS device will be extremely small), the mirrors encountered later can and will amplify this effect. This adjustment may also compensate for errors introduced in manufacturing or for other errors introduced by other mirrors, which will be discussed in more detail in Section 3.2.2.4 when the last mirror is examined more closely.

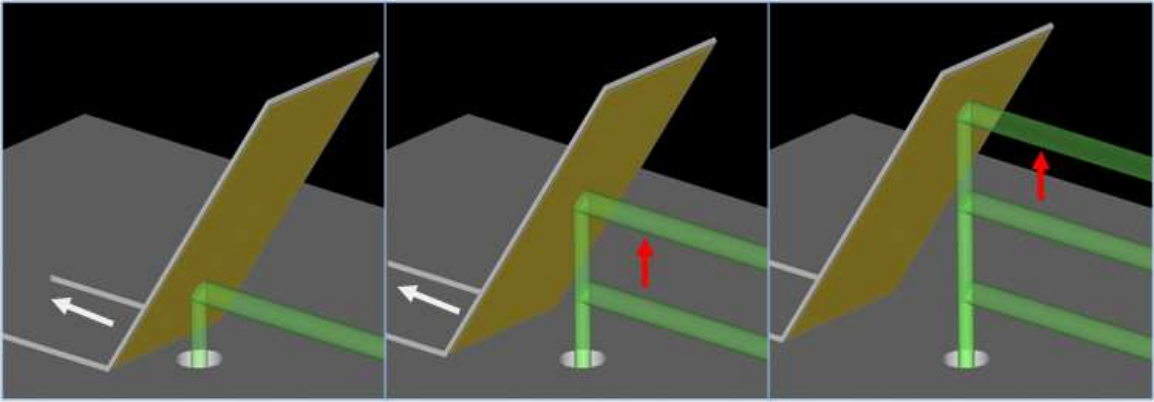


Figure 3.9: Conceptual drawing showing vertical adjustment (of a beam emitted from a VCSEL below the surface) through the translation of a mirror which is raised  $45^\circ$  from the substrate on a slidable base.

*3.2.2.2 Horizontal Beam Misalignment.* Similarly to the first mirror, the horizontal position of the beam can be adjusted using essentially the same concept as the last mirror but with the entire design rotated by  $90^\circ$ . As shown in Figure 3.10 a vertical mirror which is moved along the substrate will accomplish this motion. While the direction of motion could theoretically be in any direction along the substrate and still accomplish this task, moving the mirror in the direction of the incoming beam minimized the size requirement of this mirror as the beam will always hit in approximately the same spot on this mirror regardless of where this mirror is along its path of motion.

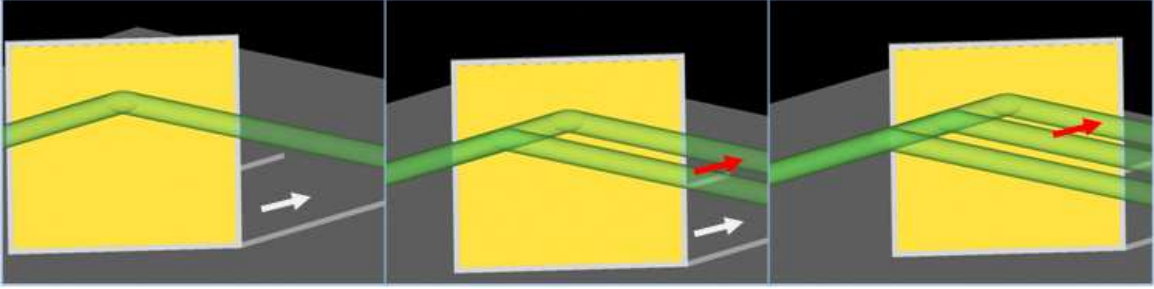


Figure 3.10: Conceptual drawing showing the horizontal adjustment (of a beam emitted horizontally from the previous mirror) through the translation of a mirror which is angled at  $45^\circ$  from the direction of its translation.

*3.2.2.3 Horizontal Beam Tilt.* The third mirror will provide a horizontal tilt to the beam by taking a horizontal mirror (which is  $90^\circ$  to the substrate) and mounting it to half a geared wheel as shown in Figure 3.11 (where the wheel is hidden from view by the mirror). If the mirror is rotated about its center line and the beam is also incident upon this center line, then the only limitation of the angle of rotation is the limit of the gear wheel itself. Contrast this to an off-center incoming beam which would hit farther from the center for more extreme angles, and eventually the mirror could be rotated such that it is completely out of the path of the beam.

*3.2.2.4 Vertical Beam Tilt.* The fourth and final mirror will provide vertical tilt to the beam through a mirror which is attached to hinges on the substrate. Above the substrate are loosely connected supports which are in turn part of a linear

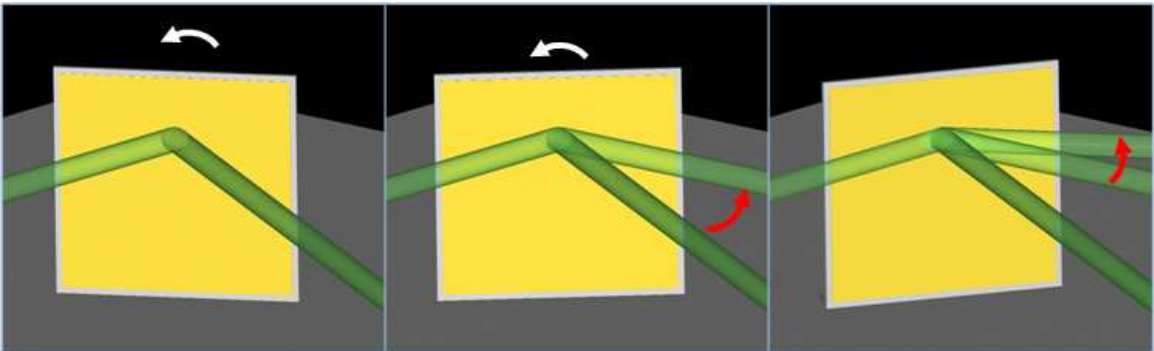


Figure 3.11: Conceptual drawing showing the horizontal rotation (of a beam emitted horizontally from the previous mirror) through the rotation of a vertical mirror attached to a wheel which is mounted on the substrate.

slide (similar to those in the first two mirrors discussed) as shown in Figure 3.12. As the slide is actuated, it alters the mirror's angle to the substrate away from the center position which is  $90^\circ$  based on the geometry of all the elements of the structure. Note that in this case, the beam will not be incident upon the axis of rotation (which by necessity for PolyMUMPs is along the substrate) and as such, there is a limit to the actuation angle beyond which the mirror will no longer be in the path of the incoming beam. Also, because the mirror is tilted out of the plane of the incoming and outgoing beams, the path of reflection would need to be compensated by the three prior mirrors once control algorithms for the mirrors were developed.

All of these mirrors will require an initial assembly step during which time the mirror itself is flipped upward manually into either a  $45^\circ$  or  $90^\circ$  position (depending on its location and purpose in the beam path). Actuation will occur using a method previously explored which uses pairs of thermal actuators ganged together to drive circular gears. These gears will in turn either rotate the mirrors directly (as in the case of the horizontal beam tilt mirror from Figure 3.11) or drive linear racks which then in turn accomplish actuation. The direction of motion is based on the phase of the signals driving the thermal actuators [50] which is not detailed here but will be covered in more detail in Chapter IV. Figure 3.13 shows a snapshot from L-Edit which demonstrates the basic principle used for all the movable mirrors in the initial designs. Using thermal actuator design mechanisms, wheel designs, and contact pads

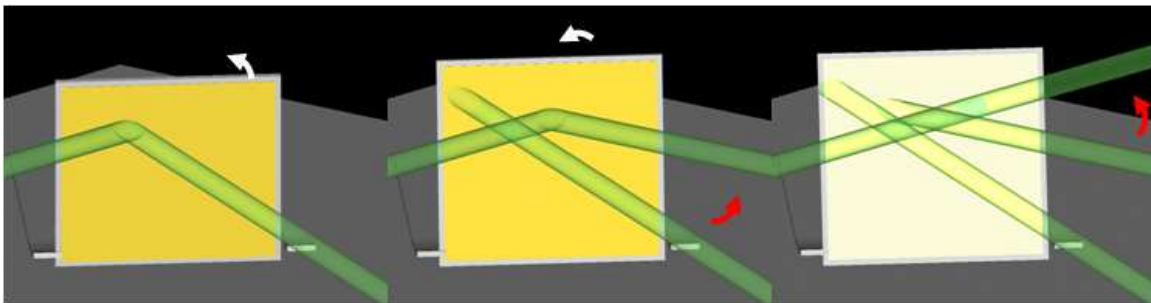
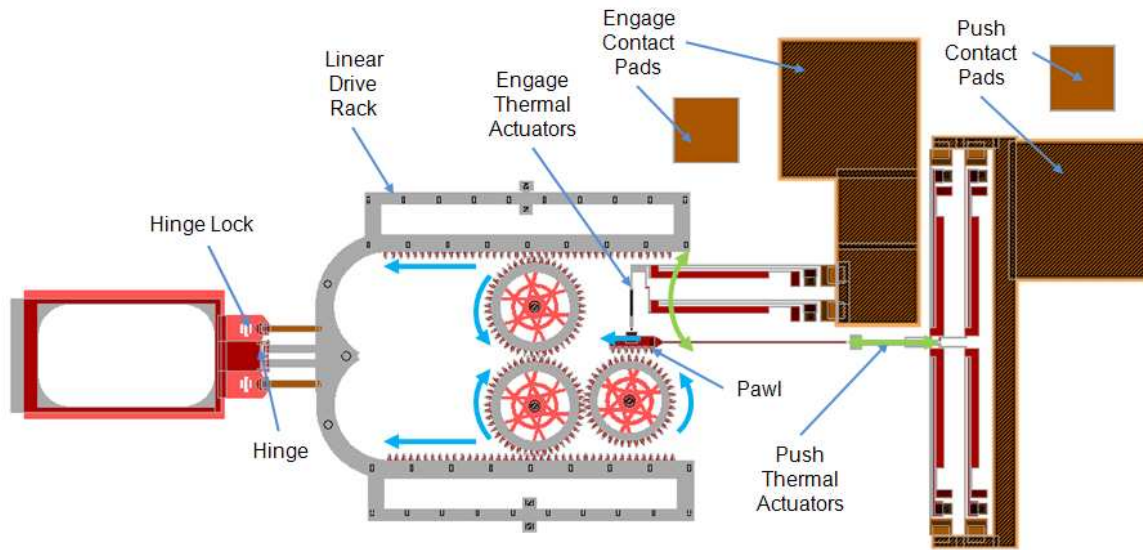
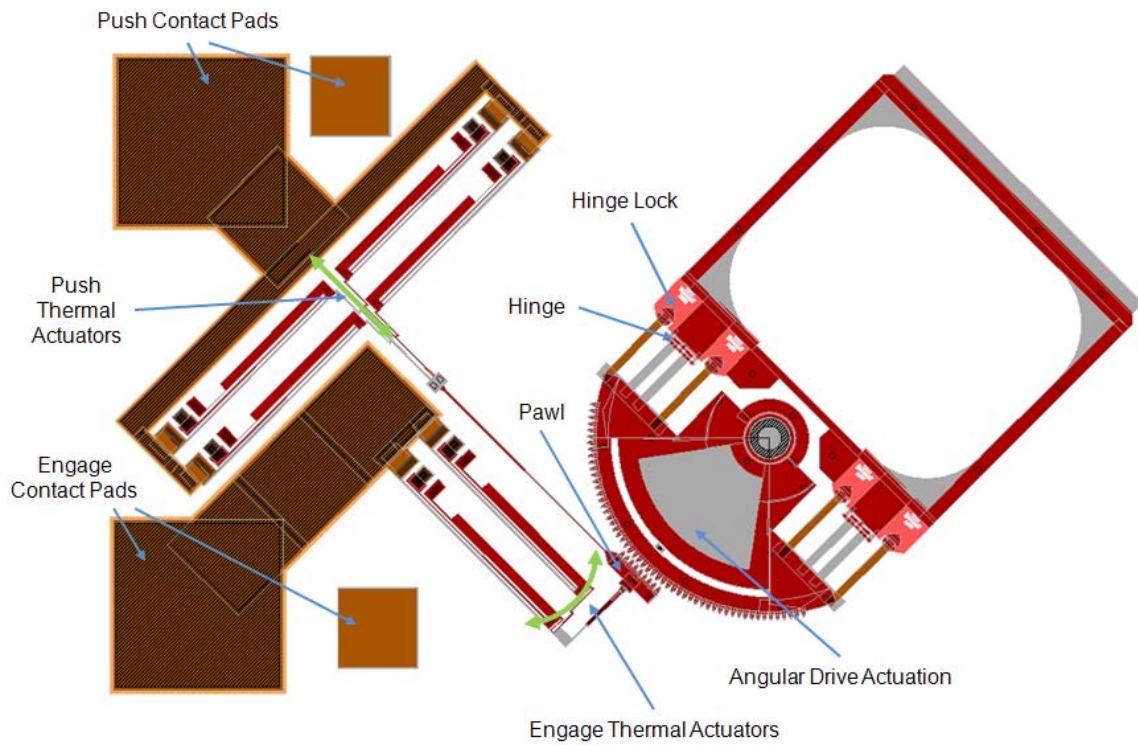


Figure 3.12: Conceptual drawing showing the vertical rotation (of a beam emitted horizontally from the previous mirror) through the tilting of a vertical mirror which is hinged to the substrate but actuated through a linear motion of the support arms.





(a)



(b)

Figure 3.13: Mirrors actuated using common design of thermal actuators a) converting the pawl motion into a linear motion of the rack and b) converting the pawl motion into a rotational motion [50] (green arrows show range of motion for banks of push and engage actuators and blue arrows show relative motion of gearing for actuation in one direction).

from one previous design project [50] and combining this with a catch hinge design and gear rack from another [51], the resulting mirrors will have a high probability of success in being assembled and moved, with the unknowns being not only the backside mirror fabrication process but also slight variations of basic design elements (number and location of thermal arms, single fused arms connecting both banks of thermal actuators to the pawl, geometry of the arms pushing the pawl, etc.).

Considering the end goal of this project, thermal actuation does offer an additional benefit in that an all optical device could in theory be constructed such that optical energy is directed at various parts of the device to cause selective heating and actuation (instead of using current) and would be the most logical direct transition between the electrical and optical versions of the design. Additionally, many of the base structures already existed from a previous project which was accomplished using PolyMUMPs and provided the best chance of success. The project in question was not of direct relevance, as it was oriented toward the development of a safe-and-arm barrier for an exploding initiator [50,52]. While the application is different the theory of operation outlined in Figure 3.14 is the same. Past attempts at this design have proved problematic with the two-member design as shown as the two arms can easily become non-planar, so instead a fused version will be attempted and will be shown in more detail in both Chapter IV and Appendix B. This particular project's working bi-axes, bi-directional thermal actuation scheme was capable of fairly fast movements which drove a stationary rotary stage. This stage could easily be adapted to hold a mirror at a pre-set angle. With minor variations, this design could also be easily modified into a linear slide controllable in the same manner but to provide linear motion in addition to the rotational motion provided by the original design. While the exact speed of these devices will need to be tested, it is conceivable that a combination of both physical beam steering and algorithmic correction could accomplish corrections for both low and high frequency disturbances accordingly.

In an effort to reach the goal presented originally, a single PolyMUMPs design was created to accomplish as many of the key achievable goals as possible. For

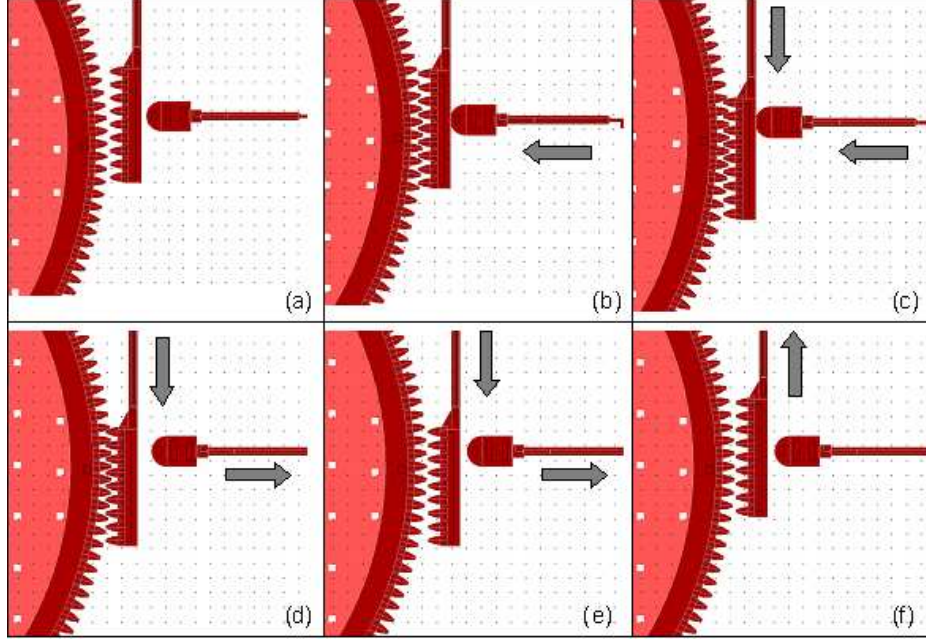


Figure 3.14: Detail of the theory of operation for a pawl drive. a) starting position for both push (vertical) and engage (horizontal) actuators, b) the pawl is pushed into the gear using the engage actuator, c) with the pawl engaged, the push actuator is energized moving the gear by a small amount, d) the engage actuator is de-energized while the push is in motion, e) the relaxation of engage actuator allows the push actuator to disengage from the gear, and f) the push actuator relaxes, returning the pawl to its rest state, then the cycle repeats causing a stepwise motion of the gear (note that reversing the cycle reverses the direction of gear rotation). [52]

the incoming beam path, two  $90^\circ$  designs were included and one  $45^\circ$  (as discussed in Section 3.2.1). For the outgoing beam path mirrors, each of the four types discussed in Section 3.2.2 were included and arranged correctly to provide a working set of mirrors. If an additional step was included, a hole could be made in the substrate at the proper location, and a VCSEL positioned below this hole. This arrangement would then be in the proper assembled position to function as a full outgoing beam path. A complete view of this design is provided in Appendix B and more specifically Figure B.2 shows the arrangement which was fabricated. These fabricated devices were then assembled and tested as much as possible within the capabilities of each device. The successful results of this testing and relevant simulations of other components will be discussed in Chapter IV.

## IV. Simulated Modeling and Test Results

Design and fabrication of these devices using PolyMUMPs was originally going to occur in three production runs over approximately seven months. In order to best utilize these three runs, the first run included variations of some of the basic elements needed for this experiment and was intended to explore the following areas:

- pyramid beam splitters with 30°, 45° and 60° degree sides
- pyramid beam splitters with both solid and framed surfaces
- pyramid beam splitters with minimal top surface
- basic self assembly using scratch drives
- movable mirror actuation using thermal actuators
- movable mirror hinge and hinge locking tests
- bottom side mirror fabrication through metal deposition onto oxide
- polysilicon to polysilicon hinge geometry tests

Following this initial run, the intent was then to make the second run a compilation of those items which worked best from the first run building complete devices but with the intent of further refining of those items from the first run which needed to be readdressed. Finally, the third (and potentially fourth if the schedule worked favorably) run would be a prototype ‘full device’ with one full incoming and outgoing beam path utilizing those technologies most likely to succeed based on the results at that point. Due to unforeseen difficulties from the foundry however, after the first run had already been submitted, all remaining runs were condensed into a single run which was significantly delayed, thereby only allowing one useful attempt at any testable structures and only 15 devices total to test. This forced the second and final run to instead be a compilation of several incoming beam path designs along side a single outgoing beam path which was based primarily on past projects which had the most success, within the space available. Because of this relatively small space, scaling was made as small as possible to fit the necessary devices onto the design

but large enough to be manufacturable. The results of each type of structure will be covered separately, along with a discussion of simulations related to each section as required where actual test results were unattainable.

#### ***4.1 Incoming Beam Path***

Considering most of the previous designs only apply to the outgoing beam path, the incoming beam path is the highest risk to fabricate using PolyMUMPs. Fortunately however, it is also considerably smaller, and thus three different beam splitter designs and two different overhead 45° mirror designs were included. The results of the fabrication of these devices did not yield working devices overall, but the issues encountered will be covered individually and followed up with simulation data which confirms the geometric soundness of the designs for these stationary structures.

*4.1.1 Backside Mirrors.* This design included several mirrors (on both the incoming and outgoing beam paths) which were intended to provide backside reflection by depositing a layer of metal on top of the sacrificial oxide. These mirrors would then be supported by a polysilicon frame after the release process and provide a suitable surface for reflection to occur to and from devices below the substrate. It was soon discovered that metal by itself would not be sufficiently strong to withstand the release process in the thicknesses which could be applied given the equipment available.

Instead, a thin layer of metal was supported by a thicker polymer material. Due to the release process and materials readily available, there were limited options to try in this step. As hydrofluoric acid is used for the release, the only metal which remains reflective is gold. Both evaporation and sputtering resulted in suitable layers of this metal directly onto clean, dry oxide, but extreme care needed to be taken during the cleaning after the lift-off resist process, as the metal is not well attached. To strengthen this thin layer of metal, a backing material needed to then be found. After a typical MEMS release, structures must then be dried using an organic solvent

(typically either methanol or isopropanol) which limits the kinds of polymers that can be used. An attempt was made using a common masking polymer (S-1818) with deionized water as the drying agent, but all the devices released resulted in extreme stiction to the surface due to trapped liquid. The best results resulted from a thin layer of gold (approximately  $0.25\ \mu\text{m}$ ) supported by  $2\ \mu\text{m}$  of SU-8, which is a negative photoresist material cured by ultraviolet light and forms an extremely strong epoxy type material when cured. As shown in Figure 4.1, this material did an excellent job of strengthening the gold it was deposited upon, but did not remain attached to the frame around each mirror.

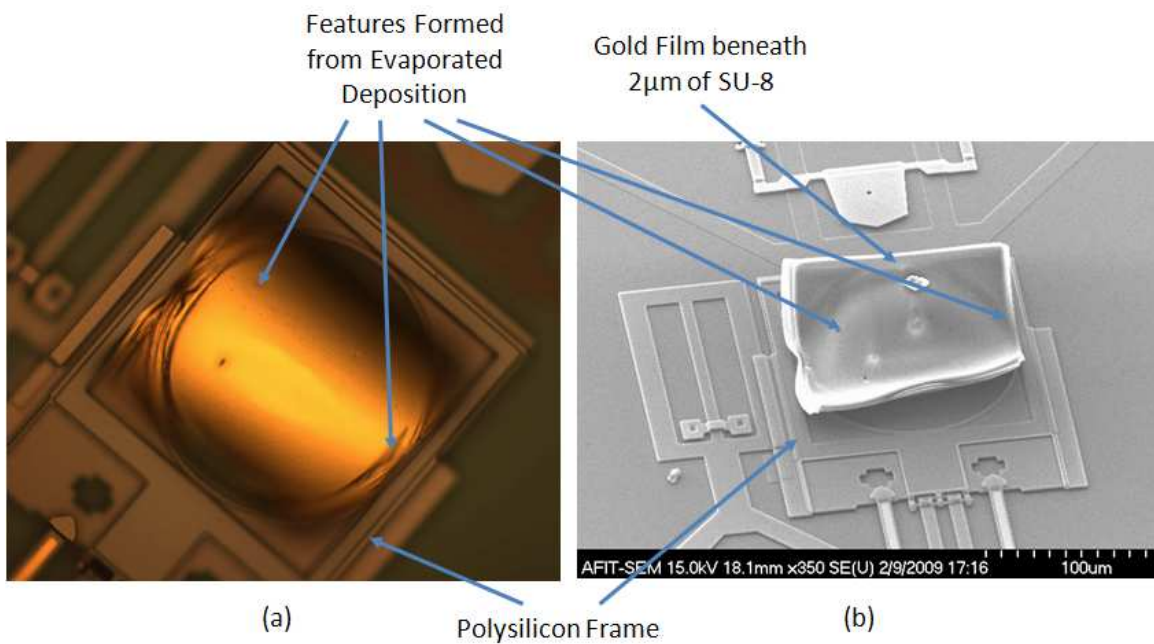


Figure 4.1: A released backside mirror (a) microscope image and (b) SEM using a 2500-Angstroms- thick layer of gold coated with  $2\ \mu\text{m}$  of SU-8, resulting in good adhesion between the metal and polymer but poor attachment of the polymer to the silicon frame.



4.1.2 *45° Overhead Mirrors.* Due to the tight constraints on available surface area, making these structures fit onto the design caused one of the key joints to fuse because of insufficient spacing between the two adjacent layers of polysilicon as shown in Figure 4.2. The left part of this figure shows the designed gap which needs to be a minimum of  $1.5\text{ }\mu\text{m}$  for smaller areas of polysilicon (as was the case with the gears elsewhere in the design) but here was insufficiently spaced, as shown in the SEM images of the devices fabricated on the right.

As the results from these devices were unable to provide any indication regarding the likelihood of success, a simulation was performed in attempt to validate the geometry of the design. Originally a Coventorware simulation was attempted but was unable to provide any results, as the bend in the jointed areas were too extreme to be

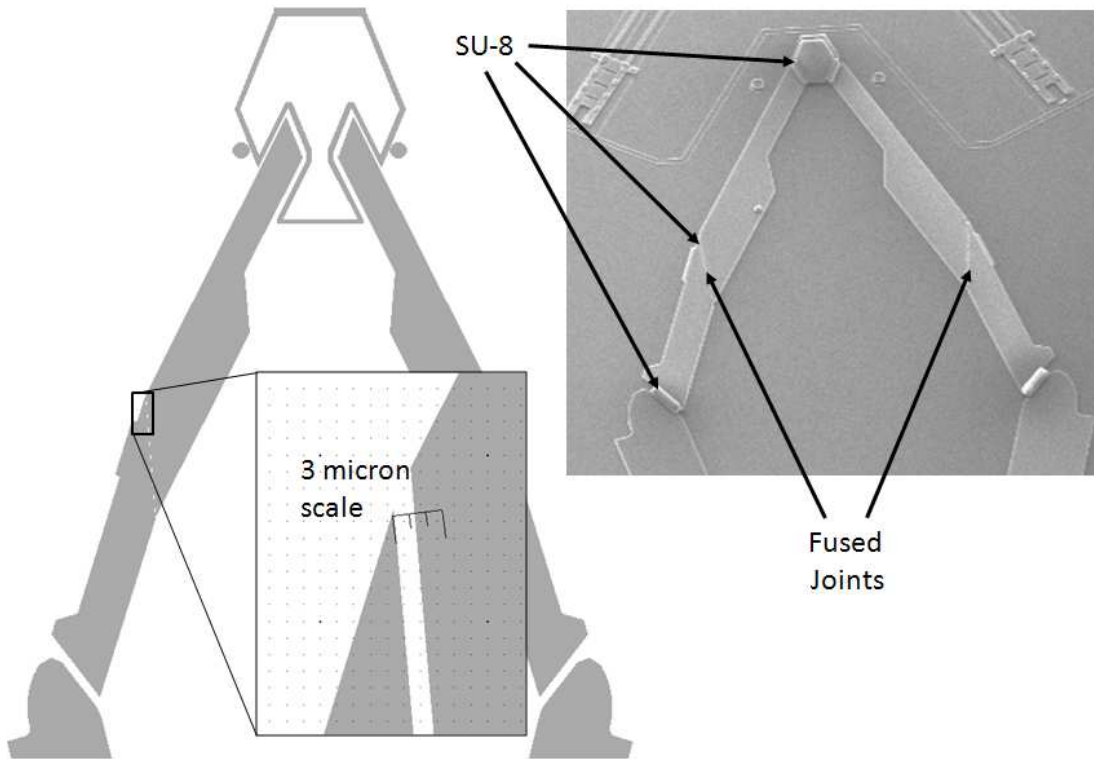


Figure 4.2: Design of  $45^\circ$  overhead mirror showing spacing on fused angle and SEM of resulting device. Discoloration along the fused joint is a result of the deposition of SU-8.

modeled using typical software modeling methods due primarily to excess distortion of the surfaces.

A mathematical solution was then developed using a kinematic method in conjunction with MATLAB to perform the actual calculations of stable angles between the sections of these arms. This approach is fairly involved, and a complete explanation is provided in Appendix A. To briefly summarize this process, a coordinate axis is established on a fixed point on the substrate, and other axes are attached to convenient parts of each moving member. Figure 4.3 shows the definition of the angles used in the development of these equations as well as the location of the fixed frame and other frames attached to each moving member. For clarity, the definitions of each angle are shown on one side while the frames are shown on the other.

The actual calculations were only performed for one side of the structure and then mirrored to the other side, as the assembly should ideally be symmetric. Also

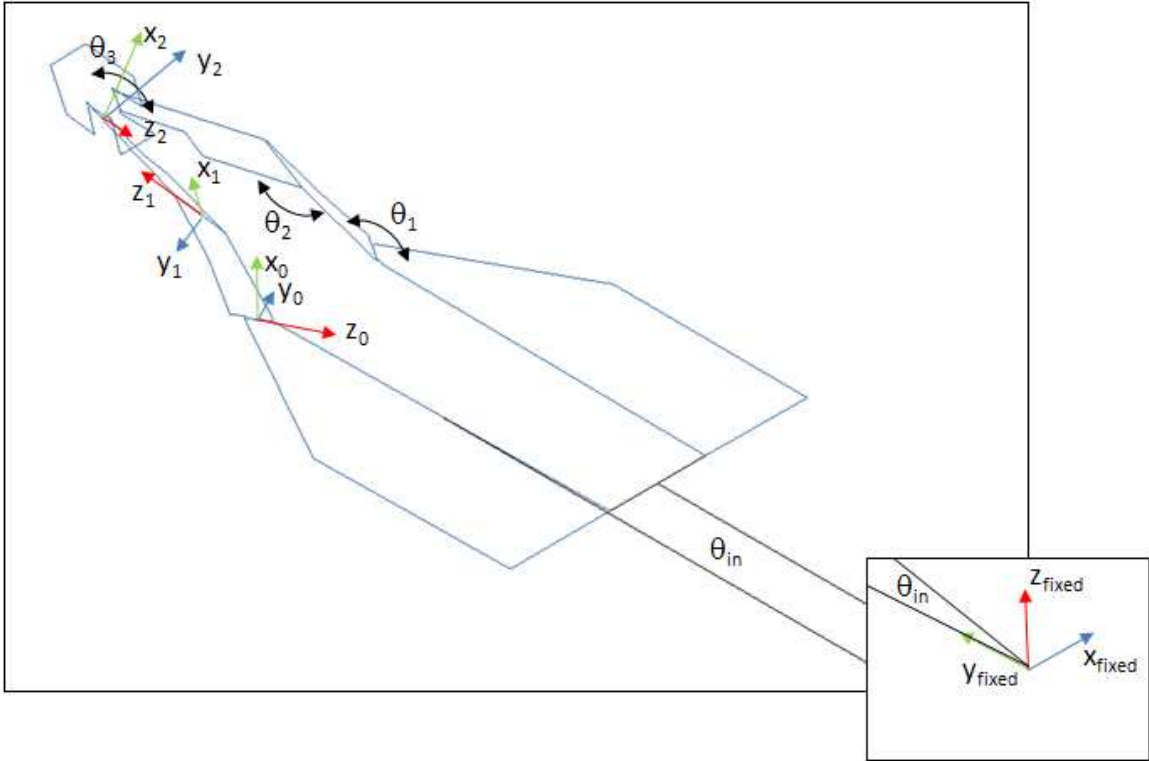


Figure 4.3: Definitions of angles used in equation derivation of overhead 45° mirror with corresponding coordinate frames shown.



note that the choice for each intermediate frame is arbitrary, but in this case, it was selected for convenience such that each z-axis lies along the axis of rotation of each joint and each x-axis lies within the plane of the next member. This allows for each angle to simply be the positive angle of rotation for that frame in around the z-axis.

Now that the reference frames and state variables are defined, four-dimensional transformation matrices can be computed which allow any point or vector in one frame to be directly calculated in another (see Appendix A for more details on the intermediate steps of this derivation). The first of these transformation matrices is found relating position and rotation of the first (fixed) axis to the first movable axis (frame 0) in terms of whatever variables relate the two, in this case just the angle of rotation of the base plate ( $\theta_{in}$ )

$${}_{fixed}^0T = \begin{bmatrix} 0.56c(\alpha) + 0.83s(\alpha) & 0.83c(\alpha) - 0.56s(\alpha) & 0 & -12.22s(\alpha) \\ 0.56s(\alpha) - 0.83c(\alpha) & 0.56c(\alpha) + 0.83s(\alpha) & 0 & 12.22c(\alpha) \\ 0 & 0 & 1 & 0 \\ 0 & 0 & 0 & 1 \end{bmatrix} \quad (4.1)$$

where  $c(\alpha) = \cos(\pi/2 + \theta_{in})$  and  $s(\alpha) = \sin(\pi/2 + \theta_{in})$ .

If this matrix is multiplied by a vector in the fixed frame, the resulting vector will point to the same location in space but will be expressed in terms of frame 0. Conversely, the inverse of this matrix can be used in a similar manner to express vectors in frame 0 in terms of the fixed frame. A second matrix is found relating the first movable axis to the second, and another from the second to the third. As the transformation from one axis to the next includes the angle of the joint at that coordinate frame, each of these matrices contain the angles of the various joints as variables. When multiplied together they allow for any point in one frame to be transformed into the any other frame (regardless of how many intermediate frames they are transformed through), or in other words:

$${}_{fixed}^3T = {}_2^3T {}_1^2T {}_{fixed}^1T. \quad (4.2)$$

Using these transformation matrices, various points on the end mirror were written in the base coordinate frame, specifically the point along the top center of the mirror (point A in Figure 4.4), the point on the bottom center (point B in Figure 4.4) and the point on the bottom left edge (point C in Figure 4.4). Both center points (A and B) will always remain within the  $y - z$  plane of the fixed frame (as the mirror should never tilt as it is assembled) so the equations which express the  $x$  value of these points can be set to zero for all states (each point yielding one equation). Similarly, the height of both the bottom points B and C should always be equal, so the two equations which describe their  $z$  values in the fixed coordinate frame can be set equal to each other, with like terms gathered and simplified, yielding the third needed equation.

These conditions provide the three equations needed to find the three unknowns (namely the angles of each of the three joints which were defined as  $\theta_1$ ,  $\theta_2$ , and  $\theta_3$ , respectively). For any mirror position, there is some angle (called  $\theta_{in}$ ) which defines

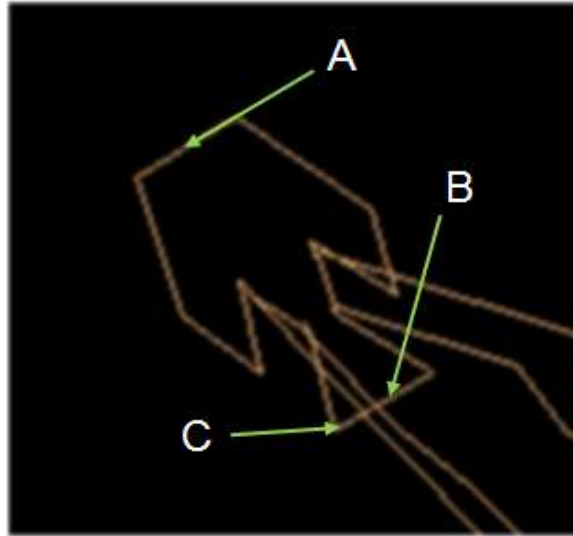


Figure 4.4: Definitions of three key points used in equation derivation of overhead  $45^\circ$  mirror with corresponding coordinate frames shown.

how much the base plates have ‘turned’ to reach that position, but in effect this is not a state variable but rather the input to the system (as the problem could also be viewed as each value of  $\theta_{in}$  results in some unique mirror angle. Using MATLAB’s symbolic mathematical capabilities, these equations were found by this method and simplified considerably. An example of one these equations is:

$$\begin{aligned}
x = & (-4334.8 * \sin(\theta_{in}) - 221.38 * \cos(\theta_{in})) \\
& + (255.85 * \cos(\theta_{in}) - 174.04 * \sin(\theta_{in})) * \cos(\theta_1) \\
& + (32.254 * \cos(\theta_{in}) + 47.415 * \sin(\theta_{in})) * \cos(\theta_2) \\
& - (7.4545 * \cos(\theta_{in}) + 10.959 * \sin(\theta_{in})) * \cos(\theta_3) \\
& + (90.234 * \cos(\theta_{in}) - 61.381 * \sin(\theta_{in})) * \sin(\theta_1) * \sin(\theta_2) \\
& + (15.526 * \cos(\theta_{in}) + 22.824 * \sin(\theta_{in})) * \sin(\theta_2) * \sin(\theta_3) \\
& + (76.772 * \cos(\theta_{in}) - 52.224 * \sin(\theta_{in})) * \cos(\theta_1) * \cos(\theta_2) \\
& + (6.7682 * \cos(\theta_{in}) - 4.6040 * \sin(\theta_{in})) * \cos(\theta_1) * \cos(\theta_3) \\
& + (14.828 * \cos(\theta_{in}) + 21.798 * \sin(\theta_{in})) * \cos(\theta_2) * \cos(\theta_3) \\
& + (35.293 * \cos(\theta_{in}) - 24.008 * \sin(\theta_{in})) * \cos(\theta_1) * \cos(\theta_2) * \cos(\theta_3) \\
& + (36.955 * \cos(\theta_{in}) - 25.139 * \sin(\theta_{in})) * \cos(\theta_1) * \sin(\theta_2) * \sin(\theta_3) \\
& - (43.435 * \cos(\theta_{in}) - 29.547 * \sin(\theta_{in})) * \sin(\theta_1) * \cos(\theta_2) * \sin(\theta_3) \\
& + (41.482 * \cos(\theta_{in}) - 28.218 * \sin(\theta_{in})) * \sin(\theta_1) * \sin(\theta_2) * \cos(\theta_3), \quad (4.3)
\end{aligned}$$

which is the equation that defines the  $x$  coordinate of the top center point on the mirror for any value of these state variables (which is point ‘A’ in Figure 4.4).

Where each of the  $\theta$  values is the current angle of one of the joints as shown above in Figure 4.3. If instead of working with angles, new variables are defined for both the sine and cosine of each angle, this (and the two other corresponding equations which are similar in form) becomes a set of nonlinear algebraic equations which can

be modeled in MATLAB. These equations were verified to produce accurate results when compared to the three dimensional graphical simulation (which will be covered next), however several attempts were made to solve these equations directly, and converging states could not be found unless the initial estimates put into the models were exceedingly close to the the actual solutions. It is possible that, given enough computational power and time, this approach could work, but a more straightforward method was available and used instead. These equations were however still used to verify the results obtained from the graphical method. By measuring the three angles from any given state in the three dimensional model and plugging those values into the equations from Appendix A, the constraints mentioned above were all met within several orders of magnitude verifying the three dimensional model and MATLAB solutions matched.

To prove this kind of a design can be assembled using a graphical simulation, AutoCAD was used as the original devices were already designed in AutoCAD. To accomplish this, some observations were made and used to manipulate the plates in three dimensions. First, it was noted that the end mirror starts at a  $0^\circ$  inclination unassembled and reaches a full  $45^\circ$  in the fully assembled position. If this is to assemble smoothly, then this mirror must move through all the angles between  $0^\circ$  and  $45^\circ$  and, for any arbitrary angle in between these limits, have a stable state. Therefore, any arbitrary angle between  $0^\circ$  and  $45^\circ$  could be selected and the system solved for that angle. First, the flattened model is placed along the substrate as shown in Figure 4.5 (a) (noting that the model is stripped to only half of the design as the other side must remain symmetric). The entire model is then rotated about the red line shown in Figure 4.5 (b) by  $30^\circ$  in this case.

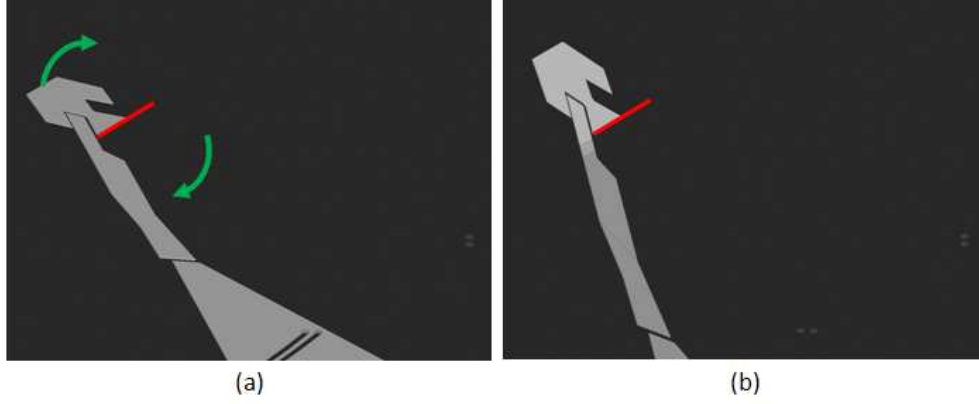


Figure 4.5: CAD drawing of the overhead arm (a) starting position and (b) after rotating mirror and arms into desired angle from substrate. Rotation occurs about the axis defined by the red line in the direction of the green arrows and all pieces are rotated together.

Next, it was observed that the top edge of the next element (indicated by the white arrow in Figure 4.6, (b)) is also perpendicular to the substrate in both the  $0^\circ$  and  $45^\circ$  positions. While it is not intuitive, it was assumed that this also remains true for all angles between  $0^\circ$  and  $45^\circ$  which allows for the determination of the angle between the mirror and this element (indicated by the red line in Figure 4.6, (a) and (b)) for any mirror position.

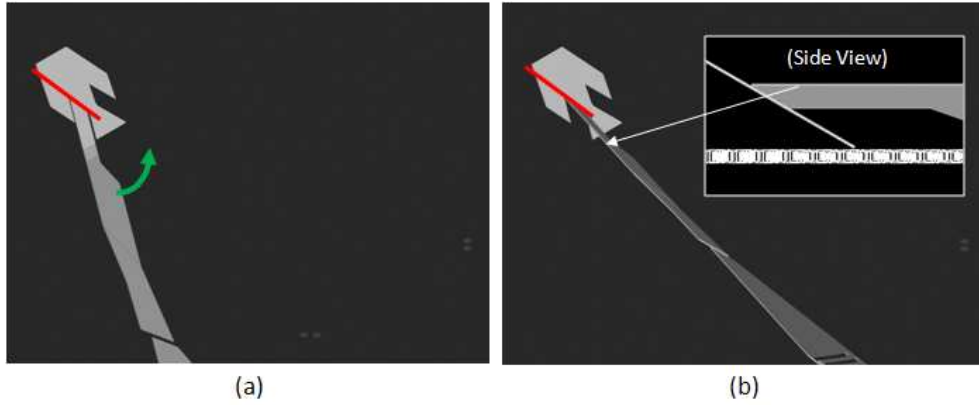


Figure 4.6: CAD drawing of overhead arm from (a) position after last step to (b) angle which brings the top edge of the next member parallel to the substrate. The mirror is fixed for this step, but all other elements are rotated together about axis 3 as though they are joined together.

To find the angle of the next joint, it was observed that the edge on the far end of this member (indicated by the white arrow in Figure 4.7, (b)) must remain flush to the substrate at all times, which is sufficient information to determine the next angle of rotation (along the red line in Figure 4.7, (a) and (b)).

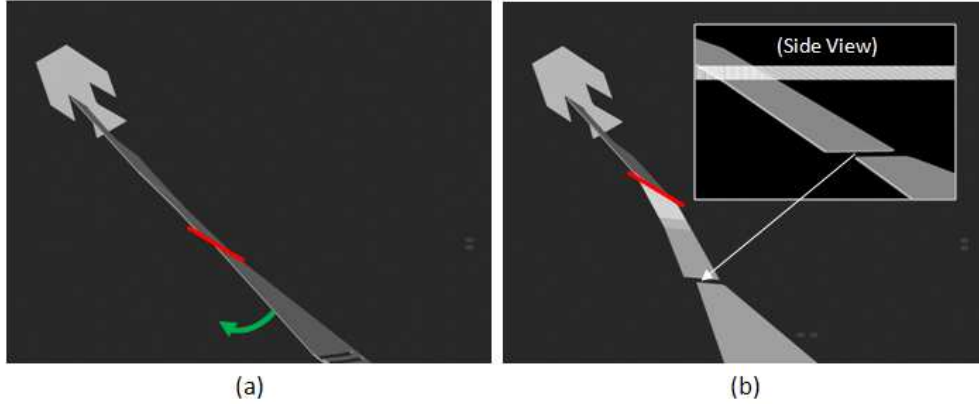


Figure 4.7: CAD drawing of overhead arm (a) before and (b) after third rotation bringing the bottom joint of arm parallel with the substrate. The mirror and top most element are fixed in this case and the bottom arm and base plate are rotated together about axis 2.

Finally, the base plate must be entirely within the plane of the substrate, and since the last joint used is part of that plate and was already brought to a parallel state, this becomes a simple rotation along the red line in Figure 4.8 (a) and (b) to bring the rest of that plate within the same plane.

The entire model is then mirrored and moved together such that the base plate lies on top of the surface of the substrate (to which it is now parallel). The tracks of the mounting posts can then be determined simply by placing posts in a fixed position on the substrate and subtracting the area intercepted for each of these interpolations, effectively sweeping out the material which would be in the way during assembly and joining these individual holes together to form a single smooth track. This process was repeated for every integer angle between  $0^\circ$  and  $45^\circ$  and in all cases, a single set of angles was found to satisfy each end mirror angle. A few intermediate positions were checked against the MATLAB model and matched (using the same process described previously), verifying the solutions produced by AutoCAD represent stable

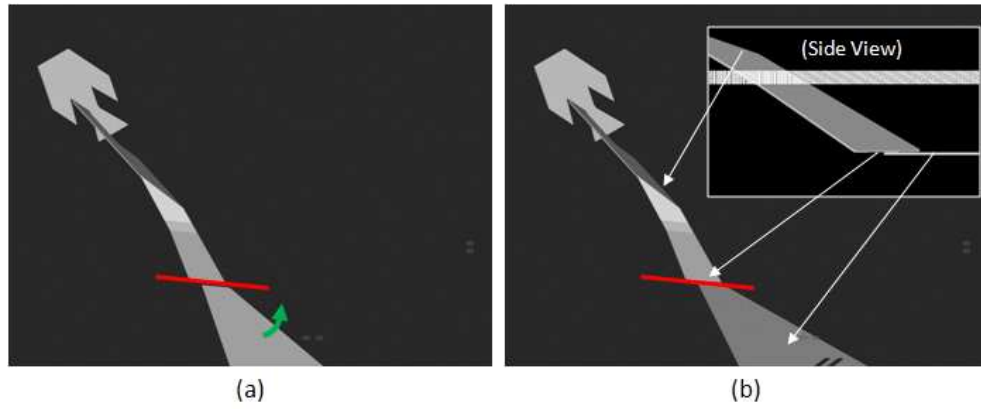


Figure 4.8: CAD drawing of overhead arm (a) before and (b) after fourth rotation bringing bottom plate parallel with the substrate. All members except the base plate are fixed and only the base plate is rotated about axis 1.

states during the assembly process. The net result of these steps are summarized in Figure 4.9 showing  $0^\circ$ ,  $15^\circ$ ,  $30^\circ$  and  $45^\circ$  respectively.

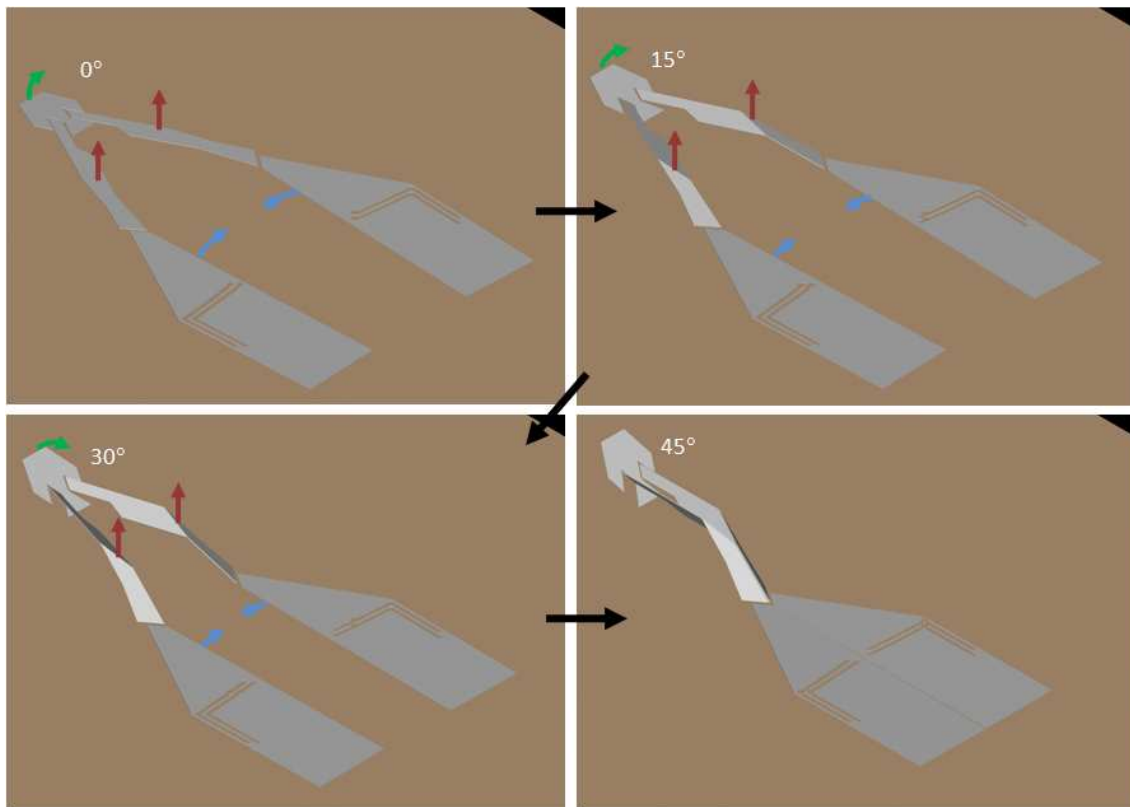


Figure 4.9: Overhead mirror in four positions encountered during assembly process from  $0^\circ$  to  $45^\circ$ .

*4.1.3 Floating Joint Structures.* For a majority of the remaining incoming beam path devices (including mirror rings for QWIP photodetection, pyramid beam splitters (see Figure 4.10) and one of the two  $45^\circ$  surface mounted mirrors), a material and technique needed to be found which would allow for two pieces of polysilicon to be joined together prior to release and later be bent into position and remain fixed after assembly. Several attempts were made at this including dissimilar metals (titanium/gold and aluminum/gold) - both of which were unsuitable due to the effects of HF on titanium and aluminum as well as the limited amount of material which could be deposited as thin layers provided little strength. As was discussed in Section 4.1.2, photoresist and SU-8 were also attempted and for similar reasons unsuccessful, as the SU-8 did not adhere well enough to keep the joints together (as demonstrated in Figure 4.10). Even if the SU-8 had shown better adhesion and had attempts to reflow this material successful, there is no guarantee that this material would have ensured these joint rotated about the intended axis and not simply twisted to conform to whatever stresses each joint was experiencing during the heating process as no form of locks or hinges were possible in this run.

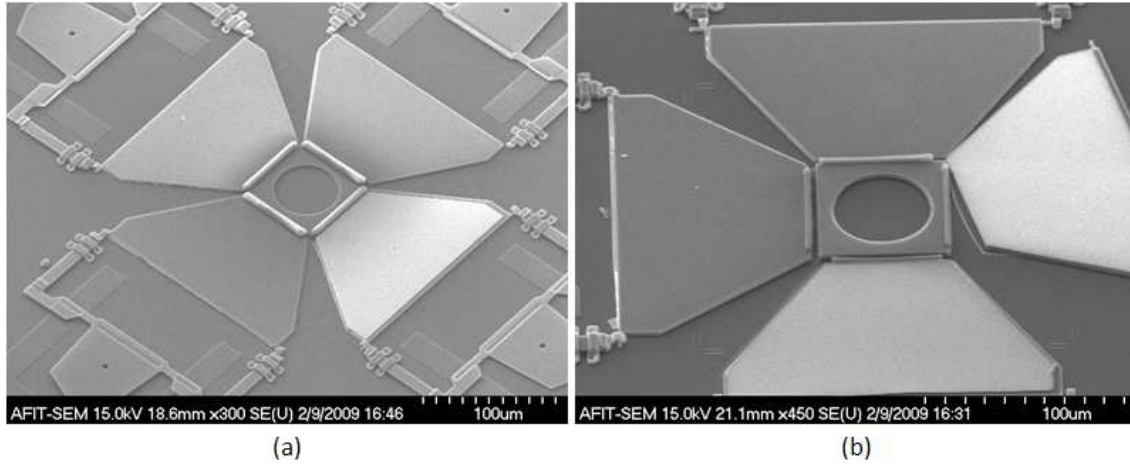


Figure 4.10: Pyramid structure with SU-8 deposited as hinging material (a) before and (b) after heating the material in an attempt to reflow and assemble the device.



## 4.2 *Outgoing Beam Path*

The outgoing beam path components overall were much more successful but did have one design flaw which prevented them from being entirely successful. To cover the results of these devices, first the devices themselves will be presented then broken down into logical subcomponents and discussed in greater detail.

*4.2.1 Beam-Positioning Mirrors.* The first two mirrors in the outgoing beam path are the vertical and horizontal beam positioning mirrors. As shown in a simplified design image in Figure 4.11, these two mirrors are very similar in design. The vertical position mirror (labeled Mirror 1) needs to be angled at  $45^\circ$  relative to the substrate and actuate linearly. The horizontal position mirror is inclined at  $90^\circ$  and also actuated linearly, but the hinges and support arms angle the mirror to reflect the beam in the proper direction, as shown by the green line in Figure 4.11 (b).

*4.2.2 Beam-Tilting Mirrors.* The last two mirrors in the outgoing beam path are the horizontal and vertical beam tilting mirrors, as shown in Figure 4.12. The first of these mirrors is the horizontal tilt mirror (labeled Mirror 3 on the left side of the figure) which is inclined at  $90^\circ$  to the substrate but fixed to a wheel which can be rotated. The beam is then directed to the vertical tilt mirror (labeled Mirror 4 on the right) which has both fixed connections to the substrate and movable connections to a linear actuator similar to those used for the first two mirrors. The net effect of these two mirrors is the ability to steer both horizontally and vertically.

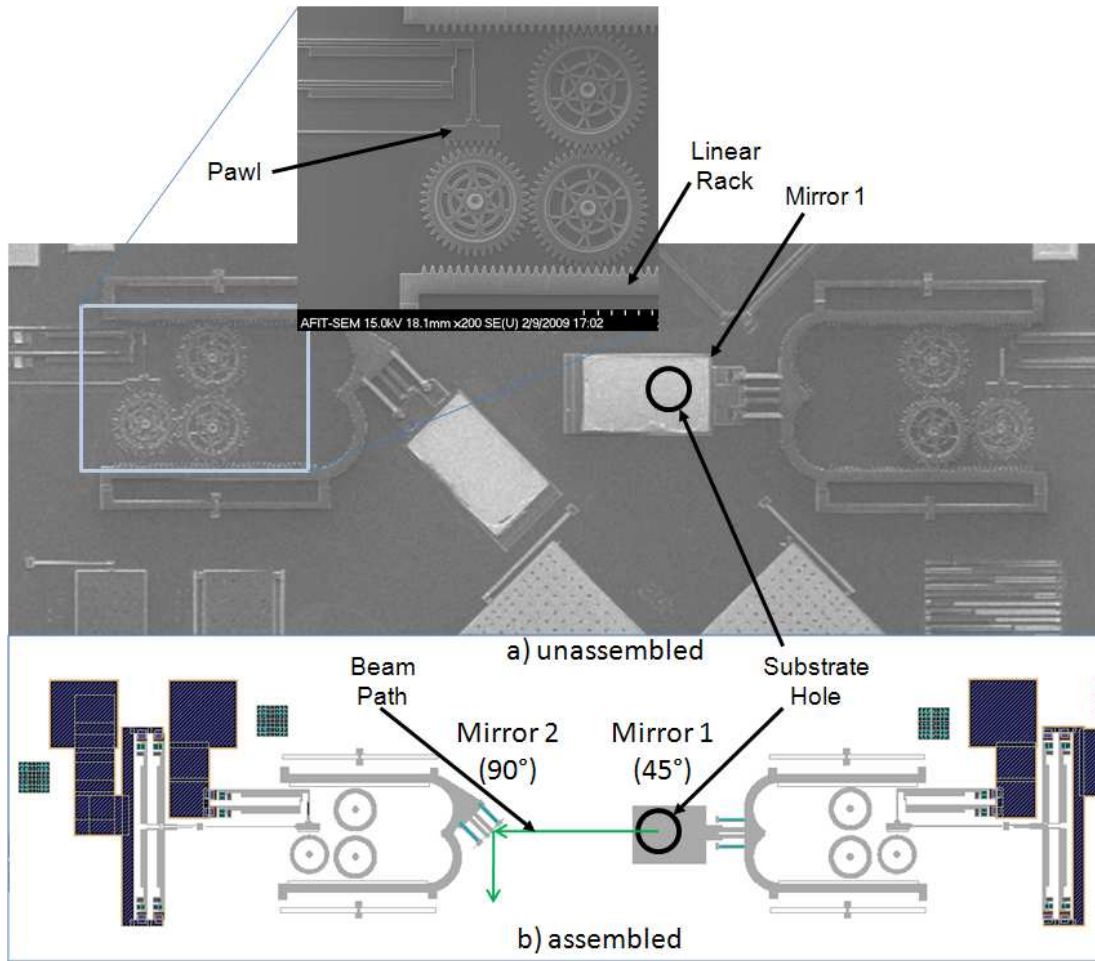


Figure 4.11: Beam position mirrors (a) unassembled and (b) assembled. The beam is emitted through the circle under the right mirror, strikes Mirror 1 which adjusts its height above the substrate and is directed to Mirror 2 which adjusts its horizontal position through the use of linear slides detailed top center.

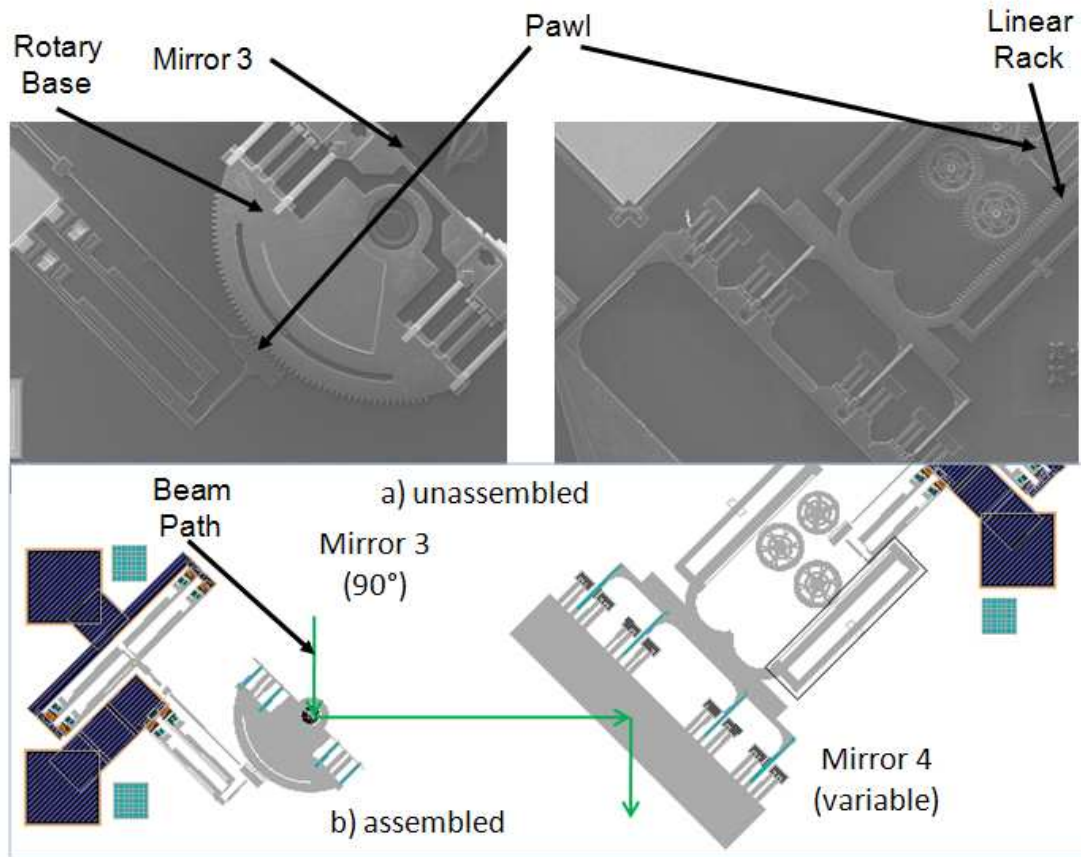
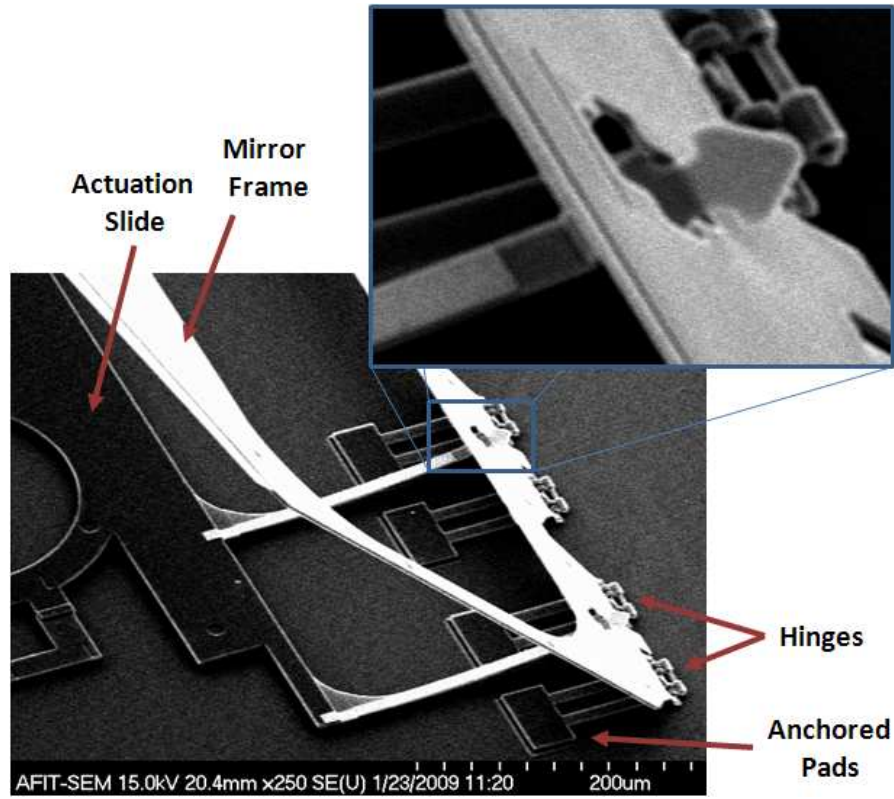
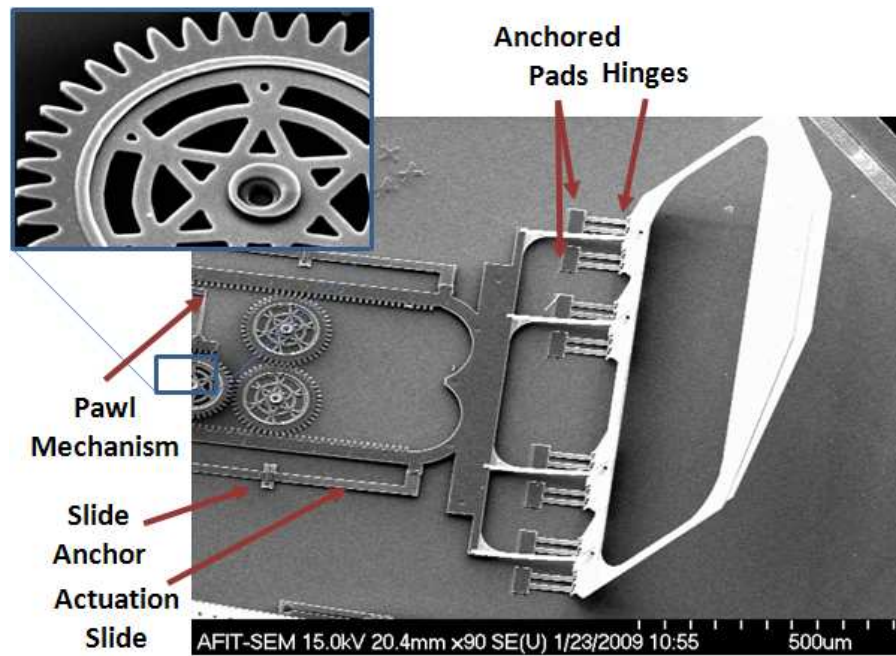


Figure 4.12: Beam-tilting mirrors in both an (a) unassembled and (b) assembled position. The beam sent from the first two mirrors first strikes Mirror 3 which is a turning mirror mounted directly to a geared platform which alters its angle while keeping the beam parallel to the substrate. Mirror 4 changes the angle of the beam relative to the substrate (and would typically be installed along the edge of the chip to allow for a downward path).

*4.2.3 Mirror Attachments.* The first PolyMUMPs run provided a first attempt at a couple of different methods of angling mirrors relative to the substrate. The best of these designs had features which were nearly releasable, but still too small to release successfully. When their dimensions were increased for the second run, every device which underwent an assembly attempt hinged successfully. The arms which were designed to catch the mirrors on the first run were far too small and instead of sliding up the mirror typically stuck to the mirror frame, bent, and broke. The new arms were widened, lengthened, and plated with gold to induce internal stress and help bend them upward immediately upon release. The result of these changes proved more successful as shown in Figure 4.13 which shows an assembled vertical tilting mirror (Mirror 4).



(a)



(b)

Figure 4.13: SEM images of assembled vertical beam-steering mirror (a) with backward tilt (including detail of one of the four latching arms) (b) the same mirror in a forward position (zoomed out to include detail of sliding actuator).

For the smaller mirrors, only a single set of hinges and two catches were included in the design due to space concerns. This made these mirrors fairly unstable during assembly, in that there is little to prevent the mirrors from tilting to the side as they are being pushed up into place. Additionally the catching arm for the mirror that is only  $45^\circ$  has a slightly enlarged open area to better fit the catch arm through the polysilicon, but was still extremely difficult to assemble indicating this opening may not have been large enough. Figure 4.14 shows the best attempt at assembling one of these smaller mirrors and as can be seen the hinge was broken during the attempt and only one arm made it through the frame.

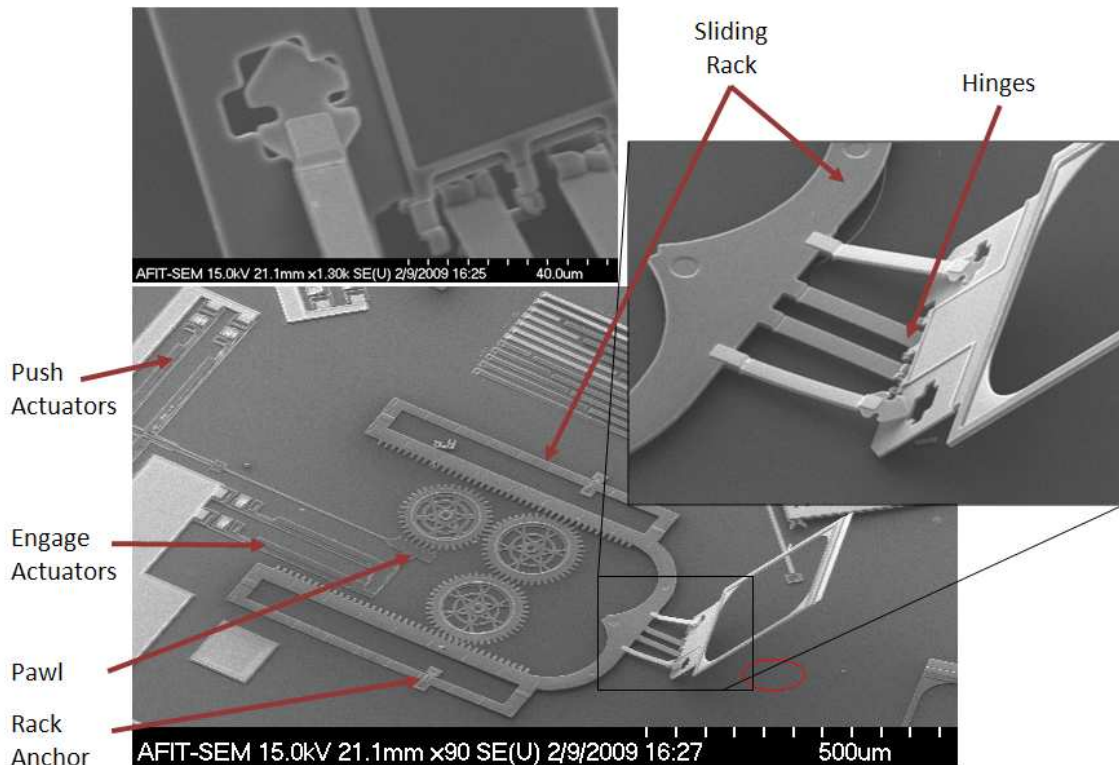


Figure 4.14: Assembled steering mirror (Mirror 1) designed to rest at  $45^\circ$  from the substrate and change the height of a vertical beam coming through the substrate (indicated by the red circle) through linear actuation.

*4.2.4 Thermal Actuation and Pawl Motion.* All four of the mirrors in the outgoing beam path are driven by identical banks of thermal actuators which drive a pawl in a rotational motion. This pawl then is designed to drive a gear with teeth of similar size in either forward or backward direction based on the order in which the push actuators (which drive the pawl forward or back and cause gear rotation) and the engage actuators (which drive the pawl in and out of its engagement position with the gear). This design is based largely on a past project which used identical thermal actuators to move a window over a hole in the substrate [50, 52]. Due to limited available space, this design was modified into a more compact form which introduced three changes, all of which affected the final design much more than anticipated but still resulted in a pawl mechanism capable of the required motion as shown in Figure 3.14.

The first of these changes involves the overall arrangement of the two banks of actuators, where one very long thin section of polysilicon was introduced which actually connected the push actuators to the pawl as shown in Figure 4.15. If the pawl is pushed forward, engaged into the gear and then pulled back this does not affect the design. When operating the mechanism in the other direction however, after pushing the pawl into the gear and then pushing the pawl away from the actuators, the arm is not sufficiently rigid to push the mirrors.

The second change was in the total number of thermal actuators used. In past projects, this has tended to be more than what was required and again, in the interest of saving space, the number was reduced. While the engage actuators only use two actuators, this is more than sufficient to engage and disengage the pawl. The push actuators however were reduced from five pairs of symmetric actuators to two pairs. As the past designs were driving much larger mechanisms than the mirrors present here, it was not anticipated that this would cause any difficulties. When the pawl mechanism is engaged in such a way that the pawl is used to pull the gear (and thus avoid the bending problem already mentioned), two banks of actuators are not capable of moving the gears used in these linear actuators as shown in Figure 4.16.



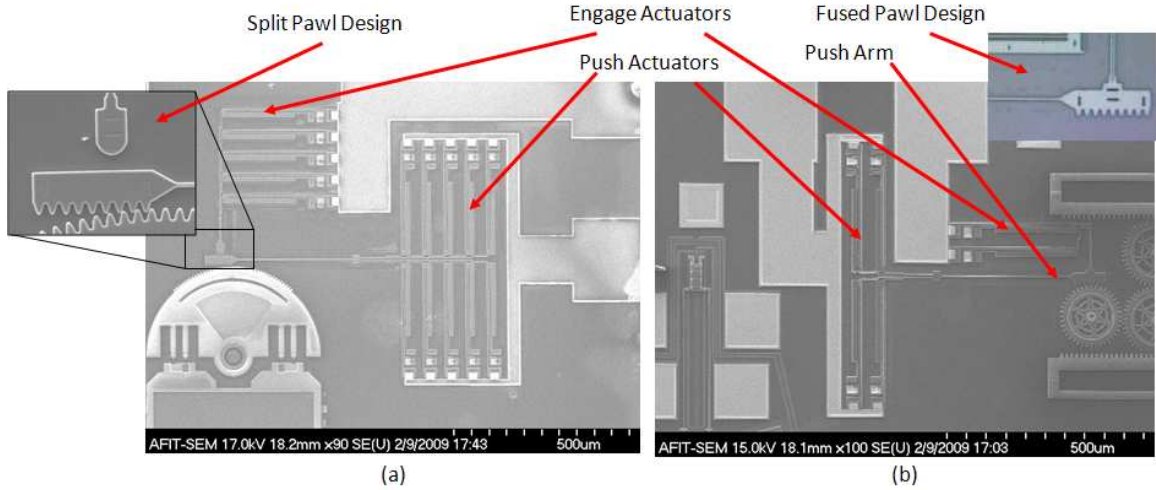


Figure 4.15: Changes in pawl drive mechanism from a) Run 83 with five banks for both the engage and push actuators to b) Run 84 with two banks each.

The third change was a successful one. In past designs, the push actuators connected to the pawl directly but the engage actuators were not physically attached. This had caused problems in that these small polysilicon elements often were no longer coplanar, so even after successful actuation they did not interact with each other as intended. In this design these two were fused which helped keep both arms in the same plane as the gear they were to engage with. In all the devices tested, this was the one part of the gearing mechanism that was never observed to go out of plane (which is a problem that was observed with other parts of the design and will be discussed next).

*4.2.5 Mirror Actuation and Gearing.* The four mirrors in the outgoing beam path share many characteristics in the way they are actuated. Three of the four mirrors are driven by linear actuation of racks and gears which convert the rotational motion of the pawl mechanism into linear motion (as shown in Figure 4.17) while one mirror is rotated directly. As was already mentioned, the pawl mechanism was unable to drive any of the mirrors in either direction (in one direction due to insufficient force and in the other direction because of both insufficient force and bending in the push arm). PolyMUMPs did show a great deal of error in gears (manifested primarily



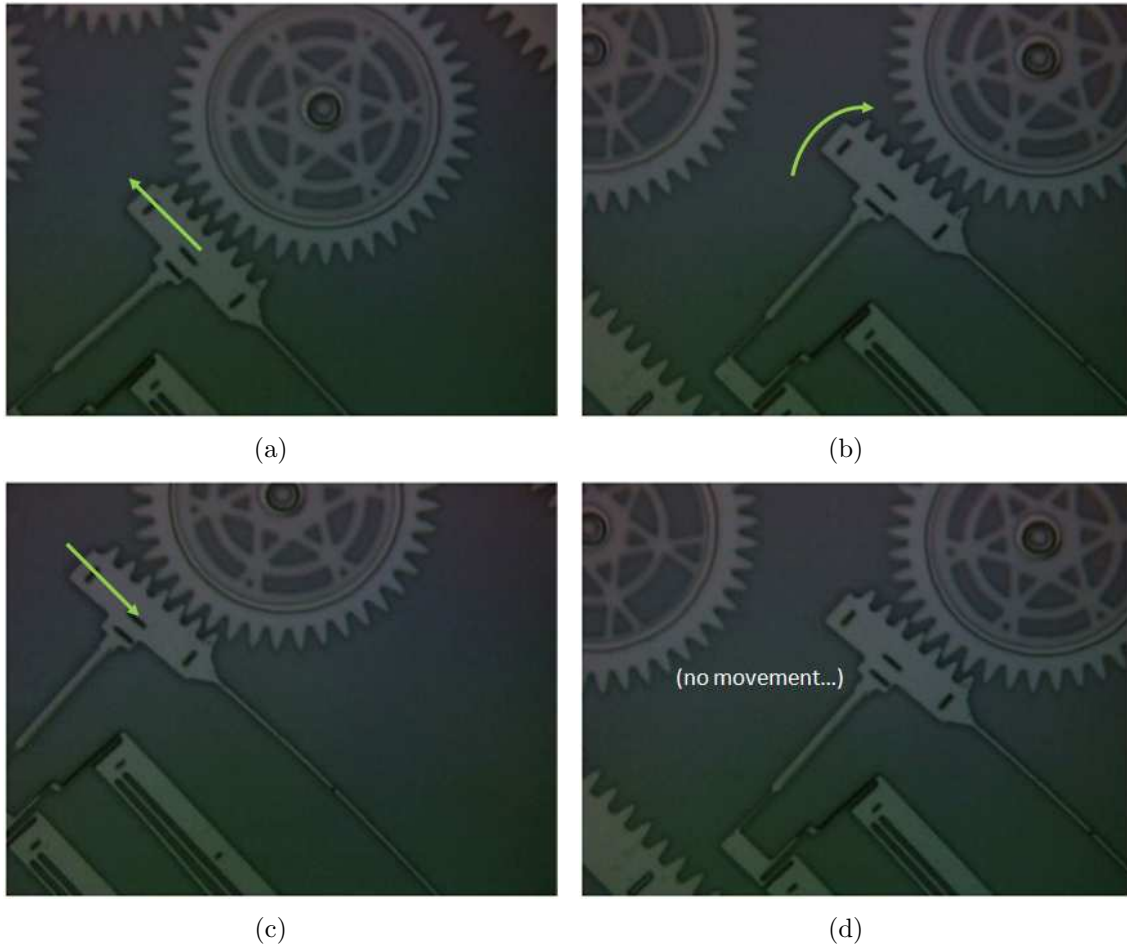


Figure 4.16: Pawl mechanism with gear present (a) push and engage actuators both at rest, (b) pawl still relaxed away from gear but pushed forward, (c) pawl pushed into gear while still pushed forward, (d) pawl no longer pushed forward but still engaged with gear (no movement due to insufficient force of actuator bank).

as gears which were off center, also shown in Figure 4.17). In spite of this error, the rack and gears still partially functioned as intended in that if the wheels were turned manually or the rack pushed manually the other components moved, but with intermittent gear skipping and out-of-plane bending.

One other potential issue which was observed involved the way in which the linear racks were attached to the substrate. To fix these slides, polysilicon staples were used on the outermost arms of the racks (visible in the images shown in Figure 4.17). The inside tracks however bent sufficiently that occasionally they would jump above

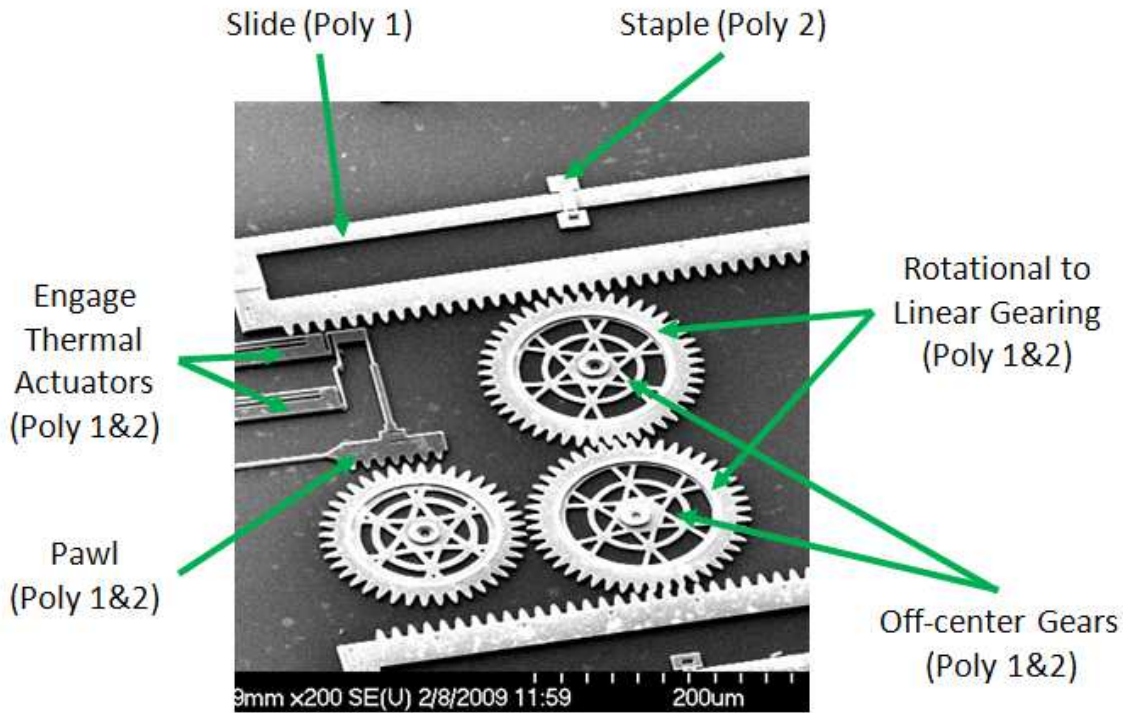


Figure 4.17: Linear actuator used to convert pawl motion into bidirectional linear translation.

the gears they should have been engaged with or twist such that they no longer traveled linearly in the direction intended.

In spite of several issues encountered, a great deal of information was obtained from this single PolyMUMPs run. For the incoming beam path:

- bottom side mirrors showed promise if SU-8 was used as a backing
- bottom side mirrors did not stick to the polysilicon used to frame them
- solid metallic type hinges are too weak if deposited in thin layers
- polymer type hinges for free floating polysilicon structures appear to be non-feasible
- overhead 45° mirrors appear to be feasible through simulation but require either high resolution or large areas to build

- single scratch drive self assembly devices do not provide enough force in PolyMUMPs to be effective

For the outgoing beam path, several observations were made as well including:

- two banks of push actuators are insufficient to move devices of this scale
- long thin sections of polysilicon are too bendable to provide enough force to push these devices
- catch arms which require a large amount of flexibility are required for this type of catch mechanism
- significantly more joints are required to support small mirrors and presumably a single catch arm should suffice
- better resolution is required in all mechanical features or they must be built on a larger scale to make mask misalignment during fabrication a negligible effect
- racks need to have some form of slidable anchor as close to the gearing as possible to avoid out-of-plane issues

With the exception of free floating hinge structures, most of the issues encountered could likely be overcome in PolyMUMPs and all issues encountered could likely be improved upon in future attempts if additional capabilities become available which will be discussed next in Chapter V.

## V. Conclusions and Recommendations

In spite of several limiting factors which prevented detailed testing of many of the components, the information which was gathered in this experiment demonstrates that certain elements are feasible and may warrant further examination. To increase the chances of such future attempts, a number of improvements will need to occur however.

### 5.1 *Processing*

While not directly related to any one functional area of the design, processing considerations are extremely important in the results of the final devices. As was mentioned previously, the PolyMUMPs process is not ideal for this application. While it may be possible that some of the designs attempted here may be successful within PolyMUMPs, other processes may provide vastly superior results and do so with much less effort, as many of the required elements may already be predesigned by the foundry which runs them. Several of the limitations of the PolyMUMPs process have already been discussed. Additional issues have also been encountered that could drastically impact process results, and include:

- inconsistencies in polysilicon doping, resulting in unpredictable internal stresses
- ghost images appearing in oxides, affecting any post-processing which may be required
- misalignment between design layers

Releasing MEMS devices can also be accomplished through various techniques, some more successful than others. While the processes developed for this experiment were for use specifically with devices fabricated using PolyMUMPs, other processes (such as SUMMiT) comprise different quality oxides of different thicknesses, so even an identically scaled design will take much longer to release than its PolyMUMPs equivalent. Additionally, some of the post-processing which was attempted required

some unconventional steps (such as the integration of organic polymers on top of existing MEMS structures) which are worth mentioning.

*5.1.1 Wet and Dry Release.* In an attempt to circumvent the issues with drying a released MEMS device which contains a solvent-sensitive polymer, several dry release runs were attempted. If perfected, this technique would allow for MEMS structures to be released without the necessity of drying any residual liquid as all HF vapor reacts with the oxide to produce vapor byproducts. One run was conducted in which a MEMS structure was left in a closed container containing a small amount of HF and it was verified that the HF concentration for this method is much too high. Instead, devices were then placed on top of a small plastic dish around which was liquid HF and the entire apparatus in a well ventilated area. Structures were released in times comparable to wet releases but an additional observation prevents this method from being reliable with current MEMS devices. A wet release, in addition to removing the oxide between MEMS devices, also is very effective at cleaning the surface of unwanted materials. When a dry release is used instead, it requires an extremely clean surface, and the oxide must be pure enough that no other substances are formed during the release which are not volatile enough to immediately leave the device. If this is not the case, those materials will remain on the surface and will affect the results negatively.

*5.1.2 Drying Technique.* For a wet release, after the MEMS device has been exposed to HF for a sufficient period of time then neutralized in solvent, the device must then be dried. Several devices were dried using the critical point dryer available at AFIT, which requires the released structure to be submersed in methanol within the drying chamber. By increasing the pressure in the chamber, the liquid around the devices is brought to its solid state. At this increased pressure, the temperature is then increased, followed by a drop in pressure which causes the solid to be sublimated directly to a gas. This process then dries devices without removing liquid directly from the sample, reducing the chances that liquids will become trapped and cause stiction.

The results from this technique however have not been completely successful. One of the primary reasons for this is the large flow of carbon dioxide into the chamber during the drying process. While there are containment vessels available to help minimize the force of this event, even with these vessels, device damage can occur. Alternatively, if the HF is neutralized with isopropyl alcohol instead, the device can be dried directly on a hotplate. Not only is this technique much faster, but it has also provided better, more consistent results. With post-processing however, both of these methods must be considered when choosing materials to deposit for hinging, self assembly, etc.

## ***5.2 Incoming Beam Path***

While overall there was little success in this area in making full structures, the information gathered is more than sufficient to help construct future attempts. Overall, there are no indications as of yet that these devices are not possible, but realizable devices would need to be reattempted before their plausibility can be confirmed. The changes required for each device vary based on the type of structure, and will be discussed individually.

*5.2.1 Bottom-side Mirrors.* Suspending a metal layer onto silicon dioxide within the confines of a polysilicon frame for the purpose of building a backside mirror was successfully accomplished. For metal depositions less than  $1.5\text{ }\mu\text{m}$  (possibly more) the strength of the joint between this metal layer and the surrounding polysilicon is not sufficient to hold the metal in place during the release. Backing this material was successfully accomplished using only approximately  $2\text{ }\mu\text{m}$  of SU-8, but in order to fix the overall mirror to the polysilicon, two changes would need to be made.

First, the area of incidence of the surrounding frame would have to be increased. The current data does not indicate how much this would need to be but there are two factors to consider. If the surrounding frame is too large, then usable device area can rapidly be used up unnecessarily. Although, if the area is too small then adhesion will not occur. Also, the masks produced to pattern the SU-8 need to be sufficiently

larger than the opening in which the metal sits. As SU-8 is a negative resist cured by exposure to UV, a slightly undersized mirror can still be used simply by overexposing the mask or intentionally backing it away from the unexposed SU-8 during the mask alignment process, but in order to maintain maximum design accuracy, the preferred approach is to properly size the mask.

The second change would be the use of an adhesion promoter. The manufacturer of SU-8 has chemicals available to do this, which due to time constraints and limited number of devices were not explorable, but may well help maintain the bond between exposed SU-8 and released polysilicon. As the effectiveness of this kind of material has not been explored, this option would need to be reviewed in conjunction with resizing the mirror, frame, and masks to help reach the ideal balance between mirror and frame dimensions.

*5.2.2 45° Overhead Mirrors.* Unfortunately these structures were not able to be explored in more detail during this experiment. As there was not a lot of prior work in this area, it was expected that would be the most difficult portion of this experiment. In spite of the fused joint, observations made from other parts of the design as well as an added capability made available have offered some promising alternatives in this area. Two distinct paths are now possible to solve the overall issue of directing a horizontal beam to a vertical beam splitter, flip chip bonding and releasable polysilicon joints. Both of these paths still have applicability and should be considered.

*5.2.2.1 Flip-Chip Bonding.* During the course of this experiment a piece of equipment, was brought online at AFIT called a flip-chip bonder. As the name implies, this device is able to essentially take two devices (MEMS, microelectronics, or one of each) and flip one on top of the other. By designing each half of the device and depositing beads of metal of a predefined thickness in key locations as shown in Figure 5.1 (a), one device is then aligned over the other and the metal is fused to both halves, joining the two devices face-to-face with each other as in Figure 5.1 (b).

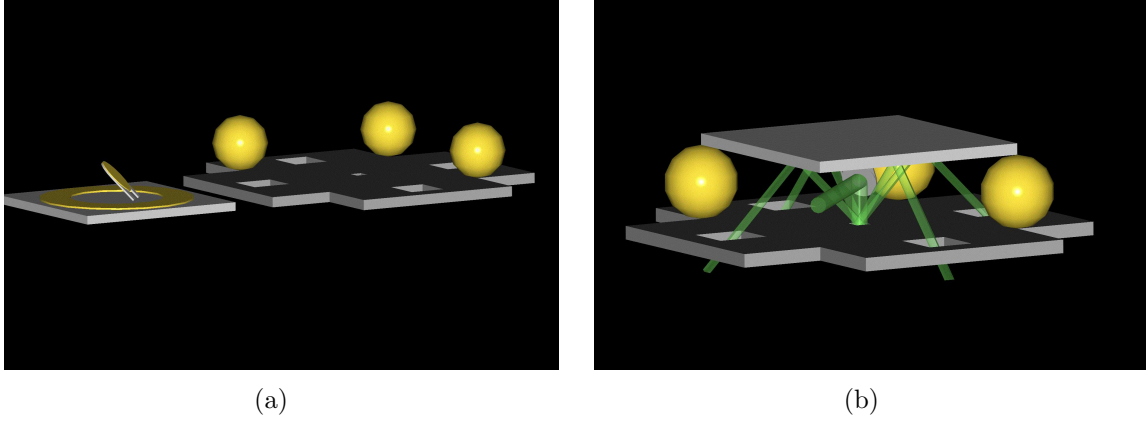


Figure 5.1: Conceptual design of  $45^\circ$  overhead mirror, beam splitter (using anisotropically etched pit for beam splitter, and deposited metal ring a) two individual halves prior to assembly and b) after  $45^\circ$  mirror has been bonded to the other device.

This approach still requires a  $45^\circ$  mirror (now fixed to the substrate), a ring of flat reflective metal surrounding the mirror and on the other half some form of beam splitter. Fixed  $45^\circ$  mirrors are a simplified version of the movable mirrors used in the outgoing beam path (and have been accomplished elsewhere as well). The mirror ring is a trivial metal deposition, and the beam splitter will be covered separately.

*5.2.2.2 Multiple Joint Folding Structures.* While flip-chip bonding does provide an immediate solution with a high likelihood of success, the possibility of exploring the more complex structures attempted here still have merit. These kinds of structures take up less space, as the area required to manually lay down spacing beads is considerable compared to a folding device. For prototyping devices such as this, flip-chip bonding is more than satisfactory. If such a design were to go into production however, the additional steps required to perform the flip-chip bonding would be eliminated if folding structures could be mastered, saving time, money, materials, and chip real estate.

Based on the observations from this experiment, the key obstacle to overcome to prove the validity of these structures is the hinging. While depositions of polymers is still a possible hinging solution, there is one other option which is almost guaranteed



to succeed, and that is the floating hinges discussed in Chapter III. The hinges used in the outgoing beam paths in PolyMUMPs worked surprisingly well. These types of structures built using a process capable of three free polysilicon layers, with tolerances at least as good as PolyMUMPs, would allow for precise control over how each member is able to rotate, and take out any guesswork in the design. Positive stop features could also be added to precisely control the fully assembled form. Polymer material could still be used on valley hinges as a form of self assembly, but the precise control of polysilicon hinges would greatly increase the odds of success and open up a wide variety of design options with structures such as these.

The related folding structure design (the suspended VCSEL mirror ring) is basically a variation of the  $45^\circ$  overhead mirror and could be accomplished using the same approach. It is still possible that it could be self assembled using a polymer at one or more of the valley folding joints. Again, this ring is replaced by the deposited metal ring in the flip-chip bonding solution, but for the same justifications already mentioned is still a design worth pursuing and still a possibility at this time.

*5.2.3 Beam Splitters.* As the only attempts possible given the space available also relied on connecting polysilicon layers using a hinging material, these devices as they are currently designed are just as problematic as the multiple-joint folding structures. As these beam splitters would only be usable with the other mirrors however, the risk in using the same design scheme was minimal. While these, too, could be designed with a floating hinge, another possibility exists which if successful would also work with either a flip-chip approach or single-level design.

Polysilicon crystalline structure exhibits some unusual properties when etched with certain reactants, such as potassium hydroxide. The crystalline structure is naturally removed in a very regular, predictable pattern which resembles an inverted four-sided pyramid as shown in Figure 5.2. If such a piece of substrate (with a 100 planar structure) were to be patterned and etched in this fashion and the pit coated with gold, this could possibly serve as a beam splitter as well. The orientation of the

mirror ring above then becomes important (as making this ring exactly parallel to the substrate may be difficult), but if the ring were simply made sufficiently large to compensate for any misalignments, this could lead to a very compact design that is much easier to manufacture than any built pyramid structure and is definitely worth pursuing.

### ***5.3 Outgoing Beam Path***

While the movable mirrors which make up the outgoing beam path were much more successful, there is still plenty of room for improvement. As with the incoming beam path, the results from these devices fall into definite categories each of which will be addressed individually.

*5.3.1 Bottom-side Mirrors.* As with the incoming beam path, the same observations and limitations apply to mirrors for this portion of the design where metal was to be supported by a polysilicon frame. The one fundamental difference in

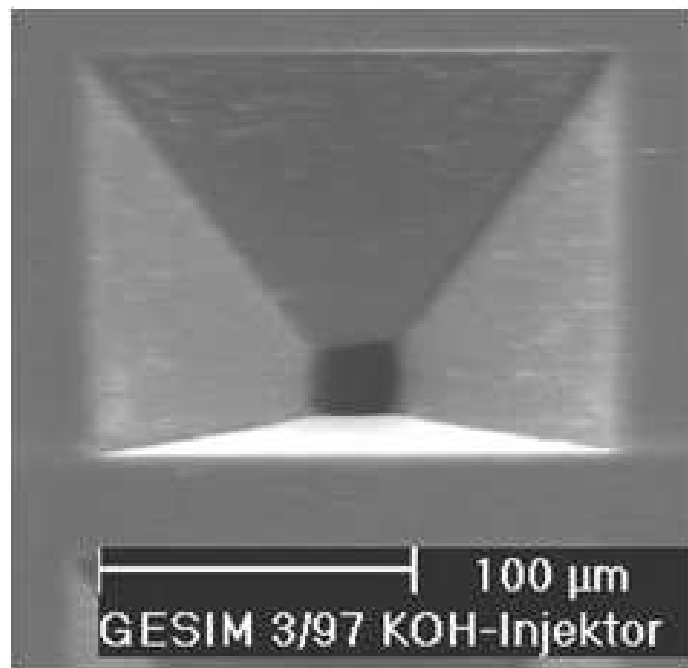


Figure 5.2: Anisotropic etch of silicon using KOH [53].

this area is that, by necessity, the mirrors in the outgoing beam path are larger. By extension, any changes which increase overall mirror size in order to accommodate the construction of these underside mirrors will likely be even larger for the mirrors in the outgoing beam path. One advantage however is that these mirrors must be hinged in order to reach their operating position, so if carefully designed, it may be possible to simply take a top-side mirror and design it to flip over entirely to accomplish this task. This would likely require more real estate than attempting to build these devices as designed now, but may be a small tradeoff should a suitable way to build these underside mirrors be problematic without conducting a custom foundry run.

*5.3.2 Mirror Hinging and Support Structure.* While this area of the experiment was relatively successful in that mirror structures were assembled using the current design, it took some time to develop the correct technique to assemble these devices and even with this experience they can be difficult to assemble. One improvement which actually could be made even using PolyMUMPs could make the assembly of these devices seem trivial compared to the current design.

Hinges used in this design were the second attempt, based on hinges from the first design which were designed to be too small. This caused problems with layers lining up correctly as well as issues with releasing such fine features. The enlarged versions used for the second run all released correctly; 100% of the hinges tested either were already released or needed very little bending to break free. The difficulty in assembling these devices was with the catch arm. This rigid piece of polysilicon was designed as part of the base (either fixed to the same base as the hinge structure or in the case of the horizontal tilt mirror fixed to the slide). Either way, these arms were rigid and needed to bend into position, which required the tip to slide along the mirror frame until it found the hole it was designed to fit into. In most cases, this was the primary source of failure in trying to assemble mirrors. While the addition of a metal layer on top of these arms help bend them upward and ultimately gave

the edge needed to be able to assemble them, there is another possibility which could improve this design even further.

If at the base of the support arms, the arms themselves were also hinged as shown in Figure 5.3, then during the assembly process these catch arms could be manipulated into position directly. This was attempted with the current design but without a hinge, these arms were far too fragile to survive being moved directly by a probe. If they were hinged however, the mirror and their supports could be individually manipulated into position, with adjustments to each piece. The support arms could literally be placed inside the grooves made for them, and the entire assembly would then be assembled without inducing any appreciable stress on the structure (aside from the initial stress which may be required to break loose the hinges).

An additional benefit to this method is a much greater control of the final mirror position. The current design uses a bent polysilicon arm to control the position of

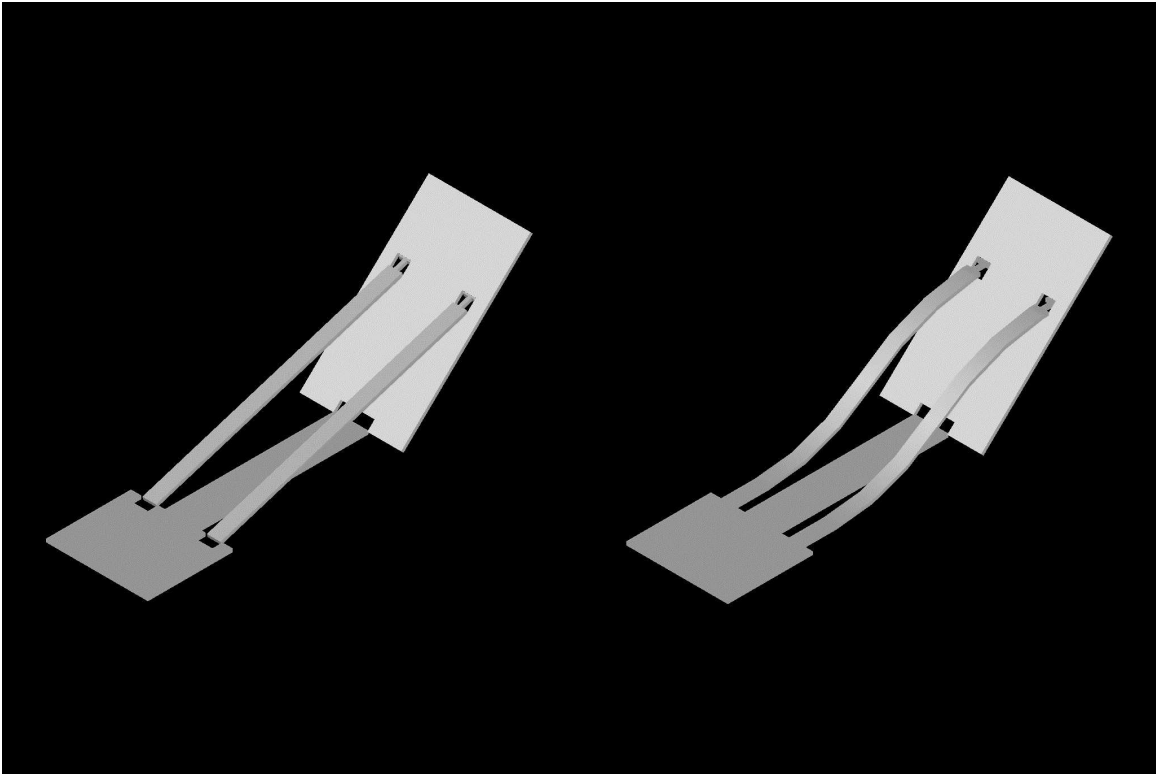


Figure 5.3: Conceptual design of hinged catches (left) vs. flexible fixed catches (right).

its mirror. Finding the perfect length to hold the mirror at a precise angle is at best a trial-and-error method and assumes that the same bending profile will occur each time resulting in the same ending angle. Also, it is entirely possible that, if heated or cooled, these arms may bend unintentionally and change the final position of the mirrors which would require position corrections to occur to compensate. A hinged structure would allow very straightforward geometry to be used to achieve the exact angle and once assembled, temperature would only expand or contract the overall structure which should not appreciably affect mirror positioning.

*5.3.3 Mirror Movement and Gearing.* The designs tested did move as expected. Gears and racks interacted correctly, and essentially this portion of the design performed its intended function. They did not however perform them well. The basic issue was the amount of error relative to the size and spacing of the gear teeth as well as layers coming out of plane with each other. To correct for out of plane parts of the design, a variety of solutions could be used including pins within tracks to control the motion of a sheet of polysilicon while keeping it close to the substrate and adding additional tracks and staples to better control the motion of these plates, etc.

The problem with overall error in the position of the gears, racks, gear teeth, etc. is more a function of the foundry process used. While its possible the overall design could simply be enlarged so that the feature dimensions became large compared to the errors in those features, the mirrors as designed are already larger than the VCSEL and photodetector technology they would be integrated with, and thus increasing the mirror size is a very inefficient solution. Instead a process which holds tighter tolerances would allow for the current correct scale to be maintained while producing gears which work much better with each other.

*5.3.4 Thermal Actuators and Pawl Motion.* As was already alluded to in Chapter IV, actuation of these kinds of assemblies has already been accomplished using nearly the same design as was tested here. The change to the design was a reduction in the number of thermal actuators ganged together. The most straight-

forward solution would be to simply increase this number (or ideally build several devices with various numbers of these mechanisms geared to a system which is as large as the largest used here). This would identify the exact amount needed to do the job.

The other problem encountered involved the bending of the long, thin beam connecting the push actuators to the pawl. This could be corrected by thickening most of the arm (but leaving at most two flexible points in the arm to allow for the in and out motion required by the engage actuator). In future designs, issues such as the required actuation voltages, relaxation time, sensitivity to backbending, etc. could be addressed by further improvements to the basic arm design used here.

*5.3.5 Additional Mirror Designs.* One final area worth recommending would be additional mirror designs. The four basic mirror designs here represented the bare minimum which would hint to the feasibility of this kind of a system. With additional foundry capabilities, several options become possible. As was mentioned in Chapter III, additional releasable polysilicon layers open up tremendous possibilities in design. Compound designs such as the combination of both vertical and horizontal beam control, adding multiple focal length mirrors in the beam path to control the beam spread, etc. all may be of tremendous benefit if this kind of a design were to be put to practical use. The fundamental work done here is only a starting point. By taking the tools constantly being designed by others and applying them to this foundation, a future researcher could quite conceivably solve this one area of photonics and help put such devices into actual use.

## **5.4 Recommendations**

Due to the wide variety of structures tested, no one device was built, tested and demonstrated full functionality as expected. Each design however did offer degrees of success and from those aspects which did not function, several possibilities exist to correct for these issues. While independent discussion of the two types of devices

is warranted, both cases would likely benefit significantly from a process with more control such as SUMMiT for a variety of reasons already mentioned.

For the fixed incoming beam path, it does not appear likely that hinging between sections of polysilicon would be successful with anything except actual polysilicon hinges. While a polymer may show promise as a method of partial self assembly and keeping assembled structures in place, depositing a ‘fold’ between two sheets of polysilicon would require much more effort to be successful. Considering that there are processes available which can give sufficient resolution to accomplish this task with free floating hinges however, this effort does not seem justified at this time. Many of the structures which were designed all seem feasible in terms of being able to be assembled geometrically, but until such time as a more tightly controlled fabrication process is used, success will be limited. Backside mirrors were also very close to successful, but additional overlap between the edge of the SU-8 and the polysilicon supporting it would be required. Pyramidal structures which are proposed here to be used as beam splitters have been built elsewhere and, though not successful here for the same hinging reasons already mentioned, these could potentially be replaced with anisotropically etched silicon and accomplish the same objective but with a sturdier structure that likely would be much easier to form. This would limit beam splitting to four discrete beams, while surface mounted could be designed for a variety of geometries. Overhead mirrors could for the short term be replaced with flip-chip bonded equivalents for proof of concept and prototype testing, but single layer structures would still be useful to pursue long-term for various manufacturing benefits.

For the controllable outgoing beam paths, the devices as designed are very close to functional. While PolyMUMPs does introduce some issues with variability in gear alignment, all of the other obstacles encountered could likely be overcome in future designs using PolyMUMPs. Issues with insufficient actuator force are a simple matter to compensate for by just adding additional banks of actuators. The long, thin strips of polysilicon bending excessively provide a bit more of a challenge but could likely be overcome by thickened beams or by replacing them with parallel beams joined at

various locations along their length. Such design modifications would require some attention to the possibility of out-of-plane issues, but with proper polysilicon staples or guides, this could be avoided. Hinges on these structures are basically functional as designed but for smaller mirrors could be duplicated more often to increase the likelihood that these mirrors could be assembled. Those catches which were successful were likely only successful because the catch and the hinge were not anchored to the same structure. In other words, because the mirror was independently adjustable to the height of the catches and those mirrors in which both were anchored to the same base required stress to bend the catches into place. Hinging these catch arms seems a simple fix which would likely accomplish the same variability required to build functional devices.



## Appendix A. Forward Kinematic Analysis

As the geometry resulting from many of the designs proposed is sufficiently complex that simulation is not possible, another approach must be taken to analyze the motion of these structures. Specifically the 45° overhead mirror results in complications because of the complex geometry and angular motion between the members. Instead, another approach can be taken to mathematically determine the motion of these members and is an approach commonly used in robotic design called kinematics.

A full description of this technique is outlined in other sources ([49]), but in summary the following outlines the transformation matrices needed to describe a cartesian coordinate system on a movable member relative to a single, stationary universal coordinate system. The matrices used to accomplish this description are given by:

$$T_{x-rotation} = \begin{bmatrix} 1 & 0 & 0 & 0 \\ 0 & c(\theta) & -s(\theta) & 0 \\ 0 & s(\theta) & c(\theta) & 0 \\ 0 & 0 & 0 & 1 \end{bmatrix} \quad (A.1)$$

$$T_{y-rotation} = \begin{bmatrix} c(\theta) & 0 & s(\theta) & 0 \\ 0 & 1 & 0 & 0 \\ -s(\theta) & 0 & c(\theta) & 0 \\ 0 & 0 & 0 & 1 \end{bmatrix} \quad (A.2)$$

$$T_{z-rotation} = \begin{bmatrix} c(\theta) & -s(\theta) & 0 & 0 \\ s(\theta) & c(\theta) & 0 & 0 \\ 0 & 0 & 1 & 0 \\ 0 & 0 & 0 & 1 \end{bmatrix} \quad (A.3)$$

$$T_{translation} = \begin{bmatrix} 1 & 0 & 0 & x \\ 0 & 1 & 0 & y \\ 0 & 0 & 1 & z \\ 0 & 0 & 0 & 1 \end{bmatrix} \quad (A.4)$$

For the derivation of the various matrices, Figure A.1 shows the angles used.

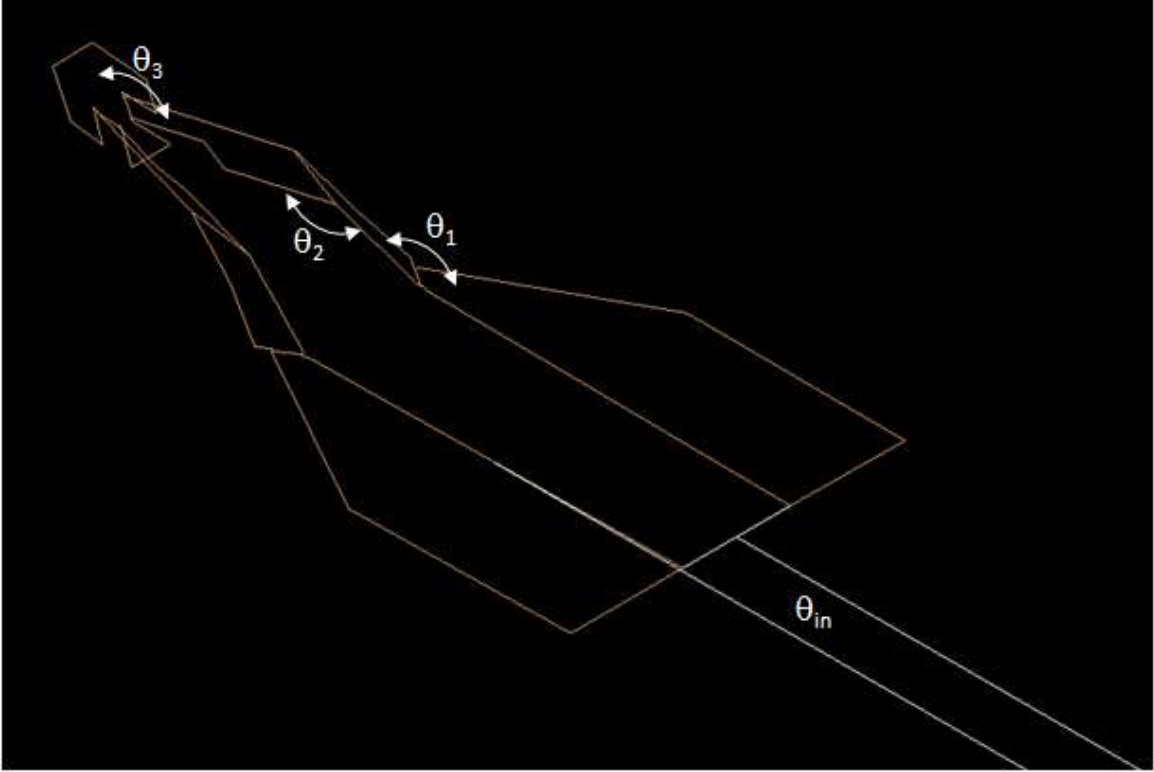


Figure A.1: Definitions of angles used in equation derivation of overhead 45° mirror.

Where  $s(\theta_{in})$  and  $c(\theta_{in})$  are shorthand for the sine and the cosine respectively. These can then be applied to the overhead mirror design, and stepping through one arm of the assembly, frame reference letters are assigned for each of the coordinate frames along the way.

First, the input angle of rotation for the baseplate is applied:

$${}^a_bT = \begin{bmatrix} c(\pi/2 + \theta_{in}) & -s(\pi/2 + \theta_{in}) & 0 & 0 \\ s(\pi/2 + \theta_{in}) & c(\pi/2 + \theta_{in}) & 0 & 0 \\ 0 & 0 & 1 & 0 \\ 0 & 0 & 0 & 1 \end{bmatrix} \quad (\text{A.5})$$

then a move to the center of first solid face

$${}^b_cT = \begin{bmatrix} 1 & 0 & 0 & 382.93225 \\ 0 & 1 & 0 & 0 \\ 0 & 0 & 1 & 0 \\ 0 & 0 & 0 & 1 \end{bmatrix} \quad (\text{A.6})$$

followed by a move to center of first joint and rotate by the first joint angle

$${}^c_dT = \begin{bmatrix} 1 & 0 & 0 & 348.29908 \\ 0 & 1 & 0 & 7.7378447 \\ 0 & 0 & 1 & 0 \\ 0 & 0 & 0 & 1 \end{bmatrix} \quad (\text{A.7})$$

$${}^d_eT = \begin{bmatrix} c(-2.72658836) & -s(-2.72658836) & 0 & 0 \\ s(-2.72658836) & c(-2.72658836) & 0 & 0 \\ 0 & 0 & 1 & 0 \\ 0 & 0 & 0 & 1 \end{bmatrix} \quad (\text{A.8})$$

$${}^e_fT = \begin{bmatrix} 1 & 0 & 0 & 0 \\ 0 & c(\theta_1) & -s(\theta_1) & 0 \\ 0 & s(\theta_1) & c(\theta_1) & 0 \\ 0 & 0 & 0 & 1 \end{bmatrix} \quad (\text{A.9})$$

Next, a move to center of second solid face

$${}^f_gT = \begin{bmatrix} 1 & 0 & 0 & -21.7867610 \\ 0 & 1 & 0 & 62.2171240 \\ 0 & 0 & 1 & 0 \\ 0 & 0 & 0 & 1 \end{bmatrix} \quad (\text{A.10})$$

$${}^g_hT = \begin{bmatrix} c(2.17987877) & -s(2.17987877) & 0 & 0 \\ s(2.17987877) & c(2.17987877) & 0 & 0 \\ 0 & 0 & 1 & 0 \\ 0 & 0 & 0 & 1 \end{bmatrix} \quad (\text{A.11})$$

followed by a move to center of second joint and rotate by the second joint angle (where all joint angles will be oriented such that they will need to rotate in the positive x direction)

$${}^h_iT = \begin{bmatrix} 1 & 0 & 0 & 115.6898820 \\ 0 & 1 & 0 & 17.6290098 \\ 0 & 0 & 1 & 0 \\ 0 & 0 & 0 & 1 \end{bmatrix} \quad (\text{A.12})$$

$${}^i_jT = \begin{bmatrix} c(0.38979515) & -s(0.38979515) & 0 & 0 \\ s(0.38979515) & c(0.38979515) & 0 & 0 \\ 0 & 0 & 1 & 0 \\ 0 & 0 & 0 & 1 \end{bmatrix} \quad (\text{A.13})$$

$${}^j_kT = \begin{bmatrix} 1 & 0 & 0 & 0 \\ 0 & c(\theta_2) & -s(\theta_2) & 0 \\ 0 & s(\theta_2) & c(\theta_2) & 0 \\ 0 & 0 & 0 & 1 \end{bmatrix} \quad (\text{A.14})$$

Next, a move to center of third solid face

$${}^k_l T = \begin{bmatrix} 1 & 0 & 0 & 21.5445490 \\ 0 & 1 & 0 & -42.2288010 \\ 0 & 0 & 1 & 0 \\ 0 & 0 & 0 & 1 \end{bmatrix} \quad (\text{A.15})$$

$${}^l_m T = \begin{bmatrix} c(-0.55608881) & -s(-0.55608881) & 0 & 0 \\ s(-0.55608881) & c(-0.55608881) & 0 & 0 \\ 0 & 0 & 1 & 0 \\ 0 & 0 & 0 & 1 \end{bmatrix} \quad (\text{A.16})$$

followed by a move to center of third joint and rotate by the third joint angle

$${}^m_n T = \begin{bmatrix} 1 & 0 & 0 & 230.2832400 \\ 0 & 1 & 0 & 36.1604920 \\ 0 & 0 & 1 & 0 \\ 0 & 0 & 0 & 1 \end{bmatrix} \quad (\text{A.17})$$

$${}^n_o T = \begin{bmatrix} c(-2.28421081) & -s(-2.28421081) & 0 & 0 \\ s(-2.28421081) & c(-2.28421081) & 0 & 0 \\ 0 & 0 & 1 & 0 \\ 0 & 0 & 0 & 1 \end{bmatrix} \quad (\text{A.18})$$

$${}^o_p T = \begin{bmatrix} 1 & 0 & 0 & 0 \\ 0 & c(\theta_3) & -s(\theta_3) & 0 \\ 0 & s(\theta_3) & c(\theta_3) & 0 \\ 0 & 0 & 0 & 1 \end{bmatrix} \quad (\text{A.19})$$

Finally, three more sets of transformation matrices are derived to arbitrary points on the mirror. The first set is a move from third joint coordinate axis to a point on the

top center of the mirror, but with the coordinate axis rotated to match the same as the universal coordinate orientation in the initial position of the assembly.

$${}^p_qT = \begin{bmatrix} 1 & 0 & 0 & -81.0011 \\ 0 & 1 & 0 & 52.5323 \\ 0 & 0 & 1 & 0 \\ 0 & 0 & 0 & 1 \end{bmatrix} \quad (\text{A.20})$$

$${}^q_rT = \begin{bmatrix} c(1.18289) & -s(1.18289) & 0 & 0 \\ s(1.18289) & c(1.18289) & 0 & 0 \\ 0 & 0 & 1 & 0 \\ 0 & 0 & 0 & 1 \end{bmatrix} \quad (\text{A.21})$$

The second of these three sets is again from the third joint's coordinate axis to a point located on the bottom center of the mirror

$${}^p_sT = \begin{bmatrix} 1 & 0 & 0 & 69.5851 \\ 0 & 1 & 0 & -8.9739 \\ 0 & 0 & 1 & 0 \\ 0 & 0 & 0 & 1 \end{bmatrix} \quad (\text{A.22})$$

$${}^s_tT = \begin{bmatrix} (1.18289) & -s(1.18289) & 0 & 0 \\ s(1.18289) & c(1.18289) & 0 & 0 \\ 0 & 0 & 1 & 0 \\ 0 & 0 & 0 & 1 \end{bmatrix} \quad (\text{A.23})$$

The third and final set is a move from third joint's coordinate axis to bottom left corner of the mirror

$${}^p_uT = \begin{bmatrix} 1 & 0 & 0 & 57.1674 \\ 0 & 1 & 0 & -39.5165 \\ 0 & 0 & 1 & 0 \\ 0 & 0 & 0 & 1 \end{bmatrix} \quad (\text{A.24})$$

$${}^u_vT = \begin{bmatrix} c(1.18289) & -s(1.18289) & 0 & 0 \\ s(1.18289) & c(1.18289) & 0 & 0 \\ 0 & 0 & 1 & 0 \\ 0 & 0 & 0 & 1 \end{bmatrix} \quad (\text{A.25})$$

To find the overall transformation matrix from any one coordinate system to another, the transformation matrices are simply multiplied together. For example, to find the coordinates for the origin (0,0,0) of the first joint's coordinate frame (f) in the universal coordinate frame (a), the product of those matrices must first be found:

$${}^a_fT = {}^a_bT {}^b_cT {}^c_dT {}^d_eT {}^e_fT \quad (\text{A.26})$$

This can be done in MATLAB, leaving the variables for the joint angles intact. These matrices are then simply multiplied by the vector (0,0,0,1) to obtain vectors for these positions in terms of the three state angles. The first key elements of these vectors is the x coordinate of the top center point of the mirror (which must always be zero as the mirror can not translate in the x direction due to symmetry) which applying this technique yields:

$$\begin{aligned}
X_{top \ center} = & (-4334.8\sin(\theta_{in}) - 221.378\cos(\theta_{in})) \\
& + (255.85\cos(\theta_{in}) - 174.04\sin(\theta_{in}))\cos(\theta_1) \\
& + (32.254\cos(\theta_{in}) + 47.415\sin(\theta_{in}))\cos(\theta_2) \\
& - (7.4544\cos(\theta_{in}) + 10.958\sin(\theta_{in}))\cos(\theta_3) \\
& + (90.234\cos(\theta_{in}) - 61.381\sin(\theta_{in}))\sin(\theta_1)\sin(\theta_2) \\
& + (15.525\cos(\theta_{in}) + 22.824\sin(\theta_{in}))\sin(\theta_2)\sin(\theta_3) \\
& + (76.772\cos(\theta_{in}) - 52.223\sin(\theta_{in}))\cos(\theta_1)\cos(\theta_2) \\
& + (6.7681\cos(\theta_{in}) - 4.6039\sin(\theta_{in}))\cos(\theta_1)\cos(\theta_3) \\
& + (14.827\cos(\theta_{in}) + 21.797\sin(\theta_{in}))\cos(\theta_2)\cos(\theta_3) \\
& + (35.293\cos(\theta_{in}) - 24.007\sin(\theta_{in}))\cos(\theta_1)\cos(\theta_2)\cos(\theta_3) \\
& + (36.955\cos(\theta_{in}) - 25.138\sin(\theta_{in}))\cos(\theta_1)\sin(\theta_2)\sin(\theta_3) \\
& - (43.435\cos(\theta_{in}) - 29.546\sin(\theta_{in}))\sin(\theta_1)\cos(\theta_2)\sin(\theta_3) \\
& + (41.481\cos(\theta_{in}) - 28.217\sin(\theta_{in}))\sin(\theta_1)\sin(\theta_2)\cos(\theta_3)
\end{aligned} \tag{A.27}$$

Similarly, the second key element is the x coordinate of the bottom center point of the mirror (which also must always be zero) and is defined by:



$$\begin{aligned}
X_{bottom \ center} = & (-4233.7\sin(\theta_{in}) - 152.60\cos(\theta_{in})) \\
& + (193.41\cos(\theta_{in}) - 131.56\sin(\theta_{in}))\cos(\theta_1) \\
& + (45.442\cos(\theta_{in}) + 66.803\sin(\theta_{in}))\cos(\theta_2) \\
& + (1.2822\cos(\theta_{in}) + 1.8850\sin(\theta_{in}))\cos(\theta_3) \\
& + (127.13\cos(\theta_{in}) - 86.479\sin(\theta_{in}))\sin(\theta_1)\sin(\theta_2) \\
& - (2.6707\cos(\theta_{in}) + 3.9261\sin(\theta_{in}))\sin(\theta_2)\sin(\theta_3) \\
& + (108.16\cos(\theta_{in}) - 73.577\sin(\theta_{in}))\cos(\theta_1)\cos(\theta_2) \\
& - (1.1642\cos(\theta_{in}) - 0.79196\sin(\theta_{in}))\cos(\theta_1)\cos(\theta_3) \\
& - (2.5506\cos(\theta_{in}) + 3.7495\sin(\theta_{in}))\cos(\theta_2)\cos(\theta_3) \\
& - (6.0710\cos(\theta_{in}) - 4.1297\sin(\theta_{in}))\cos(\theta_1)\cos(\theta_2)\cos(\theta_3) \\
& - (6.3569\cos(\theta_{in}) - 4.3242\sin(\theta_{in}))\cos(\theta_1)\sin(\theta_2)\sin(\theta_3) \\
& + (7.4716\cos(\theta_{in}) - 5.0825\sin(\theta_{in}))\sin(\theta_1)\cos(\theta_2)\sin(\theta_3) \\
& - (7.1355\cos(\theta_{in}) - 4.8539\sin(\theta_{in}))\sin(\theta_1)\sin(\theta_2)\cos(\theta_3)
\end{aligned} \tag{A.28}$$

The third key element comes from the z coordinate for both the bottom center and bottom left points as they must always be equal (again due to symmetry). If the two equations for these two z coordinates are found, set equal to each other and like terms grouped, the equation for this error in height (or the difference in the z value of these two points) is given by:

$$\begin{aligned}
Z_{difference \text{ in edge}} = & (-6.2630)\sin(\theta_1) \\
& - (3.7008)\cos(\theta_1)\sin(\theta_2) \\
& + (3.1486)\sin(\theta_1)\cos(\theta_2) \\
& + (4.7494)\sin(\theta_1)\cos(\theta_3) \\
& + (25.932)\sin(\theta_1)\sin(\theta_2)\sin(\theta_3) \\
& + (30.480)\cos(\theta_1)\cos(\theta_2)\sin(\theta_3) \\
& - (29.109)\cos(\theta_1)\sin(\theta_2)\cos(\theta_3) \\
& + (24.766)\sin(\theta_1)\cos(\theta_2)\cos(\theta_3)
\end{aligned} \tag{A.29}$$

At this point, these equations were verified by applying arbitrary values for each of the 4 angles (within allowable physical limits) and values obtained. These same angles were then physically applied to the AutoCAD model and the corresponding coordinate values were then pulled directly from the 3D model and matched the calculated values from MATLAB.

## *Appendix B. PolyMUMPs Design Overview*

This project consisted of two PolyMUMPs designs, run 83 and 84. This appendix contains a brief overview of the two submitted designs along with a breakdown of each section of each design demonstrating what devices were submitted and for what purpose.

### ***B.1 Run 83***

The first submission was a design intended to attempt structure which used some of the basic elements which would be needed in a working device, including:

- pyramids with solid vs open frame faces
- various pyramid geometries which change incident angles and minimize dead space on top of structure
- pyramid self assembly
- movable mirror assembly methods (hinge engaged from a self assembly spring push mechanism)
- movable mirror integrated with gear wheel
- linear actuated platform (for potential use with a vertical lens element)
- linear actuated angled mirror necessary for beam steering

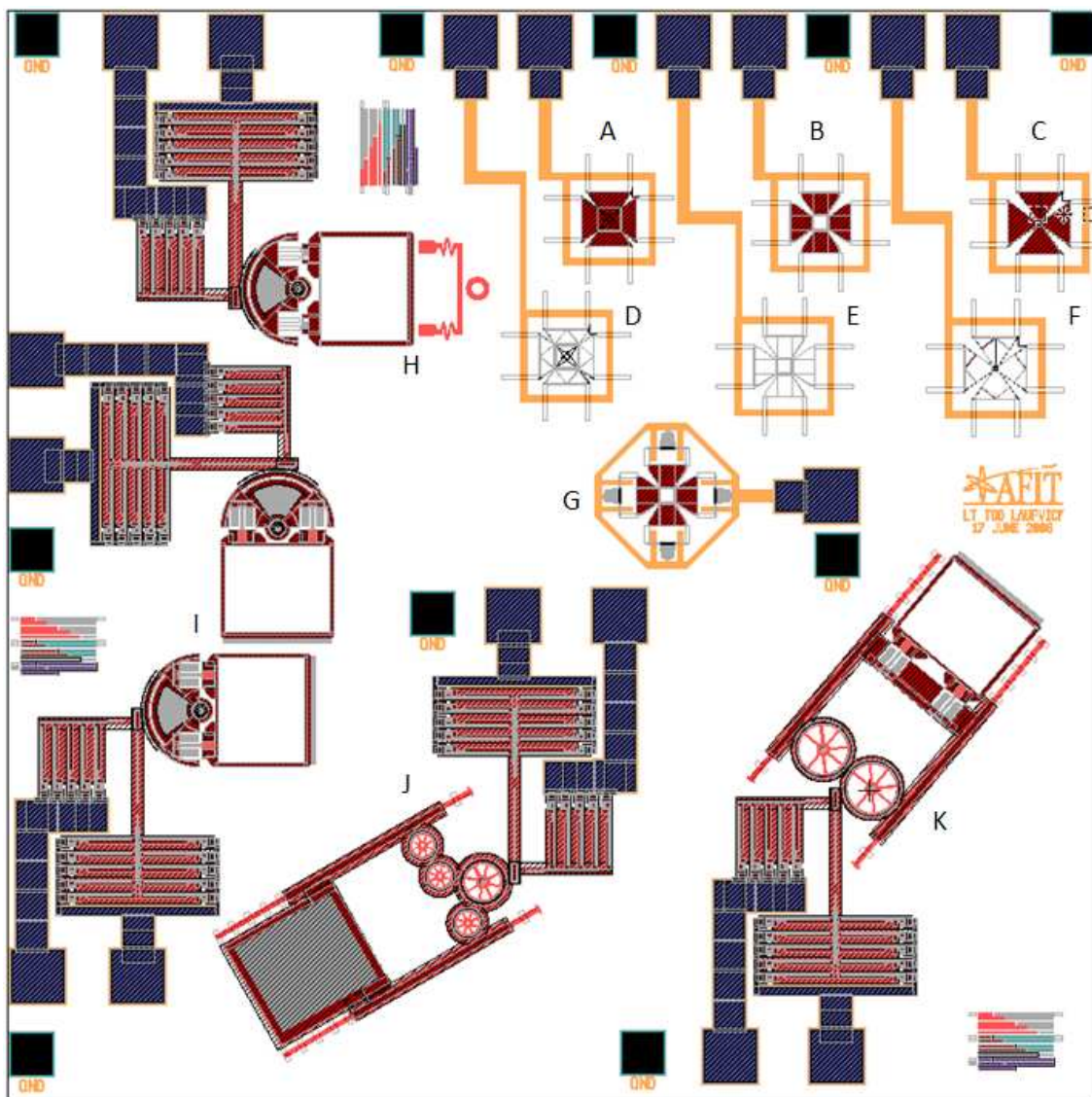


Figure B.1: LEdit submission for run 83 A) 30° solid faced mirror, B) 45° solid faced mirror, C) 45° solid faced mirror with minimal top, D) 30° open faced mirror, E) 45° open faced mirror, F) 45° open faced mirror with minimal top, G) self assembly test, H) spring push free floating hinge, I) two manual assembly horizontal mirror (x2), J) multiple gear linear drive with flat stage and K) multiple gear linear drive (alternate) with angled mirror.

## ***B.2 Run 84***

The second submission was a design intended to attempt as many designs that would fit in the given space with the largest variety of options. This design included:

- one complete outgoing beam path consisting of four mirrors (horizontal and vertical steering and turning)
- one complete incoming beam path consisting of a  $45^\circ$  overhead mirror and QWIP pyramid with overhead ring
- one additional  $45^\circ$  overhead mirror (for additional hinging attempts)
- one alternate pyramid and mirror structure for use with a standard photodetector, using polymer hinged reflecting mirrors
- one alternate pyramid and mirror structure for use with a standard photodetector, using polysilicon hinged reflecting mirrors

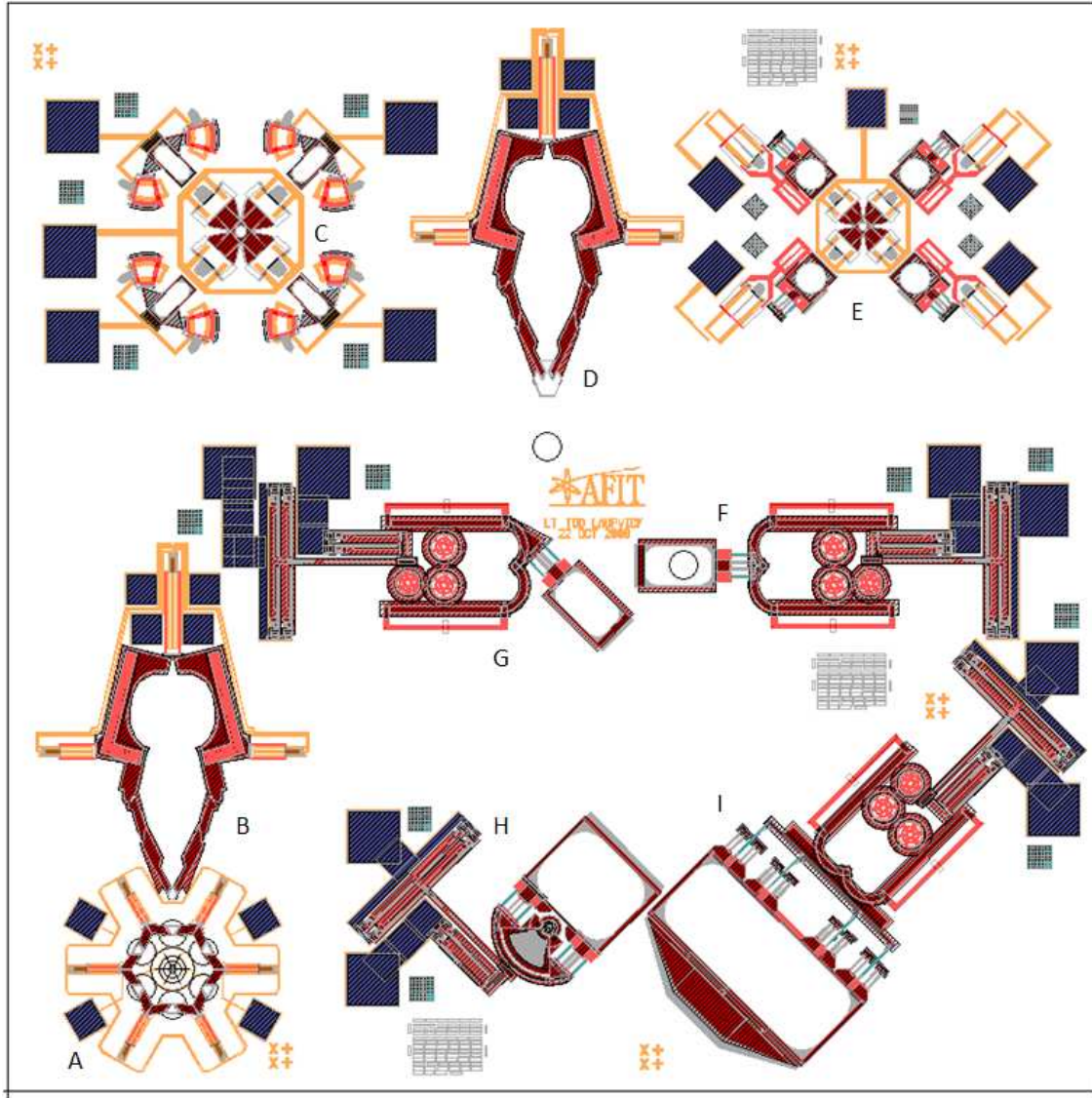


Figure B.2: LEdit submission for run 83 A) Overhead ring and pyramid for VCSEL detector, B) folding  $45^\circ$  overhead mirror, C) photodetector design with polymer hinges and scratch drive self assembly, D) second  $45^\circ$  overhead mirror with enlarged mirror surface, E) photodetector design using polysilicon hinges and alternate scratch drive partial self assembly, F) VCSEL steering mirror (Mirror 1, vertical), G) VCSEL steering mirror (Mirror 2, horizontal), H) VCSEL turning mirror (Mirror 3, horizontal), I) VCSEL turning mirror (Mirror 4, vertical).

## *Appendix C. Post Processing*

While PolyMUMPs in general provides significant flexibility of design, for this experiment certain aspects of this process were not suitable. As the devices manufactured are returned in an unreleased state however, there exists the capability of post processing the devices with additional layers prior to release.

This appendix outlines in general what post processing was intended, how it was to be performed and a general overview of results.

### *C.1 Mirrors and Hinges*

There are two purposes for which postprocessing was attempted for this experiment: mirroring and hinges.

While PolyMUMPs does include a layer of gold as the last step prior to shipping, their process does not allow for gold to be deposited anywhere except on top of the uppermost polysilicon layer. For devices intended to reflect optical signals upward (or devices capable of flipping over entirely) this would have been sufficient, but as there is a significant number of mirrors which need to direct light downward and limited space in which to do it, an alternate plan of attack needed to be developed.

Prior to releasing a MEMS device, the uppermost surface of the chip can only be comprised of one of three things: polysilicon from the uppermost deposition, oxide from the uppermost deposition or gold covering polysilicon. The concept for constructing a downward reflecting mirror is basically to find a way to deposit gold onto the oxide with a frame of polysilicon around it. After releasing the structure and removing the oxide, the gold and polysilicon frame would ideally remain with nothing between the gold and the substrate. If successful, future attempts could then include boring through the back side of the device, through the substrate into the oxide layer so that after release this bottom side mirror would then have a clear view of the hole made and allow signals to pass beneath the MEMS layer.

The hinging issue involves the foldable structures discussed throughout this work. Similar to a complex paper fold, the general idea is to construct adjacent layers

of polysilicon with no connections between them other than the oxide. If released in that state, the structures would simply fall apart but the intent is to attempt to deposit various materials between these two layers. If the material deposited is strong yet flexible enough, then these flat pieces of polysilicon would (if properly pushed together) fold along these naturally weak 'creases' rather than bending. The process is very similar to depositing mirrors (and in fact various metals were attempted) but rather than patterning the mirror area the hinges were patterned instead.

The way in which the depositions were performed varied depending on the material, but in general there were two basic processes which were followed. If the intent was to deposit a polymer photoresist then the resist was applied as normal, a mask was aligned to the device, the device was exposed to ultraviolet light and then developed to remove all unwanted photoresist. If the intent was instead to deposit various metals, then a similar process was followed to apply the negative of the desired metal using a similar process as above. After developing the photoresist however, metal was then applied (either through evaporation or sputtering). The devices were then put into an organic solvent to remove the photoresist and the gold above it, but where the photoresist was missing the gold remained attached to the surface below.

As a large variety of masks were needed for this experiment, mask files will not be included in this work. The design of these masks was simply to reproduce the feature (hinge or mirror) and enlarge slightly to allow the deposited material some overlap with the polysilicon around the feature to help attempt to keep it attached. The masks prepared for the final PolyMUMPs run included:

- Valley Hinges
- Mountain Hinges
- Top Side Mirrors
- Bottom Side Mirrors



- Bottom Side Mirrors and Mountain Hinges (both likely to require bottom-side metal)
- Top Side Mirrors and Valley Hinges (both likely to require top-side metal)
- All Mirrors and Hinges
- All Mirrors, Hinges and PolyMUMPs deposited metal
- Slightly enlarged versions of everything above (for adhesion backing)
- Negatives of everything above (to allow for any kind of resist to be used)

A process follower was developed for bottom side mirror deposition (which also works for either kinds of hinge, but adjusted to deposit metal on the top for valley hinges).

## C.2 Process Followers

Bottom Mirror Deposition and SU-8 Backing			
Init.	Process Step	Notes	Date Time
	<b>PRE-CLEANING:</b> <input type="checkbox"/> 20 min, Acetone <input type="checkbox"/> Methanol Rinse <input type="checkbox"/> Dry with nitrogen and 110°C, 5 min	<u>Start Date</u>	
	<b>CHIP MOUNTING:</b> <input type="checkbox"/> Clean and dry a 3" Si wafer <input type="checkbox"/> Apply even layer of 1818 <input type="checkbox"/> 30 sec spin at 4,000 rpm, ramp=200 <input type="checkbox"/> 110°C, 1 min <input type="checkbox"/> Individually dip back of each device into single drop of 1818 <input type="checkbox"/> Brush back of device on lint free wipe and immediately set onto center of wafer <input type="checkbox"/> Repeat with as many devices, keeping a symmetric pattern near the center of the wafer (keep layer of 1818 thin enough that none seeps up between chips) <input type="checkbox"/> 110°C, 1 min <input type="checkbox"/> Repeat with a complete ring of sacrificial devices surrounding samples (keep layer of 1818 thin enough that none seeps up between chips) <input type="checkbox"/> 110°C, 1 min <input type="checkbox"/> Using dropper, apply a thin bead of 1818 around the outside of the sacrificial ring, leaving no breaks <input type="checkbox"/> With a swab, wipe up most of bead <input type="checkbox"/> 110°C, 1 min <input type="checkbox"/> Repeat surrounding bead at least once more (more if a large number of devices are being treated) <input type="checkbox"/> 110°C, 1 min <input type="checkbox"/> Cool for a minimum of 2 minutes to allow photoresist to set <input type="checkbox"/> Ensure all devices do not slide prior to continuing, if photoresist is not entirely dry repeat heating and cooling steps as necessary	<u>Start Time</u>	
	<b>DOUBLE LOR APPLICATION:</b> <input type="checkbox"/> Cool for a minimum of 2 minutes to allow photoresist to set (if necessary) <input type="checkbox"/> Apply LOR3A ensuring all devices (both center devices and sacrificial ring) are completely covered <input type="checkbox"/> 30 sec spin at 4,000 rpm, ramp=200 <input type="checkbox"/> 110°C, 2 min <input type="checkbox"/> Cool for a minimum of 2 minutes to allow photoresist to set <input type="checkbox"/> Apply LOR3A ensuring all devices (both center devices and sacrificial ring) are completely covered <input type="checkbox"/> 30 sec spin at 4,000 rpm, ramp=200 <input type="checkbox"/> 110°C, 2 min <input type="checkbox"/> Cool for a minimum of 2 minutes to allow photoresist to set <input type="checkbox"/> Inspect wafer under microscope and look for <input type="checkbox"/> Bubbles <input type="checkbox"/> Even Application		
	<b>1818 APPLICATION:</b> <input type="checkbox"/> Cool for a minimum of 2 minutes to allow photoresist to set (if necessary) <input type="checkbox"/> Apply 1818 ensuring all devices (both center devices and sacrificial ring) are completely covered <input type="checkbox"/> 30 sec spin at 4,000 rpm, ramp=200 <input type="checkbox"/> 110°C, 75 sec (As photoresist is setting, sacrificial chips can be slid away from center devices, immediately after removing wafer from hotplate, remove center devices from wafer and cool individually) <input type="checkbox"/> If necessary, reheat wafer for 10 sec and remove remaining devices <input type="checkbox"/> Cleanup wafer with 1165 heated to 170 °C for 10 min (longer if necessary) <input type="checkbox"/> Inspect wafer under microscope and look for <input type="checkbox"/> Bubbles <input type="checkbox"/> Even Application		
	<b>EXPOSE 1818:</b> <input type="checkbox"/> Align to Negative mask of mirrors to be deposited <input type="checkbox"/> 6.0 sec Exposure on Zuss aligner		

Revision 1.00

(3 Feb 09)

Page 1

Figure C.1:

### Bottom Mirror Deposition and SU-8 Backing

	<b>1818 / LOR DEVELOP:</b> <input type="checkbox"/> 75 sec develop with LDD26 at 500 rpm <input type="checkbox"/> 30 sec DI rinse at 500 rpm <input type="checkbox"/> Dry with nitrogen at 500 rpm <input type="checkbox"/> Dry wafer with nitrogen on clean texwipes		
	<b>INSPECT LITHOGRAPHY:</b> <input type="checkbox"/> Place wafer in microscope <input type="checkbox"/> Inspect wafer alignment on microscope <input type="checkbox"/> Check Lithography: <input type="checkbox"/> Open <input type="checkbox"/> Clean <input type="checkbox"/> Sharp Definition <input type="checkbox"/> If exposed areas still show LOR, repeat development step in 10 sec increments (drying and inspecting after each repeat) <input type="checkbox"/> Rework wafer if necessary (1165 stripper for 20 min to fully clean sample)		
	<b>O<sub>2</sub> PLASMA ASHER:</b> <input type="checkbox"/> 6 min plasma asher prior to any metal deposition		
	<b>METAL DEPOSITION:</b> <input type="checkbox"/> Apply desired metals (either through sputtering or evaporation, keeping thicknesses of sputtered metals low as poor adhesion is typical) <input type="checkbox"/> Maximum of 3000 Å per layer of LOR3A		
	<b>LIFT OFF EXCESS:</b> <input type="checkbox"/> Place devices in vibrating bath of acetone, watching removal process and removing as soon as it appears all metal is lifted off <input type="checkbox"/> Methanol Rinse <input type="checkbox"/> Dry with nitrogen and 110°C, 2 min <input type="checkbox"/> Inspect wafer under microscope and look for <input type="checkbox"/> Desired Metal Coverage <input type="checkbox"/> Good Adhesion <input type="checkbox"/> Clean Devices Around Metal <input type="checkbox"/> Repeat as necessary until surface appears clean and free of excess LOR		
	<b>O<sub>2</sub> PLASMA ASHER:</b> <input type="checkbox"/> 6 min plasma asher to remove residual resist material		
	<b>SU-8 APPLICATION:</b> <input type="checkbox"/> Preheat device for a MINIMUM of 5-10 min at 110°C to remove any residual moisture <input type="checkbox"/> Apply any adhesion promoter as per manufacturer instructions (if available) <input type="checkbox"/> Place individual device on spinner and apply even layer of SU-8 <input type="checkbox"/> 30 sec spin at 4,000 rpm, ramp=200 <input type="checkbox"/> 60°C, 3 min <input type="checkbox"/> 110°C, 3 min <input type="checkbox"/> Align to desired features (negative resist so exposed areas will remain – ensure good alignment prior to exposure as SU-8 after exposure will be unremovable, mask can be backed off to slightly enlarge coverage) <input type="checkbox"/> Expose for 15 sec on Zuss aligner <input type="checkbox"/> Repeat Alignment and exposure for other features as necessary <input type="checkbox"/> 60°C, 3 min <input type="checkbox"/> 110°C, 3 min <input type="checkbox"/> Develop with SU-8 developer for 60 sec (SU-8 can't be overdeveloped if applied correctly) <input type="checkbox"/> Dry with nitrogen at 500 rpm <input type="checkbox"/> Dry wafer with nitrogen on clean texwipes	<div><u>Finish Date</u></div> <div><u>Finish Time</u></div>	

## *Appendix D. Intermediate Results*

Several intermediate results were encountered during this experiment. While not applicable to the overall successes and lessons learned, there still may be some value in documenting some of these items .

### *D.1 Foundry Issues From PolyMUMPs*

During the various postprocessing steps on both PolyMUMPs runs, various issues were documented. While many of these are typical, the difference in quality between the two runs was remarkable. As shown in (a), several features (including the framed pyramid structure shown) which were  $2\mu\text{m}$  and above were either broken or missing upon arrive or too fragile to survive any postprocessing. As these formed most of the anchoring for the pyramids on this run it prevented a great deal of testing on possible hinging schemes. Another issue which severely impacted this run is shown in (b) where ghost images of various other designs (elsewhere on the chip by not part of THIS design) were present in the oxide layer. While for most applications this may not have been an issue, as this experiment was attempting to deposit metal on the oxide, this did impact most of the mirrors present as the step height in the oxide was not insignificant compared to the amounts of gold which could be deposited. Thus, most of the mirrors which were deposited did not form single layers of metal and did not stick to the oxide and those that did showed these ghost features in the metal.

Run 84 was a much better quality run overall. While some issues were still present from the foundry (such as a few broken actuator arms as those shown in Figure D.2 (a). These were admittedly very small features so a few breaks were not unexpected, but most were intact upon delivery. Also, as run 84 was delivered late in the year, it was sent out locally to be cut and as such, several chips were present in random locations around the edges (a problem not encountered with some test samples from run 83 which were sent to a different facility to be laser cut).

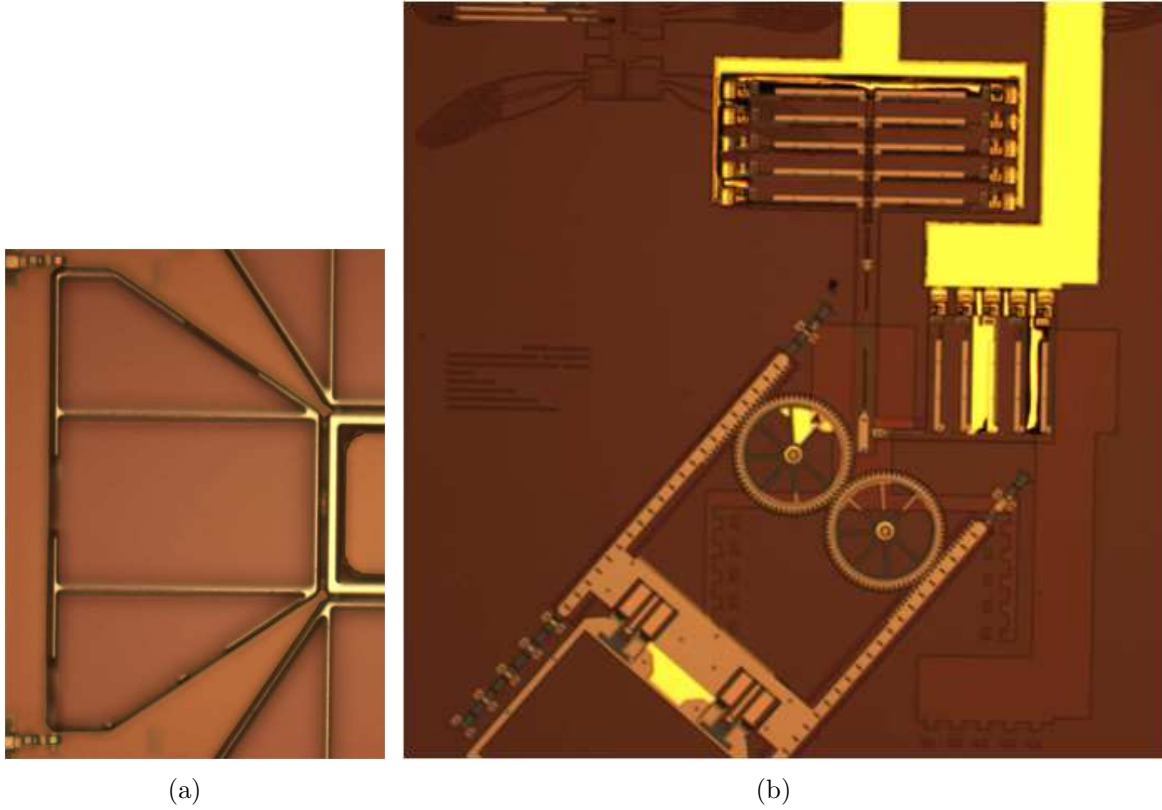


Figure D.1: Run 83 issues a) features as large as  $2\mu\text{m}$  in width missing or mis-aligned resulting in broken or missing sections in devices received from the foundry b) ghost images of two other designs overlaid in oxide layer (visible as wings in the top center of image and rectangular polygons in lower right corner)

## D.2 Post Processing

Several failed attempts were required to perfect a process which provided repeatable, usable results in various areas of this experiment. One such area was the application of a double LOR3A / 1818 mask on such small samples. While the full process of this was captured and presented as a process follower in Appendix C, some of the images from actual samples where were processed have been captured here and are worth mentioning.

One issue in any LOR deposition / development process is finding the correct exposure and development times required. The desired pattern requires the upper 1818 layer to maintain the outline of the metal to be deposited, but the LOR under-

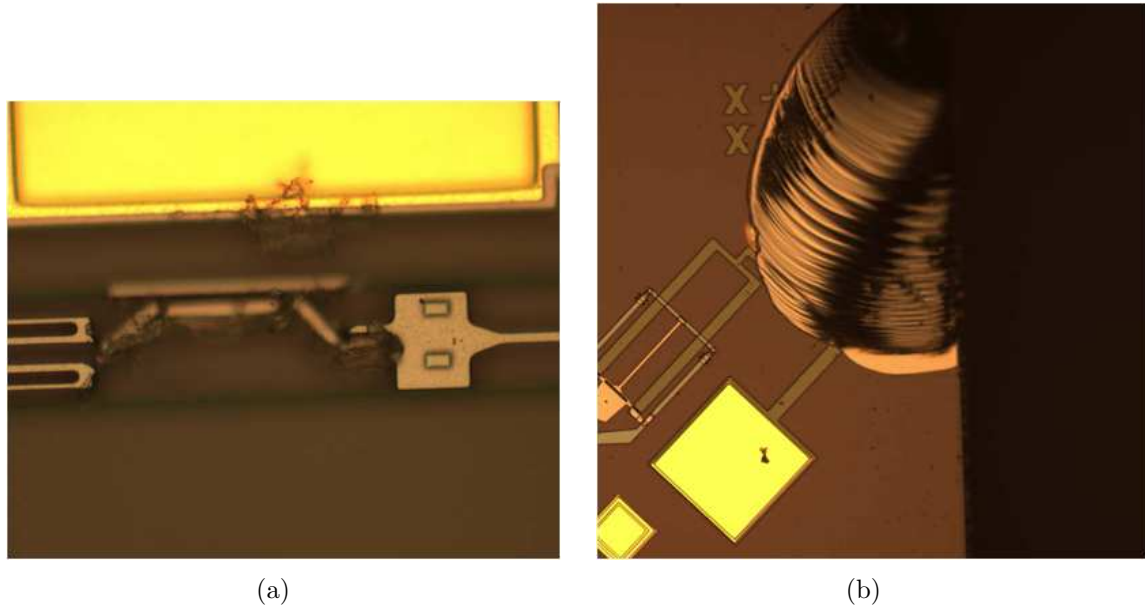


Figure D.2: Run 84 issues a) some broken polysilicon actuator beams b) edge chips were common

neath this layer must be undercut sufficiently for the lift off to occur. When done correctly (as shown in Figure D.3), both of these features should be clearly visible and the area where the metal is deposited should be completely free of any residual photoresists.

Similarly, issues arose in finding the correct method to deposit SU-8 for hinging. While this material did not ultimately work for the application it was used for, the depositions of the material itself worked well. As shown in Figure D.4, the dark brown areas patterned well over the gaps in the polysilicon below and survived the release process unaffected. Unfortunately the small overlap between the SU-8 and the polysilicon on either side did not hold well when the material was heated in an attempt to bend these hinges.

One final area worth mentioning is the differences in the two metal depositions available. While specific runs will inevitably have different results, in general the two images shown in Figure D.5 show the difference in attempting these two methods onto a PolyMUMPs device. While evaporated metal is much finer (and thus results in a

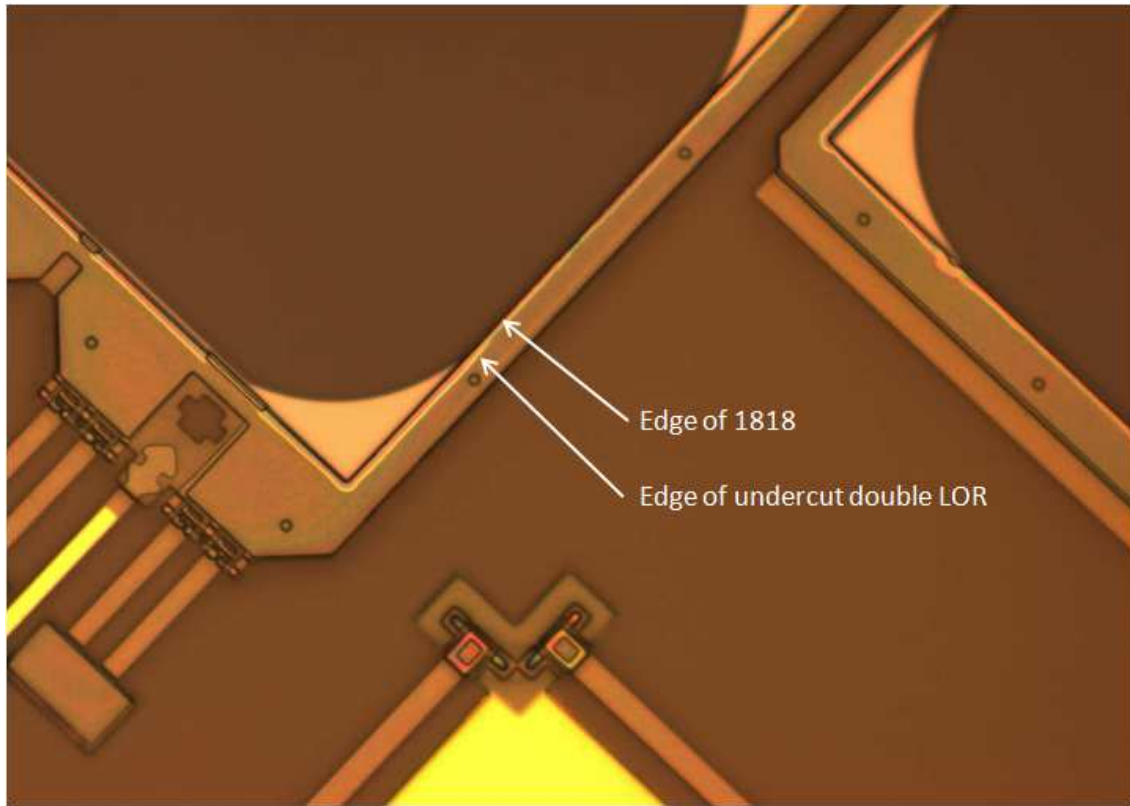
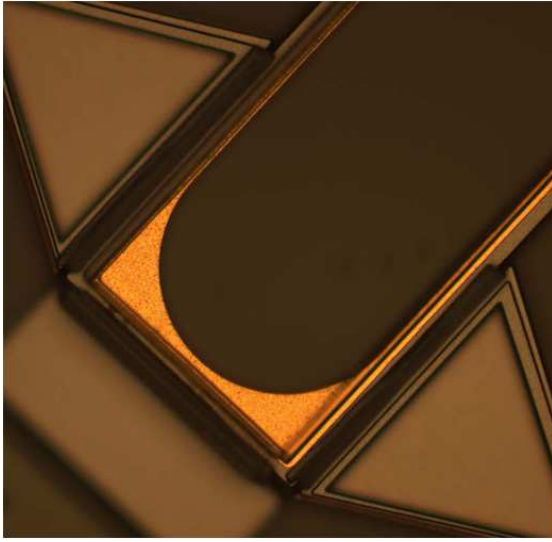
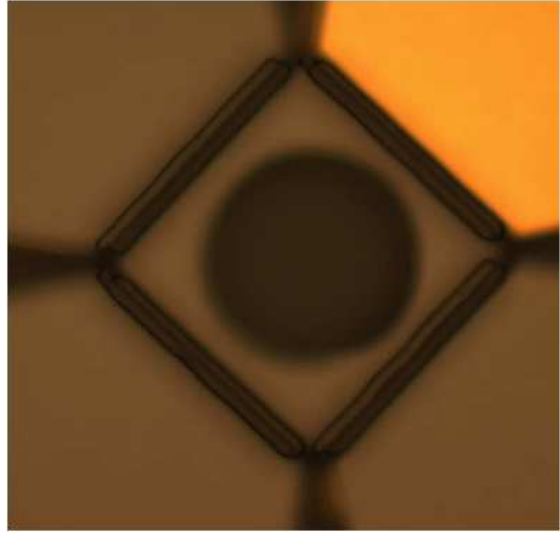


Figure D.3: Image showing a well exposed, developed and cleaned LOR / 1818 sample ready for metal deposition showing the edge of the 1818 and a clearly undercut LOR beneath

more, mirror-like finish), defects were significantly more common. More importantly the adhesion of evaporated metal was in general much worse than sputtered (approximately 10% of the evaporated mirrors survived the lift off process compared to about 80% of the sputtered).

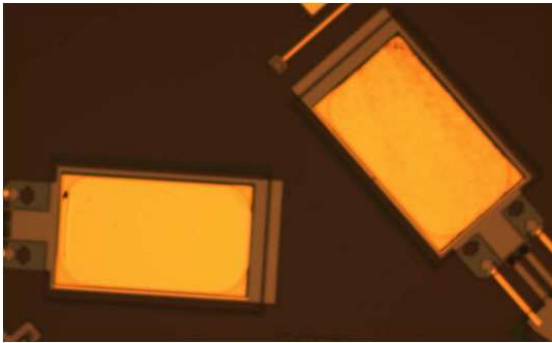


(a)

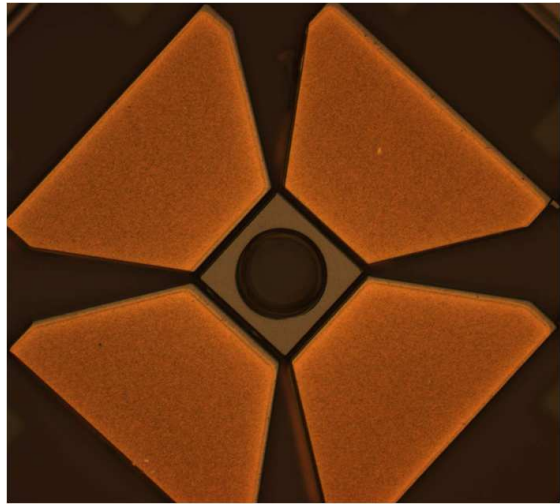


(b)

Figure D.4: SU-8 patterned hinges (shown as dark brown rectangular areas) overlapping and joining adjacent polysilicon layers in a) a  $45^\circ$  stationary mirror and b) the top of a pyramid structure



(a)



(b)

Figure D.5: Metal depositions compared a) evaporated b) sputtered



## Bibliography

1. DARPA, “Chip to chip optical interconnects.” Online [www.darpa.gov/MTO/Programs/index.html](http://www.darpa.gov/MTO/Programs/index.html).
2. R. N. Hall, “Coherent light emission from p-n junctions,” *Solid-State Electron.*, vol. 6, pp. 405–408, 0 1963.
3. S. Sze and K. Ng, *Physics of Semiconductor Devices*. Wiley-Interscience, 2nd ed., 2007.
4. Y. Wang, K. Tai, J. Wynn, M. Hong, R. Fischer, J. Mannaerts, and A. Cho, “Gaas/algaas multiple quantum well grin-sch vertical cavity surface emitting laser diodes,” *IEEE Photonics Technol. Lett.*, vol. v 2, pp. p 456–458, Jul 1990.
5. A. Tuantranont, V. M. Bright, J. Zhang, W. Zhang, J. A. Neff, and Y. C. Lee, “Optical beam steering using mems-controllable microlens array,” *Sens. and Actuators, A*, vol. 91, pp. 363–372, 7/15 2001.
6. K. Ishikawa, J. Zhang, A. Tuantranont, V. M. Bright, and Y.-C. Lee, “An integrated micro-optical system for vcsel-to-fiber active alignment,” *Sens. and Actuators, A*, vol. 103, pp. 109–115, 1/15 2003.
7. S. Riyopoulos, “Modulation waves propagating in vcsel arrays,” *Proc. SPIE Int. Soc. Opt. Eng.*, vol. v 4286, pp. p 142–147, Jan 2001.
8. D. I. Babic, J. J. Dudley, K. Streubel, R. P. Mirin, N. M. Margalit, J. E. Bowers, and E. E. Hu, “Transverse-mode and polarization characteristics of double-fused 1.52  $\mu$ m vertical-cavity lasers,” *III-Vs Review.*, vol. 9, pp. 36–40, 4 1996.
9. A. Kroner, F. Rinaldi, J. M. Ostermann, and R. Michalzik, “High-performance single fundamental mode algaas vcsels with mode-selective mirror reflectivities,” *Opt. Commun.*, vol. 270, pp. 332–335, 2/15 2007.
10. H.-P. D. Yang, I.-C. Hsu, F.-I. Lai, G. Lin, R.-S. Hsiao, N. A. Maleev, S. A. Blokhin, H.-C. Kuo, and J. Y. Chi, “Beam profile characteristics of ingaas sub-monolayer quantum-dot photonic-crystal vcsels,” *Opt. Commun.*, vol. 274, pp. 94–99, June 2007.
11. C. Pu, Z. Zhu, and Y.-H. Lo, “Surface micro-machined optical coherent detection system with ultra-high sensitivity,” *Sens. and Actuators, A*, vol. 78, pp. 36–40, 1 1999.
12. J. Yuan, F. Luo, X. Zhou, Q. Huang, and M. Cao, “Optical interconnection in embedded-fiber printer circuit boards,” *Optik - International Journal for Light and Electron Optics*, vol. 119, pp. 46–50, 1/7 2008.

13. A. Jain and H. Xie, "A single-crystal silicon micromirror for large bi-directional 2d scanning applications," *Sens. and Actuators, A*, vol. 130-131, pp. 454-460, 8/14 2006.
14. K. Hedsten, J. Melin, J. Bengtsson, P. Modh, D. Karlén, B. Lfving, R. Nilsson, H. Rdjegrđ, K. Persson, P. Enoksson, F. Nikolajeff, and G. Andersson, "Mems-based vcsel beam steering using replicated polymer diffractive lens," *Sens. and Actuators, A*, vol. 142, pp. 336-345, 3/10 2008.
15. M. Starman, Lavern A., *Characterization of Residual Stress in Microelectromechanical Systems (MEMS) Devices Using Raman Spectroscopy*. Phd dissertation, AFIT, 2002.
16. C. Thompson, Eric, "Nonmechanical multizoom telescope design using a liquid crystal spatial light modulator and focus-correction algorithm," thesis (m.s.), AFIT, Mar 2008. AFIT/GEO/ENP/08-03.
17. B. McCarthy, V. M. Bright, and J. A. Neff, "A multi-component solder self-assembled micromirror," *Sens. and Actuators, A*, vol. 103, pp. 187-193, 1/15 2003.
18. H. Xie, Y. Pan, and G. K. Fedder, "Endoscopic optical coherence tomographic imaging with a cmos-mems micromirror," *Sens. and Actuators, A*, vol. 103, pp. 237-241, 1/15 2003.
19. R. Syms, C. Gormley, and S. Blackstone, "Improving yield, accuracy and complexity in surface tension self-assembled moems," *Sens. and Actuators, A*, vol. A, no. 88, pp. 273-283, 2001.
20. R. Guerre, C. Hibert, Y. Burri, P. Flckiger, and P. Renaud, "Fabrication of vertical digital silicon optical micromirrors on suspended electrode for guided-wave optical switching applications," *Sens. and Actuators, A*, vol. 123-124, pp. 570-583, 9/23 2005.
21. "Vw eos retracting hardtop." Online [www.autoblog.com/2006/01/13/video-vw-eos-retracting-hardtop](http://www.autoblog.com/2006/01/13/video-vw-eos-retracting-hardtop), Jan 2006.
22. "Lasers and magnetic launch for cheap launches within ten years." Online [www.nextbigfuture.com](http://www.nextbigfuture.com), May 2007.
23. EPFL, "Master of architecture and civil engineering." Online <http://enac.epfl.ch/>, 2008.
24. H.-M. Cheng, M. Ewe, R. Bashir, and G. Chiu, "Modeling and control of piezoelectric cantilever beam micro mirror and micro laser arrays to reduce image banding in electrophotographic processes," *J. Micromech. Microeng.*, vol. 11, pp. 1-12, 2001.
25. F. Filhol, E. Defa, C. Divoux, C. Zinck, and M. T. Delaye, "Resonant micro-mirror excited by a thin-film piezoelectric actuator for fast optical beam scanning," *Sens. and Actuators, A*, vol. 123-124, pp. 483-489, 9/23 2005.

26. U. Krishnamoorthy, K. Li, K. Yu, D. Lee, J. P. Heritage, and O. Solgaard, "Dual-mode micromirrors for optical phased array applications," *Sens. and Actuators, A*, vol. 97-98, pp. 21–26, 4/1 2002.
27. Y. Lu, I. Dajani, and R. J. Knize, "Ultrafast laser assisted fabrication of zno nanorod arrays for photon detection applications," *Appl. Surf. Sci.*, vol. 253, pp. 7851–7854, 7/31 2007.
28. P. Servati, A. Colli, S. Hofmann, Y. Q. Fu, P. Beecher, Z. A. K. Durrani, A. C. Ferrari, A. J. Flewitt, J. Robertson, and W. I. Milne, "Scalable silicon nanowire photodetectors," *Physica E: Low-dimensional Systems and Nanostructures*, vol. 38, pp. 64–66, 4 2007.
29. S. D. University of California and N. S. Foundation, "News from the field, nanowires make great photodetectors." Online [http://www.nsf.gov/news/newssumm.jsp?cntn\\_id=109844&org=IRM&from=newsField](http://www.nsf.gov/news/newssumm.jsp?cntn_id=109844&org=IRM&from=newsField), 2008.
30. D. Kane, "Single nanowire photodetector." Online <http://www.eurekalert.org/multimedia/pub/3858.php>, July 2008.
31. "Why nanowires make great photodetectors." Online <http://www.physorg.com/news96728801.html>, April 2007.
32. S. Krishna, "Inas/ingaas quantum dots-in-a-well photodetectors," vol. 5957, p. 595702, SPIE, 2005.
33. H. C. Liu, H. Luo, C. Y. Song, Z. R. Wasilewski, A. J. S. Thorpe, and J. C. Cao, "Design of terahertz quantum well photodetectors," *Infrared Phys. Technol.*, vol. 50, pp. 191–193, 4 2007.
34. P. D. Grant, H. C. Liu, M. Buchanan, and R. Dudek, "Ultrahigh frequency quantum well infrared photodetectors," vol. 6297, p. 629708, SPIE, 2006.
35. C. L. Jelen, S. Slivken, G. J. Brown, and M. Razeghi, "Multicolor 4- to 20-um inp-based quantum well infrared photodetectors," vol. 3629, pp. 147–154, SPIE, 1999.
36. J. Bundas, K. Patnaude, R. Dennis, D. Burrows, R. Cook, A. Reisinger, M. Sundaram, R. Benson, J. Woolaway, J. Schlesselmann, and S. Petronio, "Two-color quantum well infrared photodetector focal plane arrays," vol. 6206, p. 62060G, SPIE, 2006.
37. J. Li, K. K. Choi, and D. C. Tsui, "Voltage tunable four-color infrared detector using semiconductor superlattices," vol. 5881, p. 588102, SPIE, 2005.
38. M. Erdtmann and M. Razeghi, "Monolithic integration of gainas/inp quantum well infrared photodetectors on si substrate," vol. 4288, pp. 163–170, SPIE, 2001.
39. R. Calarco, M. Fiordelisi, S. Lagomarsino, and F. Scarinci, "Near-infrared metal-semiconductor-metal photodetector integrated on silicon," *Thin Solid Films*, vol. 391, pp. 138–142, 7/2 2001.

40. S. D. Gunapala, S. V. Bandara, A. Singh, J. K. Liu, E. M. Luong, J. M. Mumolo, and M. J. McKelvey, "Quantum well infrared photodetectors for low-background applications," vol. 3379, pp. 225–234, SPIE, 1998.
41. A. Singh and D. A. Cardimona, "Design issues relating to low-temperature dark current in quantum well infrared photodetectors," vol. 2999, pp. 46–54, SPIE, 1997.
42. H. Melchior, "Sensitive high speed photodetectors for the demodulation of visible and near infrared light," *J. Lumin.*, vol. 7, pp. 390–414, 1973.
43. D. M. Paganin and T. E. Gureyev, "Phase contrast, phase retrieval and aberration balancing in shift-invariant linear imaging systems," *Opt. Commun.*, vol. 281, pp. 965–981, 3/1 2008.
44. L. Seifert, H. J. Tiziani, and W. Osten, "Wavefront reconstruction with the adaptive shackhartmann sensor," *Opt. Commun.*, vol. 245, pp. 255–269, 1/17 2005.
45. M. Cap, "Polymumps process information." Online [www.memscap.com](http://www.memscap.com).
46. S. N. Labs, "Summit process information." Online [mems.sandia.gov/samples](http://mems.sandia.gov/samples).
47. S. N. L. MEMS Technologies Department, "Summit v(tm) five level surface micromachining technology design manual," April 2008.
48. S. N. Laboratories, "Summit(tm) process details." CD for Distribution, 2007.
49. J. J. Craig, *Introduction to Robotics, Mechanics and Control*. Addison-Wesley Publishing Company, 2nd ed., 1989.
50. C. Platteborze, R.C., "Microelectromechanical systems (mems) safe-and-arm barrier for low-energy exploding foil initiators (leefi)," thesis (m.s.), AFIT, March 2008. AFIT/GEO/ENP/08-01.
51. L. Miller, Virginia, "Conceptual mems devices for a redeployable antenna," thesis (m.s.), AFIT, Sep 2007. AFIT/GE/ENG/07-30.
52. C. Bellott, Mark M., "Microelectromechanical systems (mems) safe and arm device," thesis (m.s.), AFIT, March 2007. AFIT/GE/ENG/07-03.
53. GeSiM, "3d structuring." Online [http://www.gesim.de/front\\_content.php](http://www.gesim.de/front_content.php), 2009.

## *Index*

The index is conceptual and does not designate every occurrence of a keyword.

AutoCAD, 36, 37, 55, 57, 93

C2OI, 1

CMP, 30

Coventorware, 50

DARPA, 1

HF, 29

LPCVD, 30

MATLAB, 51, 54, 55, 57, 90, 93

MEMS, iv, 1–4, 6–9, 11, 12, 15–19, 24–27,  
31, 35, 41, 48, 71, 72, 74, 98

MTO, 1

PECVD, 31

photodetector, 4, 22, 23, 35, 80, 96, 97

PolyMUMPs, iv, 10, 12, 24, 27–32, 37, 39,  
40, 43, 45, 47, 63, 67, 69–71, 76,  
78, 82, 94, 98–100, 103, 105

QWIP, 24, 25, 59, 96

SacOx, 30

SEM, 9, 10, 13, 15, 18, 20, 49, 50, 64

SU-8, 49, 50, 59, 69, 73, 74, 82, 105, 107

SUMMiT, 10, 25, 30–32, 39, 71, 82

thermal actuator, 10, 20, 43–45, 47, 66, 80

VCSEL, 4, 6–11, 22, 35, 40, 41, 46, 76, 80,  
97

# REPORT DOCUMENTATION PAGE

Form Approved  
OMB No. 0704-0188

The public reporting burden for this collection of information is estimated to average 1 hour per response, including the time for reviewing instructions, searching existing data sources, gathering and maintaining the data needed, and completing and reviewing the collection of information. Send comments regarding this burden estimate or any other aspect of this collection of information, including suggestions for reducing this burden to Department of Defense, Washington Headquarters Services, Directorate for Information Operations and Reports (0704-0188), 1215 Jefferson Davis Highway, Suite 1204, Arlington, VA 22202-4302. Respondents should be aware that notwithstanding any other provision of law, no person shall be subject to any penalty for failing to comply with a collection of information if it does not display a currently valid OMB control number. **PLEASE DO NOT RETURN YOUR FORM TO THE ABOVE ADDRESS.**

<b>1. REPORT DATE</b> (DD-MM-YYYY) 26-03-2009			<b>2. REPORT TYPE</b> Master's Thesis		<b>3. DATES COVERED</b> (From — To) Sept 2007 — Mar 2009	
<b>4. TITLE AND SUBTITLE</b>  Chip To Chip Optical Interconnection Using MEMS Mirrors					<b>5a. CONTRACT NUMBER</b> DACA99-99-C-9999	
					<b>5b. GRANT NUMBER</b>	
					<b>5c. PROGRAM ELEMENT NUMBER</b>	
<b>6. AUTHOR(S)</b>  Tod Laurvick, Capt, USAF					<b>5d. PROJECT NUMBER</b> ENG 08-180	
					<b>5e. TASK NUMBER</b>	
					<b>5f. WORK UNIT NUMBER</b>	
<b>7. PERFORMING ORGANIZATION NAME(S) AND ADDRESS(ES)</b> Air Force Institute of Technology Graduate School of Engineering and Management (AFIT/EN) 2950 Hobson Way WPAFB OH 45433-7765					<b>8. PERFORMING ORGANIZATION REPORT NUMBER</b>  AFIT/GE/ENG/09-27	
<b>9. SPONSORING / MONITORING AGENCY NAME(S) AND ADDRESS(ES)</b>  Air Force Research Laboratory (Dr. Rajesh Naik, Senior Scientist) 3005 Hobson Way, Bldg 651 WPAFB, OH 45433-7707 937-785-3808 ext. 3180, Rajesh.Naik@WPAFB.af.mil					<b>10. SPONSOR/MONITOR'S ACRONYM(S)</b> AFRL/MLPJE	
					<b>11. SPONSOR/MONITOR'S REPORT NUMBER(S)</b>	
<b>12. DISTRIBUTION / AVAILABILITY STATEMENT</b>  Approval for public release; distribution is unlimited.						
<b>13. SUPPLEMENTARY NOTES</b>						
<b>14. ABSTRACT</b>  This experiment explores the use of MEMS mirrors to direct subsurface optical signals to another device and reception of those signals for use in chip to chip communications. Devices were built in PolyMUMPs to control horizontal and vertical beam direction and tilting in the outgoing signal and MEMS beam splitters for the incoming signal. Several elements of the outgoing beam path were successful and those which needed improvement indicate a high probability of success with limited trials needed and currently successful design elements could still be improved within the scope of PolyMUMPs. The incoming beam path elements were not successful as designed and would require the flip chip bonding unit now available at AFIT, or could be realized with a high probability of success and minimal design work with a more sophisticated fabrication process (such as SUMMiT).						
<b>15. SUBJECT TERMS</b>  MEMS, beam steering, VCSEL, photodetector						
<b>16. SECURITY CLASSIFICATION OF:</b>			<b>17. LIMITATION OF ABSTRACT</b>  UU	<b>18. NUMBER OF PAGES</b>  124	<b>19a. NAME OF RESPONSIBLE PERSON</b> Maj LaVern A. Starman, PhD (ENG)	
<b>a. REPORT</b>  U	<b>b. ABSTRACT</b>  U	<b>c. THIS PAGE</b>  U			<b>19b. TELEPHONE NUMBER</b> (include area code) (937)255-3636, x4618; lavern.starman@afit.edu	